공학박사학위논문

인간과 상호작용하는 휴머노이드용 로봇 팔과 손의 개발에 대한 연구

The Anthropomorphic Robotic Arm and Hand for Interactive Humanoids

2007년 8월

서울대학교 대학원

기계항공공학부

백 규 진

인간과 상호작용하는 휴머노이드용 로봇 팔과 손의 개발에 대한 연구

The Anthropomorphic Robotic Arm and Hand for Interactive Humanoids

지도교수 이 교 일

이 논문을 공학박사 학위논문으로 제출함

2007년 6월

서울대학교 대학원
기계항공공학부
백 규 진

백규진의 공학박사 학위논문을 인준함

2007년 8월

위 원 장 : _____

부위원장 : _____

위 원 : _____

위 원 : _____

위 원 : _____

ABSTRACT

Humanoid robots are designed and built to bear similitude to humans. Ultimately, they are to resemble the sizes and physical abilities of humans in order to function in human-oriented environment and work autonomously but to pose no physical threat to humans. Humanoid robots need to exhibit artificial skin and facial expressions to create extremely lively human appearances. A humanoid robot that resembles human in its appearance and in its movement is built using powerful actuators paired with gear-trains and joint mechanisms, motor drivers that are all encased in a package no larger than that of the human physique. In this paper, I propose the construction of the humanoid-applicable anthropomorphic 7-DoF arm completed with 8-DoF hand. A novel mechanical design of this humanoid arm makes it compact enough not only to be compatible with currently available narrating-model humanoids, but also powerful and flexible enough to be functional; the number of degrees of freedom endowed in this robotic arm is sufficient for executing a wide range of tasks including dexterous hand motions. The developed robotic arm is an interactive humanoid robot, with the safety feature actualized in both the software and hardware aspects. Software-wise, the humanoid arm adapts an algorithm to sense and interpret the incoming external force and escapes toward a safe direction. Hardware-wise, it is designed and built to be light

and compliant to minimize shocks in case of a collision.

The thesis covers the following:

- the development of the anthropomorphic arm and hand hardware for safe human interactions
- the development of an algorithm for detecting an external force input using inverse dynamics
- the development of safe escape algorithms without using the conventional multi-axis Force-Torque sensors, torque sensors or contact sensors.

Keywords: humanoid arm, humanoid hand, human robot interaction, interactive robots, safe robot arm, robot motion generation, humanoid robot.

Student number: 2002-21182

Table of contents

List of tables

List of figures

Chapter 1: Introduction

The word “robot” was first coined by a screenplay writer, Karel Capek (1920), in his play “Rossum’s Universal Robots”. In his play, humanlike robots work at a factory and receive maltreatment from their human employer until a scientist endows them emotion and cause them to rebel and kill humans. Novelist Isaac Asimov (1950) was the first to use the term “robotics” for the field and in his novel, “I , Robot,” where he defined the famous three laws of robotics:

- A robot may not injure a human being or, through inaction, allow a human being to come to harm.
- A robot must obey orders given by human beings except where such orders would conflict with the First Law.
- A robot must protect its own existence as long as such protection does not conflict with the First or Second Law.

With the advancement of technology, more powerful actuators, smaller and sensitive sensors and faster computers, which are quintessential for developing humanoids robots, have become widely available. The story of the factory humanoids that went on a strike in Capek’s play may be a bit far fetched, but given the current technology, it has become feasible to build complex enough of a humanoid robot that could hurt human if no safety law is predefined.

1.1 Humanoid robots

Humanoid robots, are a new breed of robots that are evolving fast, and are commonly distinguished from the conventional industrial robots. The first and most apparent difference is in the humanoids' appearance. Some humanoids even exhibit artificial skin, painted/actuated facial expressions, and intricate masks that are extremely lively and humanlike.

The second distinguishing feature lies in the actuation methods. In order to exercise in an anthropomorphic fashion, a humanoid needs to have enough actuated motional degrees of freedom to execute most of human actions; therefore, a redundant actuation is inevitable in most cases. For arms, 7-degrees of freedom (DoF, from the shoulder to the wrist) allows performing most human motions, and for hands, it varies from 5 to 24 under actuated joints, depending on the types of motion. Such redundancy in the humanoid limbs is essential in reproducing flexible and smooth movements of a human. For finesse and lively actions, these multi-joints also need to be actuated with sufficient torque.

Lastly, humanoids are robots which are designed for social and interactive tasks. They often, if not always, share their work space with human operators and/or other robots. Working closely with an unpredictable environment, humanoids are expected to interact with an opponent in expressing its state, reacting to events and performing tasks safely at all times.

1.2 Objectives

The current robotic technology has yet to build a humanoid robot that fully satisfies all three criteria. For humanoids that focus on their appearances, the number of DoF is reduced to produce minimal motion while keeping the exterior design compact; however, the range and speed of the reproduced motions are compromised. For humanoid robots that exercise in an anthropomorphic fashion, the robot are armed with powerful actuators; however, this jeopardizes the overall appearance as the joints become too large to be considered as a humanoid robot arm. It is also challenging for a compactly designed humanoid to execute lively motions while being conscious of its environment and safe interaction. Therefore, this work aims to develop robotic arm and hand that satisfies the functionality criteria without arbitrating its focus on anthropomorphic design.

1.3 System Overview

In this paper, I propose a humanoid-applicable 7-DoF anthropomorphic arm with a 8-DoF hand. The compact mechanical design of this humanoid robotic arm is slim enough not only to be compatible with currently available narrating-model humanoids, but also powerful and flexible enough to be functional. DC motors are installed in a compact gear-train and joint mechanical frame while maintaining the appearance of a human arm. Furthermore, the number of DoF endowed in the arm

is sufficient for executing a wide range of tasks including fine hand motions. For an interactive humanoid robot, it is also imperative for the arm to be conscious of its environment for safety while sharing the work space with humans: the safety feature of the arm is actualized in both the software and hardware aspects. Software-wise, the humanoid arm adapts an algorithm to sense and interpret the incoming external force and escaping toward a safe direction. Hardware-wise, it is designed and built to be light and compliant to minimize shocks in case of a collision.

The rest of the thesis presents the research and development process of the humanoid-applicable anthropomorphic arm and hand. Chapter 2 gives the literature review on humanoids and humanoid applicable technology as well as robot human safety issues. Chapter 3 presents the kinematics and dynamic modeling of the arm including the dynamics of the arm while in motion, hand gripping and impact dynamics effect on the hand and the rest of the joints. The paper proceeds to the discussion of the method of the redundant link motion planning from collected knot points in Chapter 4 including the design factors for a safe HRI trajectory. In Chapter 5, I describe the novel design features of the arm and hand, built from the biomechanical data collected for this study. I introduce the actuator specifications and modularized motor controller along with the communication protocol used for the system in Chapter 6, and the test-bed evaluations regarding the mechanical

performance of the arm in Chapter 7. Lastly, the concluding chapter summarizes the research work on the interactive robotic arm along with the suggestions for future work regarding the safety and hardware.

Chapter 2:
Hardware & Literature Review

Among the vast research on robotic arms and manipulators in the field of robotics, this chapter looks at the work on humanoid applicable robotic arms and hands. Here, the robot architectures and hardware designs that focus on the anthropometry of the mechanism, the safe Human Robot Interaction (HRI) and the ability to reproduce human movements are of the utmost interest. Humanoid robots' novelty lies largely in its mechanism design; the humanoids require compact packaging while delivering enough torque and speed for task executions. The two features are conflicting criteria as actuators' volume and weight are directly proportional to their power production. To overcome this physical constraint, researchers often resort to reducing the mechanical specifications of the hardware. Decreasing the number of DoF, reducing the range of motion, payload, or sacrificing the overall size/weight for the mechanical performance are some of the ways implemented in order to build humanoid robots. The following sections cover some of the exemplary models.

2.1 Robotic arms

I investigate interactive, collision and impact sensitive robotic arms with multi-DoF here.

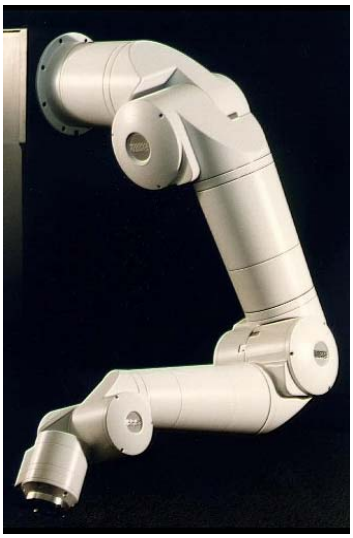

Figure 2.1 Robotics Research Co. K-1207i (http://www.robotics-research.com/)

Robotics Research Co. (RRC) has developed an industrial robotic arm with modularized joint parts and a slim mechanism design. Its 7-DoF joints can actively change its joint compliance for the safe HRI. However, due to the use of harmonic drives in each joint, the joint torque control may be ineffective at reducing the impedance of the manipulator for a high control bandwidth. In addition, even at a low control bandwidth, the joint would have a limited compliance due to the nature of the harmonic drives.

(a) **(b)**

Figure 2.2 DLR light-weight robot (a) DLR II (b) DLR III

DLR's Light-Weight Robot (Hirzinger et al. 2001, 2002; Butterfass et al. 1998a, 1998b) is composed of weight-reduced safety brakes and modular system where the individual joints are connected via carbon-fiber structures. Similar to the human arm, the robot has 7-DoF and where the complete electronic components are integrated into the arm. Having each joint equipped with a motor position sensor, a joint position sensor and a joint torque sensor, the third generation model is quite applicable for humanoids. However, DLR III Light-Weight Robot weighs 13.5 kg. Although the load to weight ratio is high, a lighter arm would be desirable for a life sized-humanoid robot arm with restricted space and actuation power. This model also uses harmonic drives as a gear-train that have a nature of limiting the range of joint compliancy even though it saves much room for compactness.

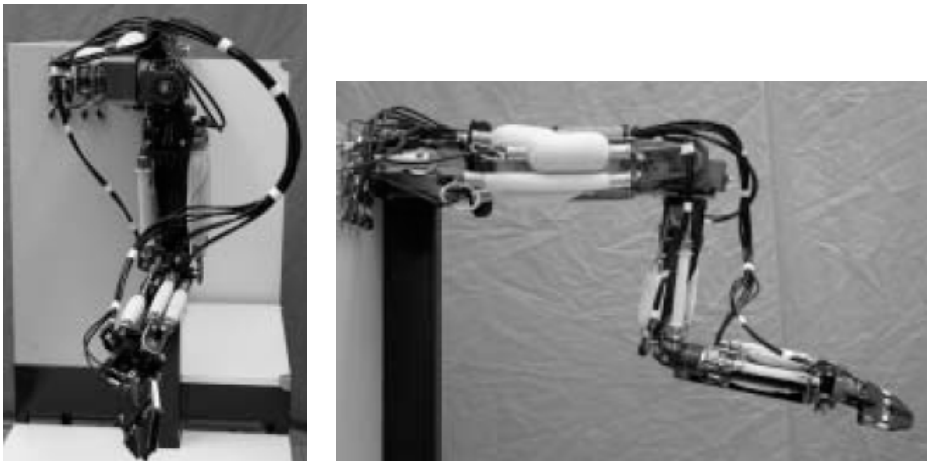

Figure 2.3 INSA 7-DoF Anthropomorphic arm (Tondu 2005)

For an arm without harmonic drives, INSA's 7-DoF Anthropomorphic arm gives almost the full range of motions of the human arm as it serves 7 DoF motion in its joints. Also due to the nature of the McKibben pneumatic actuator, the arm is quite compliant for safer human interactions. However, due to its overall size and weight, its use in direct humanoid robot applications is quite limited. The Soft Arm (Bicchi et al. 2002) also features compliant joints that are actuated by McKibben pneumatic actuators; thus, the use of compressors is inevitable even though they are quite difficult to work with when designing a compact robot body.

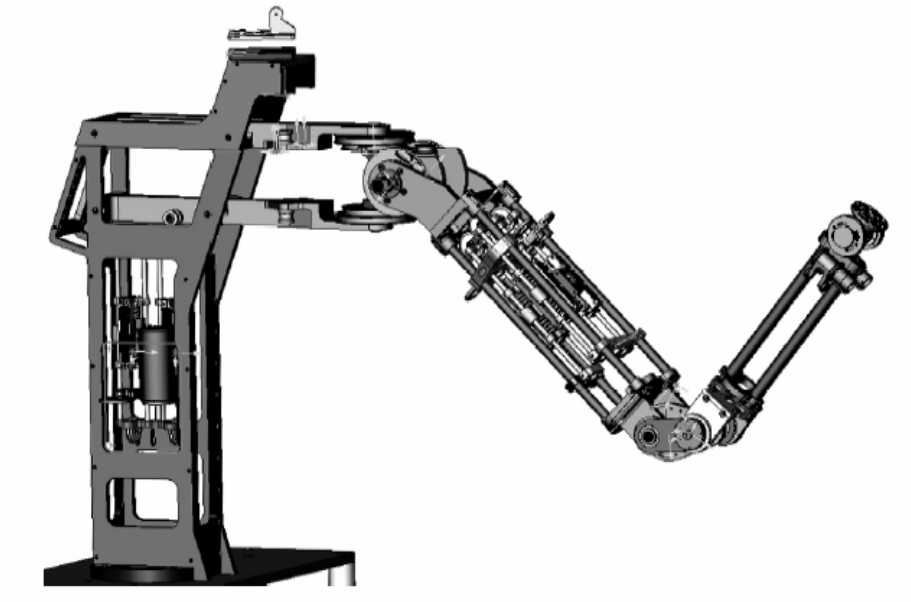

Figure 2.4 CARDEA arm (Brooks et al. 2004)

As a compliant humanoid robotic arm, CARDEA uses the Series Elastic Actuators (SEA). CARDEA has a spring in series with the output of a DC motor so that the SEA can determine the joint torque by sensing the spring deflection. This spring also serves to protect the gear-train from impact forces that the arm may encounter. Although the use of SEA enables CARDEA to satisfy the compliancy issue under human environment, it has too large a base for realistic applications and only serves 5 DoF. The limited actuation DoF also narrows the range of motions.

While realizing the importance of compliancy, it is still important to have a larger payload at the end effector without loosening the range of control bandwidth. The Distributed Elastically Coupled Macro Mini Actuation (DECMMA) arm (Zinn et al.

2004a, 2004b, 2004c) for example takes this into consideration and uses a double actuation system. For higher frequency actions with lighter loads, it uses a smaller joint actuator; and for larger loads with low frequencies, it uses larger actuators at the base. The application of this actuating system, however, is too large for humanoid robot applications.

2.2 Robotic Hands

Industrial robotic arm manipulators may resemble human hands in the sense that there is a base that acts like the palm and serially linked multi joints that act like fingers. However, for a realistic humanoid that follows closely the human biometrics, we prefer five-fingered mechanisms. Here are some models that have a high dexterity with potential applications in humanoid robotic hands.

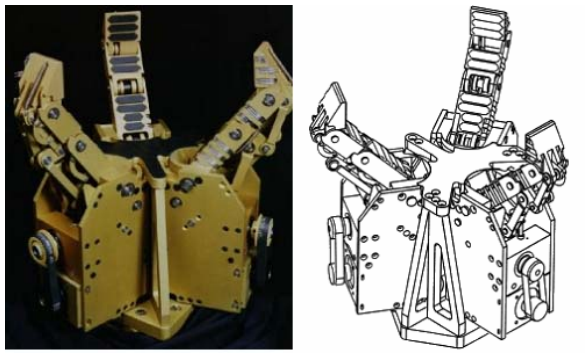

Figure 2.5 The 12-DoF Robotic hand of Laval University

Fig 2.5 is the 12-DoF robotic hand made in 1996 in LAVAL University (Laliberte 2002). Two fingers grip and the last finger is used to stabilize the grab. Its focus is on fast and stable and finger grasp; however, the overall size, shape and the orientation of fingers is far from humanoid application.

Figure 2.6 The Fast Robotic Hand of Tokyo University (Namiki et al. 2003)

The Fast Robotic Hand has a high control bandwidth for grabbing objects using vision sensing. It has a payload of 4N at the fingertip. The angular speed of the wrist is 1800deg/s with each finger's working range of 360-degree rotation; this range would be beyond the capabilities of human hands.

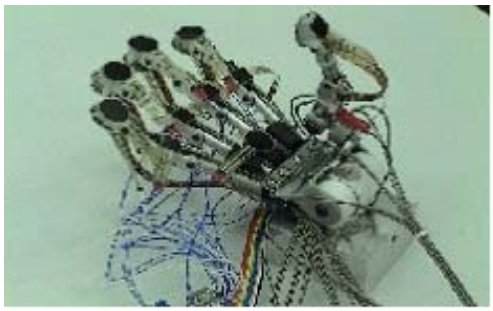

Figure 2.7 The tendon driven robot hand of Zurich University

The tendon driven robot hand (Gomez et al. 2006) uses artificial muscles as actuators. At the fingertips, the robot has contact sensors and a total of 13 servo motor actuated DoF. It uses bending sensors to confirm the finger position and pressure sensors to cover the palm. Due to the nature of tendon driving, the wires protrude out of the finger links, making it possibly dangerous to work with while in a closed interaction with human operators.

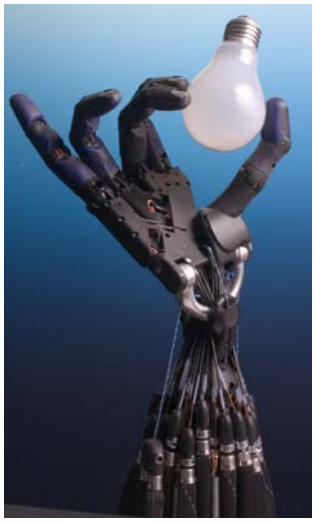

Figure 2.8 Shadow hand (Shadow Robot Co. 2003)

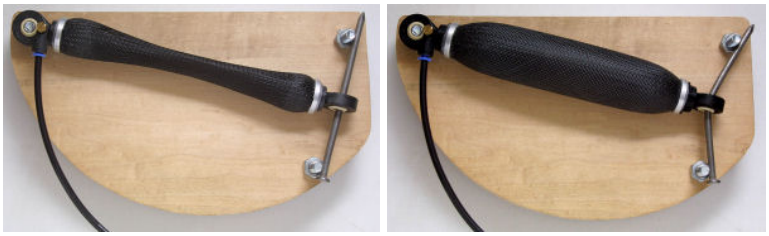

Figure 2.9 Air Muscles

The Shadow hand was first developed in 1997. It is actuated by a pneumatic actuator called Air muscles. In the fingers, it has a total of 12-DoF and has extra 4-DoF in the palm. Without the air compressor, the hand weighs 4.5kg. The fingers are driven by tendons while position, torque, and force feedback-controlled. Using a control glove, Master-Slave manipulation is also possible. The movement is quite smooth, almost resembling human movements. However, due to the actuator's

nature and its heavy weight, it is inappropriate for installing the whole hardware system on an autonomous life-sized humanoid arm.

Figure 2.10 GIFU Hand III (Mouri et al. 2002, Kawasaki et al 2002)

The GIFU hand features 16-DoF in five fingers. It measures 251mm in length and weighs 1.4kg in total. Its contact sensors on its palm and fingers have a total of 859 detecting points and its readings are used to determine the grasping status. Although it does have five fingers and the human biometric conscious size, GIFU hand is quite heavy for the humanoid robot applications.

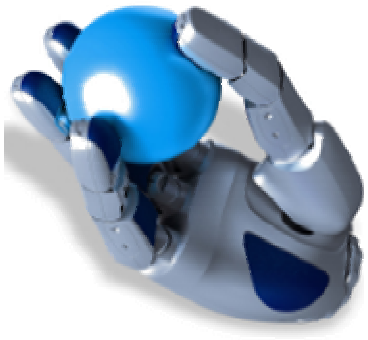

Figure 2.11 DLRIII (Borst et al. 2002)

The DLR's latest hand model features four fingers with 13-DoF in total with custom fitted DC motors in each joint. The sophisticated packaging is attractive while the fingers sense external forces with inlaid torque and position sensors. However, its size is larger than the average human hand if concerned with building a real-life sized humanoid robot.

Kaneko developed a 13-DoF, multi-fingered hand that has a smaller mechanical packaging while being dexterous enough to hold light objects (Kaneko et al. 2007). However, the number of fingers is limited to four; UBIII Hand on the other hand (Biagiotti et al. 2005) is light and has five fingers with human-sized dimensions. It uses contact sensors which are mounted on each links to determine incoming forces for task executions.

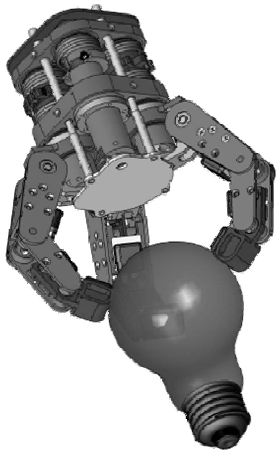

Figure 2.12 The Complaint and Force Sensing Hand (Edsinger-Gonzales 2004)

As a force sensing hand, Edsinger-Gonzales's hand utilizes SEAs (Series Elastic Actuators) to sense the grasped objects. It is a unique approach to the mechanism design as it uses no other force, torque or contact sensors. Figure 2.12 shows a robotic hand that has three fingers which are sensitive enough to hold a light bulb while supporting 16-DoF.

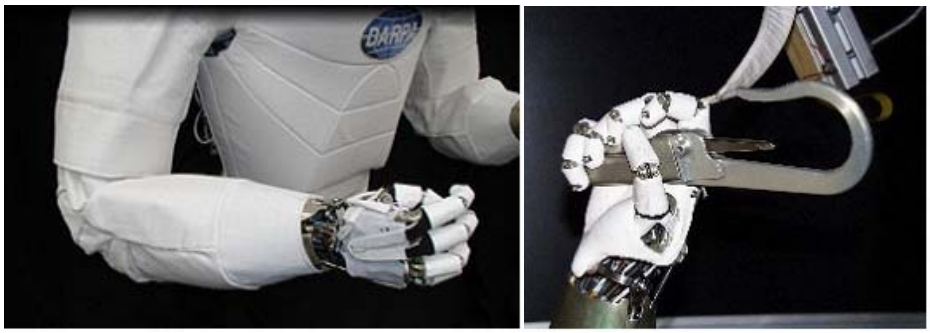

Figure 2.13 Robonaut arm and hand (Lovchic et al. 1999, 2000, 2001)

NASA's Robonaut arm and hand show the superior mechanism over the other models covered in this chapter. The part dimensions are biologically inspired and their components are robust enough to be used in space. The arm uses thermal vacuum rated motors, harmonic gear drives and numerous sensors in each joint. With multiple patents on its complex parts, this hardware is built for executing tasks in space where the weight and the production price of the whole arm is the least of concern compared to its mechanical performance. Therefore, the size and the weight are too large for the on earth applications for human interactions.

Currently known robotic hands that are presented in this chapter and some more models have been categorized with their characteristic tabulated in Appendix A.

Summarizing the works on anthropomorphic arms and hands, the following graphs show the trend in the design criteria and the physical compromises that the models have made by updating the survey (Alba & Ponticelli 2005) with some new hand models and with an emphasis on their applicability to a life-sized humanoid robots. The data on the weights and operational velocity, and payload would have been useful to make the design criteria index for the existing models. But even without such data, it is apparent that the greatest challenge lies in executing multiple articulations while keeping the weight and volume minimal.

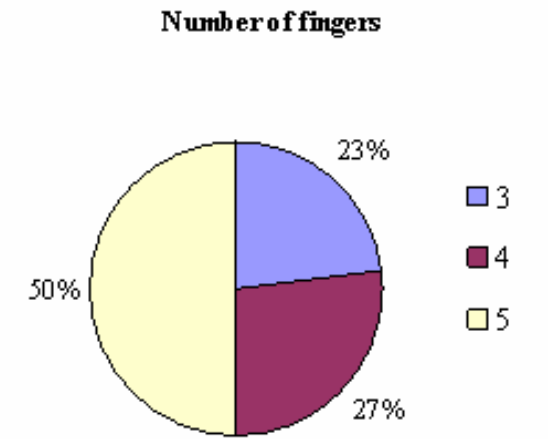

Figure 2.14 Number of fingers in robotic hands (survey of 26 hands)

Due to the limited palm and hand size and the variety of task choices, half of the hands presented in the diagram have less than five fingers. If the dexterity of the hands is of the only concern, having all five fingers is not as critical. However, the lack of fingers does not provide a sufficient test-bed for a task of reproducing realistic five fingered human motions (i.e. sign languages, reproduction of bio-mimetic motions).

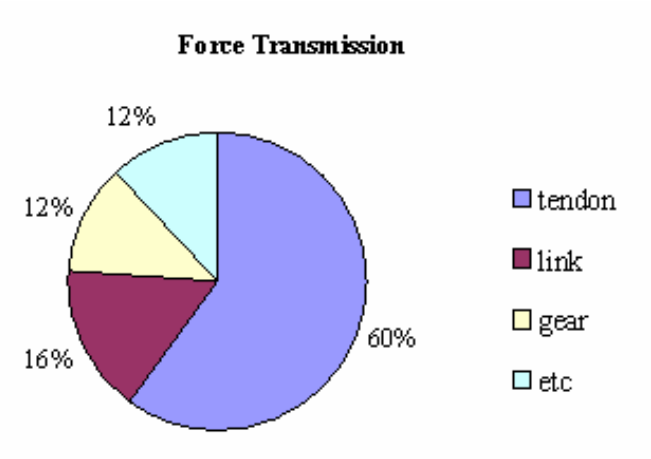

Figure 2.15 Method of power transmission in robotic hands

(Survey of 26 hands)

The method of power transmissions vary with the actuator types. Most electrical rotary motors use tendons (passive and active pulling), links, and gear power transmission methods. Most pneumatic and hydraulic actuators and artificial muscles use tendon pulling methods. Some hands use a combination of force transmission methods.

Table 2.3 shows a summarized actuator to DoF ratio of the researched hands along with the value for the newly developed hand, the Anthropomorphic hand (named SNU MnM in the graph).

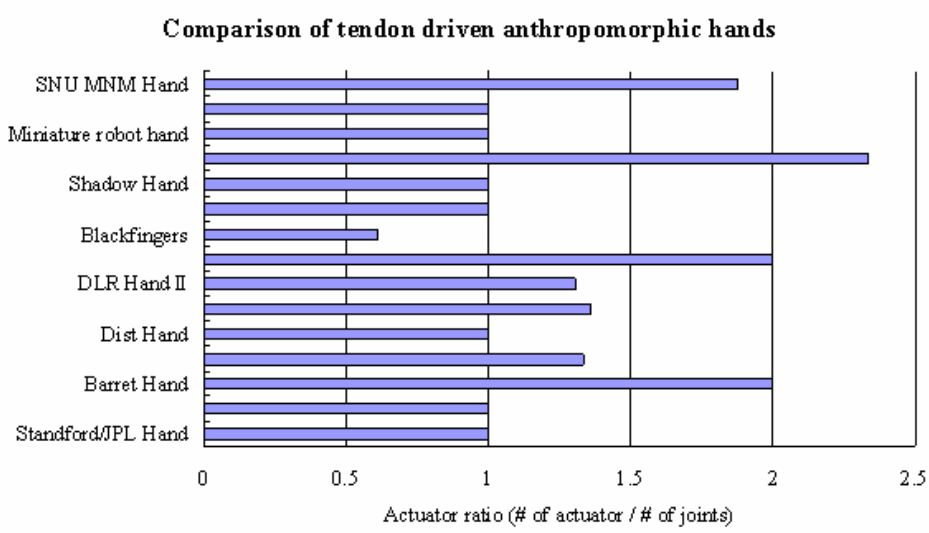

Figure 2.16 Tendon driven hands' actuator ratio

2.3 Humanoid robots

A number of attractive robotic hand and arm models are presented in the previous section. Separately, they show a high probability of being applied to life-sized humanoids. However, it is rare to find an example where such designs are actually incorporated into one machine (a hand and an arm put together) and function while keeping the overall characteristics and biometrics of the parts. Also, having such limbs be HRI-safe is still a definite challenge in the robotics field. This section covers examples of the existing humanoid robot with a set of arm and hand. There has been examples of robots with HRI conscious designs like the Companion (Fig

2.17); however, these robots are less concerned with the resemblance to human, and lack the multi-degrees of freedom range of motion.

Fig 2.17 InTouch's The Companion

(http://www.intouchhealth.com/products.html)

The Companion is a 1.2m high robot on wheels that holds an LCD screen displaying a medical professional operator from a remote location. The Companion is designed to wander the nursing home facility greeting people in its path and giving them simple but necessary medical feedbacks. Its HRI is critical; thus, IR sensors and camera detect close objects. It has no separate arm or manipulator, limiting its physical interactions with humans to its 2 dimensional floor trajectory.

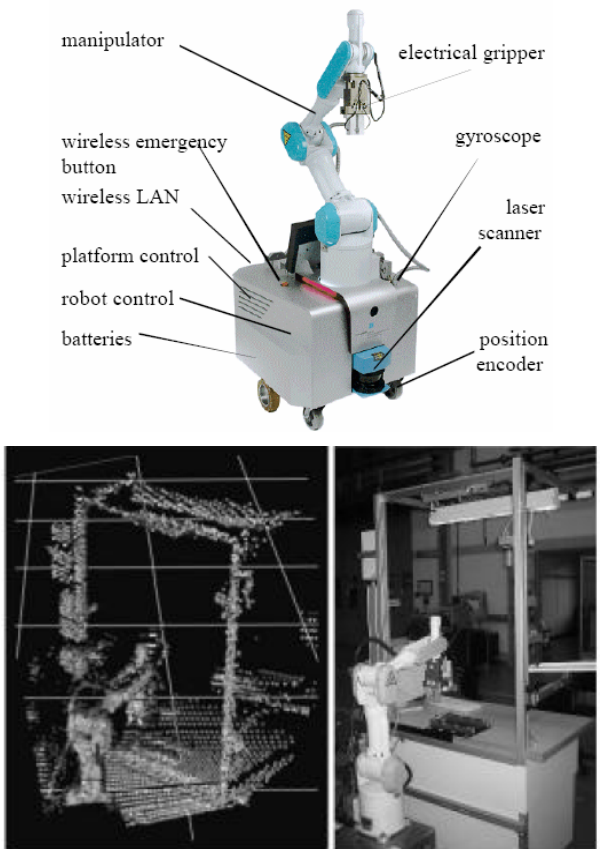

Figure 2.18 Rob@work and its 3D laser scanned image of the work environment

Rob@work (Helms et al. 2002) in Fig 2.18 ensures safe HRI by having multiple sensors to realize every position of its manipulator during task executions. It has been equipped with a tilting sensor head containing a laser scanner and two cameras. Care-O-bot (Fig 2.19), developed by the same group uses a tilting head sensor and a remote controller to work inside homes of elderly.

Figure 2.19

Care-O-Bot, human assisting anthropomorphic robot (Hans et al. 2004)

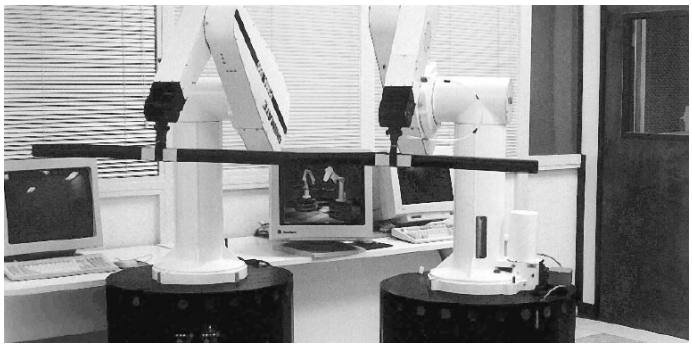

Figure 2.20 Interactive 6-axis F-T sensor installed PUMA arm

Interactive and co-working PUMA arms with a multi-axis Force-Torque (F-T) sensor can check for collision and this feature is much desired in sociable and interactive humanoids (Fig 2.20). But as an industrial robot, its mechanical

capacity is over designed for humanoid applications and its size makes it undesirable for humanoid robot applications.

Some of robotic arms and hand/manipulators with safe HRI include Rob@work, Care-o-bot, and PUMA arms; however, despite their abilities to interact safely with human operators, their appearances are far from life-sized a humanoid robot.

Figure 2.21 The Kendo sparring robot, MUSA (Bang et al. 2005, Lee 2007)

MUSA is a martial art practice partner robot that senses the opponents' sword moves and chooses the proceeding trajectories. Safe yet effective HRI, life-sized arms are essential. The size and mechanical performance, and HRI are critical for fast paced martial art practices and MUSA meets these requirements without

having to use the commonly used multi-axis F-T sensors or joint torque sensors. Four DoFs are endowed in each arm while the sword is held up with additional DoF in the wrist. There is no separate hand component in MUSA.

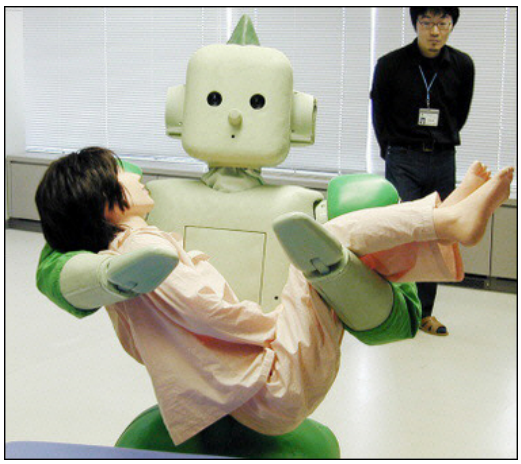

Figure 2.22 Medical service robot RI-MAN lifting an 18kg human doll

Riken Brain Science Institute's RI-MAN (Odashima 2006, Onishi 2007) also shows robotic arms that would be suitable for humanoid applications. A variety of sensors provide RI-MAN with a sense of vision, hearing, touch, and smell for safe human interactions such as locating and lifting humans. Its arms have 6 DoF each, but its payload capacity is not yet able to lift a real human (Fig 2.22 shows an 18kg human doll). Its soft skinned exterior and dollish face allow for friendly interactions with nursing home patients. RI-MAN's robotic arms are specifically built for safe HRI; therefore, its use of sensors is extensive.

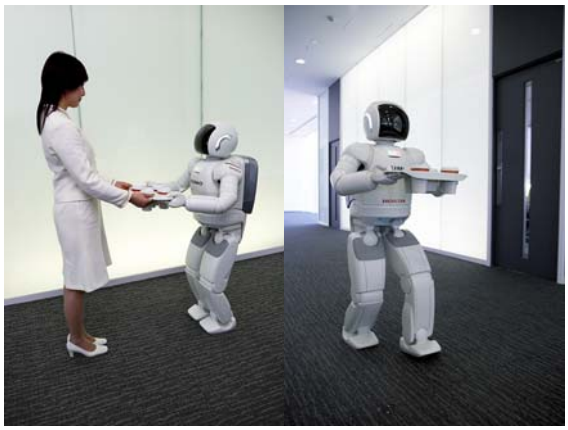

Figure 2.23 ASIMO with 6 axis F-T sensor mounted arm for human interaction (Honda 2005)

Honda's ASIMO also senses the load on its hands using F-T sensor in its wrist, and is able to carry objects given to it and return it when interacting with human operators. Its hands have five fingers but limited dexterity as it has only 4 -DoF.

Figure 2.24 Human interactive HRP-2 (Kaneko 2004)

Human interactive HRP-2 is able to interact with humans and produce useful tasks

such as lifting while leveling the board. It has two 6-axis F-T sensors installed in its wrist for sensing the externally applied forces.

Humanoid robots such as HUBO (http://hubolab.kaist.ac.kr), MUSA, RI-MAN, ASIMO, and HRP-2, present realistic, human-sized exterior with flexible movements in its redundant DoF endowed arms. However, they often lack the DoF to reproduce human-like motion trajectories or have limited dexterity in the hands.

2.4 Safe HRI strategies

In conventional settings of industrial robots where they are not required to share the work space with humans, the injury inflicted by robots are limited to the machine's malfunctions or the operators' misconduct. This being said, if the robot is isolated from human operators, little or no precaution measures are taken regarding the safety of the operator; one just needs to keep clear of the robots' workspace at all times. In many cases, industrial robots are kept behind the fence. However, for humanoid robots that are designed to encounter frequent and random HRI, neither communicational nor mechanical isolation is an option; for most humanoid robots it would be impossible to carry out their task of physical strength-supporting (for the elderly and disabled), entertaining, or communicating with their human operators.

In order to ensure the safety of both humanoid robots and human operators, several

criteria must be considered. Pervez and Ryu (2007), Ikuta (2003), Kulic & Croft (2005, 2006), Khatib (1999), Bicchi & Tonietti (2001, 2004) and Zinn (2004a, 2004b) are some of many researchers whose work encompass HRI. According to their studies, the research on HRI largely divides into three categories: the first is defining and quantifying the level of safety, the second is minimizing this level through hardware design and the third is controlling humanoids with software.

In the case where the robots' hardware encompasses an infra-structure, or robot body with multiple sensors, safety measures prior to a collision can be taken. Based on the readings of the sensors such as multi-angled cameras, IR distance sensors, or even electromyography (Kulic & Croft 2005), the robotic arm and manipulator can slow down, alter the motion trajectory (Brock & Khatib 2002), or altogether stop when a hazardous situation is identified. Also, any potentially dangerous situation can be notified to the operator before it occurs.

For autonomous, compact sized robots that are not equipped with such infrastructure, or vision-based system, which is costly both in computation and in economical sense, the robot is left to determine the dangerous situation only after an accident occurs. Upon a collision, robot chooses a trajectory path to minimize or stop from being a physical threat to the operator by analyzing the sensor readings (multi-axis F-T sensors, joint torque sensor, and position sensors).

For the ultimate safety, however, the intrinsic safety of the robot should also be

considered. The intrinsic safety of the robot can be taken as the initial and the "guaranteed safety" of the robot without the sensors (failed sensors) or even with a high bandwidth control. In such cases, the robot is unable to surveillance the surroundings, and make appropriate adjustments such as altering motion trajectory or actively controlling the robot manipulators' joint compliancy (Zinn, Hirzinger, RRC). Therefore, one can consider the natural joint compliancy, weight, surface coating material, shape, and surface friction for determining the safety of the robot hardware (Ikuta et al. 2003). Or simply, as Bicchi (2002) puts it, passively complaint joints along with low inertia (low body mass) are the two basic elements of an inherently safe mechanism design that would ensure minimum safety during HRI.

Chapter 3:
Robotic arm and hand modeling

This chapter presents the work on the anthropomorphic arm and hand control and joint manipulation. Here, I cover the inverse dynamics process, the dynamics software simulation, and the joint torque calculations for impact force for the developed robotic arm and hand. I have included most parameter tables that are needed for the calculation.

3.1 The anthropomorphic robotic arm dynamics

The main physical differences between the human arm's biomechanics and a humanoid robotic arm are the actuation source and its location. Human arm joints can only be roughly approximated in the mechanical sense due to the complex nature of the human anatomy (Sakai et al. 2006, Lenarcic 1999). The arm joint assimilates a ball and socket joint, but with an unfixed point of rotation. These joints are actuated by complex co-ordinations of extension and compression of thin and thick muscle strips. Even the use of the SMA actuated artificial muscles or pneumatic actuators, and ball and socket joint only simulate this mechanical functionality with much limitation. While the detail on the process of mechanical design is covered in Chapter 6, the mechanism of the developed anthropomorphic

arm is extremely human biometry conscious. The calculations of expected torque load at each joint position can directly correspond to the load a human arm would experience at the according joints.

For such calculation, the torque load experienced in each joint can be solved iteratively from one link to another. The Newton and Euler method summarized by Spong & Vidyasagar (1989) and Craig (2003) is applied to the system of the seven modularized links. One of the links can be simplified as shown in Fig 3.1. where *(i+1)*th link is directed toward the hand

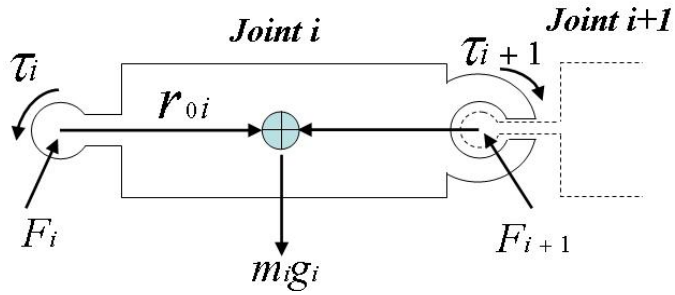

Figure 3.1: The i[th] link of the arm

The location of link *i*'s end point is at the location of *Fi*; therefore, the *i*th motor angle rotation is made at the end point of link *(i+1)*. Using the Newton-Euler method for stepwise link rotations from the base to the tip of the end-effector, the summation of forces and torque about the link i can be written out as (3.1) and (3.3) (Spong & Vidyasagar 1989).

$$F_i = R_i^{i+1} \cdot f_{i+1} + m_i g_i = m_i a_{c,i} \qquad (3.1)$$

$$\tau_i - R_i^{i+1}\tau_{i+1} + f_i \times r_{oi} - (R_i^{i+1} f_{i+1}) \times r_i = I_i\alpha_i + \omega_i \times (I_i\omega_i)$$

$$\tau_i = R_i^{i+1}\tau_{i+1} - f_i \times r_{oi} + (R_i^{i+1} f_{i+1}) \times r_i + I_i\alpha_i + \omega_i \times (I_i\omega_i) \qquad (3.2)$$

The rotational velocity ω of the link is found in the world coordinate frame (Spong & Vidyasagar 1989, Murray et al. 1993).

$$\omega_i^0 = \omega_{i-1}^0 + z_{i-1} \cdot \dot{q}_i \qquad (3.3)$$

Here ω_i^0 is the axis rotating speed in the world frame, which is detected by observing point *q*. Then, this *q* is also given in the world coordinate while ω is the rate of changing i^{th} axis frame (shown in Fig 3.2).

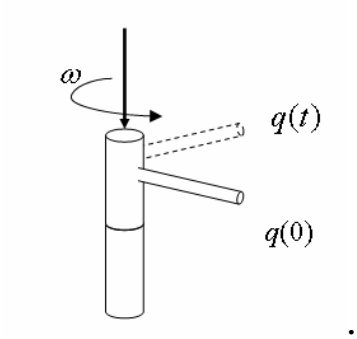

Figure 3.2 Rotational velocity of q about axis i

The point on this local frame is q(0) at time 0 and q(t) at time t; then, $\dot{q}$ is found as follows.

$$\dot{q}(t) = \omega \times q(t) \qquad (3.4)$$

For simplicity, the cross product term simplifies (Murray et al. 1993) to

$\dot{q}(t) = \hat{\omega} \cdot q(t)$, where

$$\hat{\omega} = \begin{bmatrix} 0 & -\omega_3 & \omega_2 \\ \omega_3 & 0 & -\omega_1 \\ -\omega_2 & \omega_1 & 0 \end{bmatrix}.$$

In order to use the inertial term of the arm links that are obtained from the CAD software (local frame), the coordinate system has to match the rest of the equation. For this purpose, the joint coordinates are converted into the local coordinates. And they are found when all the joints are converted back from each joint's direction of revolute joint axis, J (equation 3.5 through 3.7). Subscript 1 in J_{i_1} stands for the first row values of the i^{th} joint.

The mass center and the joint orientation coinciding with the base frame are summarized in Table 3.1 and the moment of inertia of all the links are shown in Table 3.2.

Table 3.1 Joint link center of mass, link mass and joint direction (base frame)

		Link numbers (shoulder=0 ~ palm=6)						
		6	5	4	3	3	1	0
Center of mass in base coord. [mm]	X	0	-9	2	6	10	5	0
	Y	0	-3	4	0.8	0	6	47
	Z	-585	-500	-424	-311	-224	-70	0
Link mass [kg]		0. 2	0. 002	0. 93	0. 4	0. 45	1. 3	0. 45
Joint rotation dir.		X	Y	Z	X	Z	X	Y

Table 3.2 Moment of inertia of seven joint links of the anthropomorphic arm

		Link numbers (shoulder=0 ~ palm=6)						
		6	5	4	3	2	1	0
Moment of inertia in base coord. [kg.mm^2]	Ixx	484	1.5	1980	191	536	2716	844
	Iyy	572	1	1860	156	481	2737	335
	Izz	160	0.7	298	136	149	442	852

$$J_{i\_1} = R_1^0 R_2^1 \cdots R_{i+1}^i \cdot \begin{pmatrix} 1 \\ 0 \\ 0 \end{pmatrix} \tag{3.5}$$

$$J_{i\_2} = R_1^0 R_2^1 \cdots R_{i+1}^i \cdot \begin{pmatrix} 0 \\ 1 \\ 0 \end{pmatrix} \tag{3.6}$$

$$J_{i\_3} = R_1^0 R_2^1 \cdots R_{i+1}^i \cdot \begin{pmatrix} 0 \\ 0 \\ 1 \end{pmatrix} \tag{3.7}$$

Each joint's J term produces three $[3\times 1]$ matrices. By concatenating the three terms, the q coordinate in the world frame is obtained.

$$q = \begin{bmatrix} J_{i\_1} & J_{i\_2} & J_{i\_3} \\ [1\times 3] & [1\times 3] & [1\times 3] \end{bmatrix} \tag{3.8}$$

And now, ω can be considered as the change in q during the time period from *k-1* to *k+1*. Knowing this, the rotational velocity at joint i, ω, is found by adapting a numerical analysis method.

$$\omega_i(o) = \frac{\omega_i(k+1) - \omega_i(k-1)}{2} \tag{3.9}$$

Then, the body centered linear acceleration in the world coordinate frame is found as a_i .

$$\dot{\omega}_i = \dot{\omega}_{i-1} + z_{i-1}\ddot{q}_i + \omega_i \times z_{i-1}\dot{q}_i \tag{3.10}$$

$$a_i = a_{e,i-1} + \dot{\omega}_i \times r_{oi} + \omega_i \times (\omega_i \times r_{oi}) \tag{3.11}$$

Where $a_{e,i-1}$ is the linear acceleration at the endpoint of the (i-1)th link, $\dot{\omega}_i$ is the change in the angular velocity and it is accumulatively found from the previous links. Following the same logic, the linear velocity is

$$V_i = V_{e,i-1} + \omega_i \times r_i \tag{3.12}$$

In order to convert the body inertia given in the local frame to the world frame, the following are considered ; using the J matrices found in (3.5), (3.6) and (3.7), the resulting local coordinate torque, $I_i\alpha_i$ is

$$I_i\alpha_i = \left[I_x \cdot (\alpha_i \cdot J_{i\_1}) \quad I_y \cdot (\alpha_i \cdot J_{i\_2}) \quad I_z \cdot (\alpha_i \cdot J_{i\_3}) \right]. \tag{3.13}$$

To convert this to the world frame from this local frame, use (3.13).

$$I_i\alpha_i = \begin{bmatrix} J_{i\_1x} & J_{i\_2x} & J_{i\_3x} \\ J_{i\_1y} & J_{i\_2y} & J_{i\_3y} \\ J_{i\_1z} & J_{i\_2z} & J_{i\_3z} \end{bmatrix} \cdot \begin{bmatrix} I_{xx} \cdot (\alpha_i J_{i1}) \\ I_{yy} \cdot (\alpha_i J_{i2}) \\ I_{zz} \cdot (\alpha_i J_{i3}) \end{bmatrix} \tag{3.14}$$

Now, the torque reflected on to the motor by the gears is obtained as the following.

$$\tau_{geari} = I_{geari\_1} \cdot (gear\_ratio_{i\_1})^2 \cdot \ddot{\theta}_i \cdot \left[J_{[3\times3]}\right] + I_{geari\_2} \cdot (gear\_ratio_{i\_2})^2 \cdot \ddot{\theta}_i \cdot \left[J_{[3\times3]}\right] \tag{3.15}$$

The torque load from the motor's rotor is also reflected on to the motor by the square of the total gear ratio.

$$\tau_{rotori} = I_{rotori} \cdot (gear\_ratio_i)^2 \cdot \ddot{\theta}_i \cdot \left[J_{[3\times3]}\right] \tag{3.16}$$

When the effects of all the torque are summed up, it leads to (3.17) to get the torque effect of the current link to the next link.

$$\tau_{i+1} = \tau_i - \tau_{ri} + \tau_{roi} + \tau_{geari} + \tau_{rotori} \tag{3.17}$$

The corresponding gear ratios, rotor and gear inertia are found in the following tables.

Table 3.3 Moment of inertia of the rotors and gears

		Link (shoulder=0 ~ palm=6)						
		6	5	4	3	2	1	0
Moment of inertia Base cood. [kg.mm^2]	I_rotor	0.38	0.38	0.76	2.6	1.1	4.2	4.2
	I_gear1	0.851	0.672	0.623	10.5	0.63	19.1	27
	I_gear2	2.37	1.89	0	0	0.998	0	0

Table 3.4 Joint gear ratios

	Link (shoulder=0 ~ palm=6)						
	6	5	4	3	2	1	0
Gear ratio	135	135	65	70	96.25	81	100
Gear1 ratio	15	16.2	8.67	9	21.38	9	10
Gear2 ratio	2	3.6	0	0	6.11	0	0

Table 3.4 shows the gear ratios of each joint. Here, the Gear ratio is the total speed reduction done by the gear-train, and gear1 and gear2 ratio stand for the ratios in between the spur gears in the middle of the gear-train.

3.2 Motion Simulation

In conjunction with calculations and 3D CAD software data, various motions of the developed anthropomorphic arm are produced through a motion dynamics software. The humanoid arm's CAD file has been transferred to the motion dynamics software to be evaluated. For this research, RecurDyn® software is utilized for both kinematics and rigid multi-body dynamic analysis. This allowed for confirming the arm's motion range and its joint torque. An animated motion sequence is also viewed while each joint's linear and angular velocity and acceleration are plotted.

From the plotted graphs, the joint torques for applied motion has been

found. The 3D software enables an immediate dynamic evaluation of the mechanical system. Therefore, the arm can be put in any arbitrary position and moved with any desired speed, making possible for any probable motion to be inspected while viewing the animation. The animation process is especially useful when viewing the motion of the fingers and detecting their working range for various types of grasping, which include power and precision grasps.

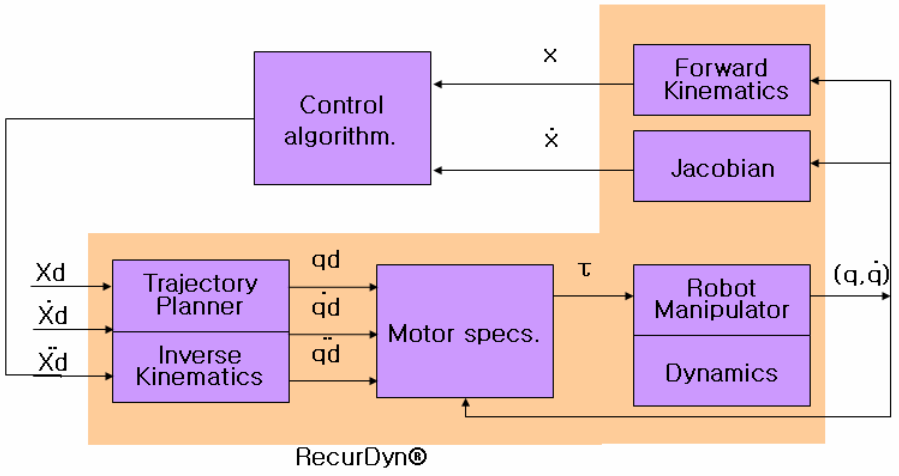

Figure 3.3 Schematics of RecurDyn® dynamics simulator process

Once a desired motion trajectory is set, RecurDyn® can read in the values to produce dynamics results. The resulting torque profile is reviewed for the motor torque sufficiency. The arm shown is not the exact model that is built; however, the position of the center of gravity for each link and the location of joints are close to the developed model. The motion simulation in Fig 3.4 shows the simulation of a

hammering motion. Fig 3.5 shows the animated finger motions for a pen-holding task.

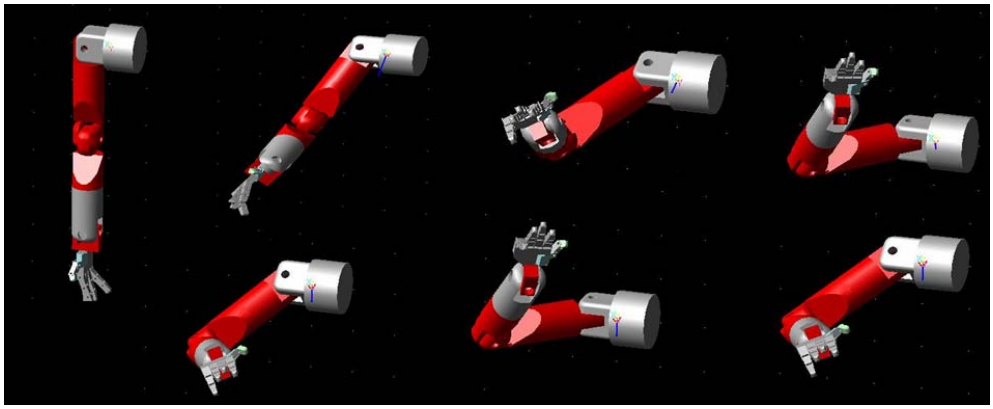

Figure 3.4 Motion simulation of a hammering arm

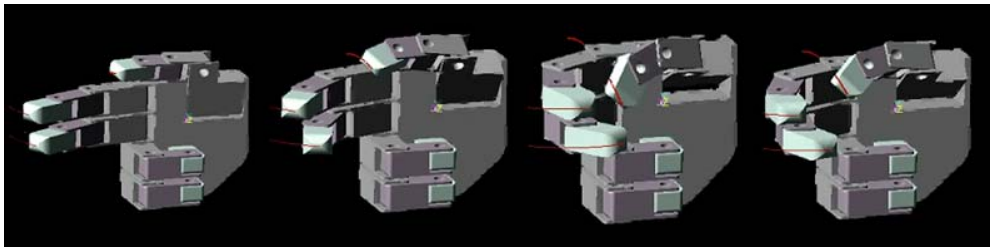

Figure 3.5 Motion simulation of a pen-holding hand

3.3 Collision Evaluation

An incoming disturbance on a robot arm can be considered as a wrench (Murray et al. 1993); the generalized force acting on a rigid body has six components, three of

which are the linear components of a pure force and three of which are the angular components of a moment acting on a point. For example, the impact on the palm on point A (Fig.3.6), can be written as

$$m_{Palm} = \begin{bmatrix} F_A \\ \mathrm{T}_A \end{bmatrix}, \tag{3.18}$$

where $F_A \in R^3$ is the linear component, and $\mathrm{T} \in R^3$ is the rotational component where R^3 is the real number domain. Poinsot's theorem states that every collection of wrenches applied to a rigid body is equivalent to a force applied along a fixed axis plus the torque value applied to the object. In the case of the anthropomorphic 7-DoF robot arm, the reaction joint torque is already measured for each given trajectory. The impact wrench on the arm or on the palm can be found since any of the two wrenches are considered to be equivalent if they generate the same work for every rigid body motion. Each link of the anthropomorphic 7-DoF arm is considered to be a rigid body, and unless there is an externally applied impact, the total work done by each joint is conserved for any movement; and, the wrench (the impact force) can be found.

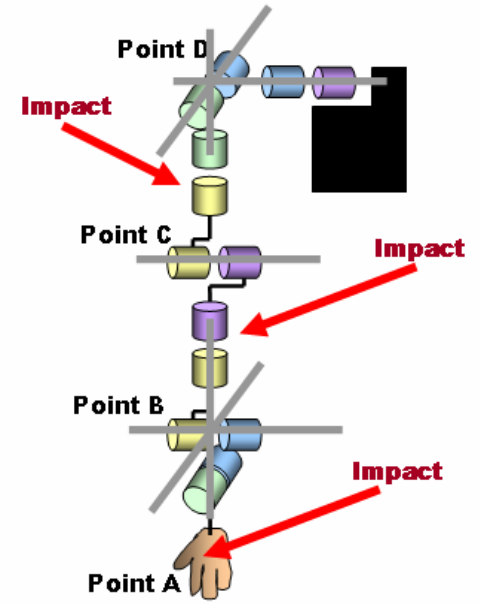

Figure 3.6 Impact location and joint orientation

In Fig 3.6, the arm is largely divided into three components for calculation: the palm as point A, the three joints in the wrist as point B, the elbow joint as point C and the three joints in the shoulder as point D. Then I consider the wrenches in these four locations: along the fixed axis of the rigid body, the linear component of the wrenches is equivalent to (3.19).

$$F_A = F_B = F_C = F_D \tag{3.19}$$

And the torque components of the wrenches are simply the additions of the torque values on the subsequent joints as shown in (3.20) through (3.22).

$$T_B = T_A + \overrightarrow{l_{AB}} \times F_A \tag{3.20}$$

$$T_C = T_B + \overrightarrow{l_{BC}} \times F_B \tag{3.21}$$

$$T_D = T_C + \overrightarrow{l_{CD}} \times F_D \tag{3.22}$$

As it was stated before, all the joint coordinates must be set up in the uniform coordinates. Figure 3.7 shows the orientation of the arm and the seven axes. The rotation matrices of each joint are given as the following.

$$R_6^5 = \begin{bmatrix} \cos\theta_0 & 0 & -\sin\theta_0 \\ 0 & 1 & 0 \\ \sin\theta_0 & 0 & \cos\theta_0 \end{bmatrix} \qquad R_5^4 = \begin{bmatrix} 1 & 0 & 0 \\ 0 & \cos\theta_1 & -\sin\theta_1 \\ 0 & \sin\theta_1 & \cos\theta_1 \end{bmatrix}$$

$$R_4^3 = \begin{bmatrix} \cos\theta_2 & -\sin\theta_2 & 0 \\ \sin\theta_2 & \cos\theta_2 & 0 \\ 0 & 0 & 1 \end{bmatrix} \qquad R_3^2 = \begin{bmatrix} 1 & 0 & 0 \\ 0 & \cos\theta_3 & -\sin\theta_3 \\ 0 & \sin\theta_3 & \cos\theta_3 \end{bmatrix}$$

$$R_2^1 = \begin{bmatrix} \cos\theta_4 & -\sin\theta_4 & 0 \\ \sin\theta_4 & \cos\theta_4 & 0 \\ 0 & 0 & 1 \end{bmatrix} \qquad R_1^0 = \begin{bmatrix} 1 & 0 & 0 \\ 0 & \cos\theta_5 & -\sin\theta_5 \\ 0 & \sin\theta_5 & \cos\theta_5 \end{bmatrix}$$

(3.23)

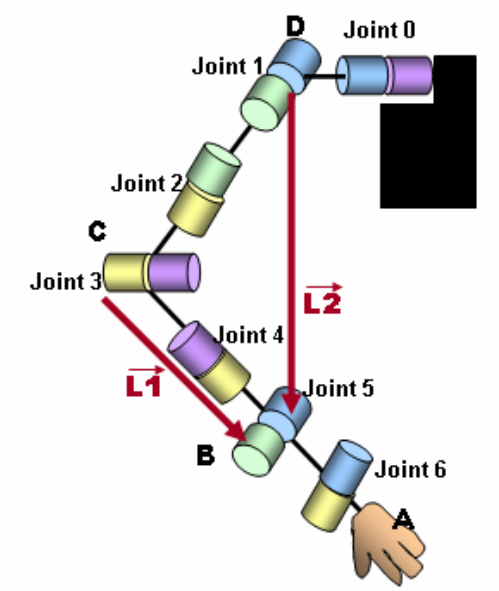

Figure 3.7 Joint sequence and lever arm directions

The torque loads on each joint are decomposed and converted into the respective values in the shoulder coordinates. Starting from the wrist (joint 6), the total rotations would be Ad_6^0 in the shoulder coordinate frame. It can be written as $P_6 = Ad_0^6 \cdot P_0$, where

$$Ad_0^6 = R_1^0 \cdot R_2^1 \cdot R_3^2 \cdot R_4^3 \cdot R_5^4 \cdot R_6^5 . \tag{3.24}$$

Similarly, the transformation matrix can be written for the consequent joints by eliminating its prior joint rotations and can be written as

$$Ad_0^i = R_1^0 \cdot R_2^1 \cdots R_{i+1}^i . \tag{3.25}$$

The space coordinates are set to be equivalent to the last shoulder joint, joint 0; for

brevity, I drop the subscript 0 and thus the equation $Ad_0^i = Ad_i$ holds. Following this,

$$\begin{bmatrix} Ad_4 \\ Ad_5 \\ Ad_6 \end{bmatrix} \cdot \mathrm{T}_B = \begin{bmatrix} \tau_4 \\ \tau_5 \\ \tau_6 \end{bmatrix}, \quad [Ad_3] \cdot \mathrm{T}_C = [\tau_3], \quad \text{and} \quad \begin{bmatrix} Ad_0 \\ Ad_1 \\ Ad_2 \end{bmatrix} \cdot \mathrm{T}_D = \begin{bmatrix} \tau_0 \\ \tau_1 \\ \tau_2 \end{bmatrix} . \qquad (3.26)$$

Here, τ_i is the measured torque value in each i^{th} joint. When the impact is only on the point B, the torque reading in joint 0 through joint 2 are considered. When there is an impact right on the wrist, I denote its wrench m_3, where it is $m_3 = \begin{bmatrix} F_3 \\ \mathrm{T}_3 \end{bmatrix}$.

For convenience, I divide the linear force component F_3 into two parts: I call the force along the shoulder axis link L_2 as F_{32} while I call the force component perpendicular to this as F_{31}. Therefore, from the definitions, the relation $F_{31} \perp L_2$ holds. The orthogonal nature of all these vectors leads to the relationship

$$\frac{F_3}{\|F_3\|} = \frac{\mathrm{T}_3}{\|\mathrm{T}_3\|} \times \frac{L_2}{\|L_2\|}, \qquad (3.27)$$

where L_2 is $\overrightarrow{l_{BD}}$ as seen in Fig 3.7. (3.27) can be expanded to

$$\therefore F_3 = \frac{\|\mathrm{T}_3\|}{\|L_2\|} \cdot \left(\frac{\mathrm{T}_3}{\|\mathrm{T}_3\|} \times \frac{L_2}{\|L_2\|} \right)$$

$$= \frac{1}{\|L_2\|^2} \cdot \mathrm{T}_3 \times L_2 . \qquad (3.28)$$

Solving for F_3, T_3 is obtained as:

$$\begin{aligned} \mathrm{T}_3 &= Ad_3 \cdot \{L_1 \times (F_{31} + F_{32})\} \\ &= Ad_3 \cdot (L_1 \times F_{31} + L_1 \times F_{32}) \\ &= Ad_3 \cdot (L_1 \times F_{31}) + Ad_3 \cdot (L_1 \times \frac{L_2}{\|L_2\|} \cdot f_{32}) \qquad (3.29) \\ \therefore Ad_3 \cdot (L_1 \times L_2 \cdot \frac{f_{32}}{\|L_2\|}) &= \mathrm{T}_3 - Ad_3 \cdot (L_1 \times F_{32}), \qquad (3.30) \end{aligned}$$

where L_1 is the direction vector from D to C point found to be, $\overrightarrow{l_{BD}} - \overrightarrow{l_{CD}} = \overrightarrow{l_{BC}}$, and f_{32} is the magnitude of F_{32}. Solving for f_{32} in (3.30), the value for f_{32} is obtained as the following:

$$\begin{aligned} f_{32} &= \{Ad_3 \cdot (L_1 \times \frac{L_2}{\|L_2\|}) = \mathrm{T}_3 - Ad_3 \cdot (L_1 \times F_{32}) \\ &= \frac{\mathrm{T}_3 - Ad_3 \cdot (L_1 \times F_{32})}{Ad_3 \cdot (L_1 \times \frac{L_2}{\|L_2\|})}, \qquad (3.31) \end{aligned}$$

where $F_3 = F_{31} + f_{32} \cdot \frac{L_2}{\|L_2\|}$.

Now consider the whole arm, where the same sequence of equations can be used. However the torque reading in the joints must compensate for the effect of other joints first. As stated earlier, the wrench on the palm is

$$m_{Palm} = \begin{bmatrix} F_A \\ \mathrm{T}_A \end{bmatrix}. \qquad (3.32)$$

And this wrench will transfer the linear component to point B where F_B can be written out as (3.33) by the definition of vector sums. The definition of the

subscript F_{B1} (perpendicular to the lever arm) and F_{B2} (parallel to the lever arm) are similar to the case described above.

$$F_B = F_{B1} + F_{B2} = F_{B1} + f_{B2} \cdot \frac{L_2}{\|L_2\|} \tag{3.33}$$

And from (3.26),

$$\mathrm{T}_B = \begin{bmatrix} Ad_6 \\ Ad_5 \\ Ad_4 \end{bmatrix}^{-1} \cdot \begin{bmatrix} \tau_6 \\ \tau_5 \\ \tau_4 \end{bmatrix}, \tag{3.34}$$

where $\begin{bmatrix} \tau_6 \\ \tau_5 \\ \tau_4 \end{bmatrix}$ are the measured torque readings.

At point C, the torque reading can be similarly written out as (3.26), producing (3.35):

$$\tau_3 = Ad_3 \cdot \mathrm{T}_C = Ad_3 \cdot \mathrm{T}_B + Ad_3 \cdot (L_1 \times F_B) \tag{3.35}$$

Take the similar form from (3.31), substitute in $L_2 \times F_B = \mathrm{T}_D - \mathrm{T}_B$ (3.22) for f_{B2} in (3.33). The torque on the elbow already considers the torque experienced in the wrist. Hence f_{B2} is

$$f_{B2} = \frac{(\tau_2 - Ad_2 \cdot \mathrm{T}_B) - Ad_2 \cdot (L_1 \times F_{B1})}{Ad_2 \cdot (L_1 \times \frac{L_2}{\|L_2\|})} \quad . \tag{3.36}$$

Substituting (3.36) into (3.33) produces (3.37):

$$F_B = \frac{1}{\|L_2\|^2} \cdot (T_D - T_B) \times L_2 + \frac{(\tau_2 - Ad_2 \cdot \mathrm{T}_B) - Ad_2 \cdot (L_1 \times F_{B1})}{Ad_2 \cdot (L_1 \times \frac{L_2}{\|L_2\|})} \cdot \frac{L_2}{\|L_2\|} \tag{3.37}$$

T_D is already known from Equation (3.22). T_A is found from (3.20), and F_A is known from the wrench applied at point A, $m_{Palm} = \begin{bmatrix} F_A \\ \mathrm{T}_A \end{bmatrix}$. The same types of equations can be solved out for the second case where the additional three joints in the wrist are considered.

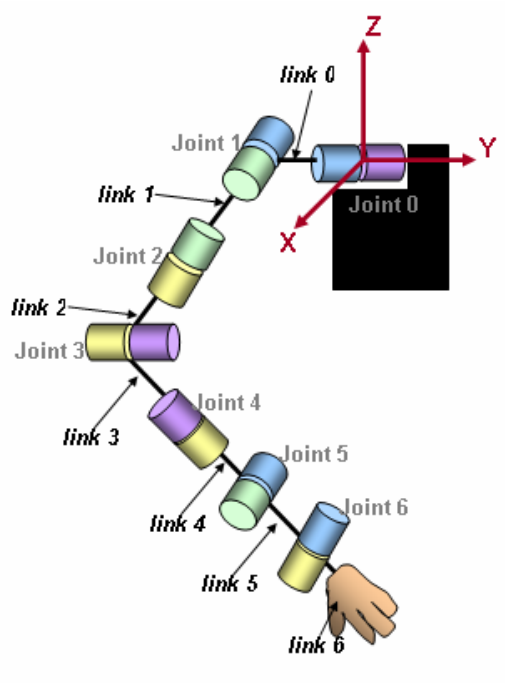

Figure 3.8 Joint and link orientation of the anthropomorphic arm.

In order to solve for the dynamic behavior of the robotic arm using the equations described in the previous pages, each link's inertial effect on the motor joints must be considered. Table 3.1 through 3.4 show the corresponding values of the moment of inertia in all the links that are converted into the base coordinate

frame. As it was mentioned earlier, the link moment of inertia values are retrieved from CAD software.

3.4 Joint stiffness control

The joint stiffness is actively controlled in real-time depending on the collision during the motion trajectory execution process by changing its control parameters, P and D. The average DC motor can be represented as a function of time (Guru 2001, Altintas 2000), written as:

$$V_a(t) = R_a I_a(t) + L_a \frac{dI(t)}{dt} + k_b \frac{d\theta_m(t)}{dt} \tag{3.38}$$

And its torque is given as

$$T_m(t) = J_e \ddot{\theta}(t) + B\dot{\theta}(t) + T_{Load}\,. \tag{3.39}$$

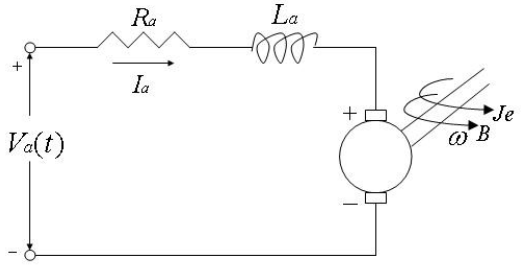

Figure 3.9 The DC motor representation with electric symbols

Using the Lapalce transformation, (3.38) and (3.39) leads to

$$V_a(s) = R_a I_a + L_a s I(s) + k_b \theta_m(s) \tag{3.40}$$

$$T_m(s) = J_e s^2 \theta(s) + Bs\theta(s) + T_{Load}(s) \qquad (3.41),$$

where $T_m(s) = K_m I_a(s)$ is given out as the motor current constant by the motor manufacturers as shown in Table 3.5

Table 3.5 DC motor characteristics

		2232 024SR	2642G 048	3242G 048	3257G 048
Terminal resistance (ohm)	R	16.40	23.80	19.70	6.56
Tq constant (Nm/A)	Km	0.0321	0.0698	0.0820	0.0762
EMF const (Vsec/rad)	Kb	0.0321	0.0698	0.0820	0.0762
Rotor inductance (H)	L	7.10.E-04	2.20.E-03	2.20.E-03	1.10.E-03
Rotor inertia (kgm^2)	J	3.80.E-07	1.10.E-06	2.60.E-06	4.20.E-06
No load speed (rad /sec)	Tm	743.13	669.87	565.20	617.53
Mechanical const (ms)	τm	0.006	0.0054	0.0075	0.0047

Considering the gear ratio *n*, (3.39) becomes

$$T_m(t) - T_{Load}(t) \cdot \frac{1}{n} = J_e \ddot{\theta} + B_m \dot{\theta}, \qquad (3.42)$$

where the effective inertia J_e is found as the sum all the inertia (from the armature and the load) reflected on to the motor, $J_e = J_a + \frac{J_{Load}}{n^2}$. Looking at the whole system of the motor in Fig 3.9, when $T_s = 0$

$$(Jes^2 + B_m s)\theta_m(s) = K_m\left(\frac{V(s) - sK_b \cdot \theta_m(s)}{Ls + R}\right) - \frac{1}{n}T_s(s) \qquad (3.43)$$

$$\frac{\theta_m(s)}{V(s)} = \frac{K_m}{s\left[(J_e s + B_m)(Ls + R) + K_m \cdot K_b\right]} = \frac{\frac{K_m}{B_m R}}{s\left[\left(\frac{J_e}{K_m} + 1\right)\left(\frac{L}{R}s + 1\right) + \frac{K_m K_b}{B_m R}\right]} \tag{3.44}$$

When $V = 0$,

$$\frac{\theta_m(s)}{T_s(s)} = \frac{-(Ls + R)}{s\left[(Ls + R)(J_e s + B_m) + K_m \cdot K_b\right]} \tag{3.45}$$

Since the electrical and mechanical time constant parameters are given as follows:

$$\tau_e = \frac{L_a}{R_a} \qquad \tau_m = \frac{J_e}{B},$$

(3.44) simplifies to (3.46):

$$\frac{\theta_m(s)}{V(s)} = \frac{\frac{K_m}{B_m R}}{s\left[(\tau_m s + 1)(\tau_e s + 1) + \frac{K_m K_b}{B_m R}\right]} = G(s) \tag{3.46}$$

Then, the transfer function is given as follows:

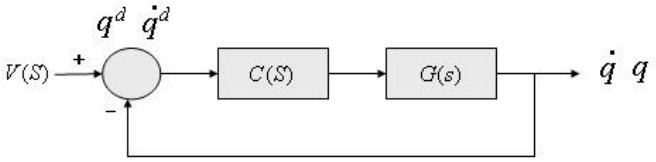

Figure 3.10 Control block diagram of the PD controlled motor driver

Looking at the transfer function,

$$G(s) = \frac{K}{Ms^2 + Bs}$$

$$G(s) = \frac{\frac{K_m}{R}}{s\left[\left(J_e s + B_m + \frac{K_m \cdot K_b}{R}\right)\right]} \tag{3.47}$$

The constants are

$$K = \frac{K_m}{R}$$

$$B_{eff} = B_m + \frac{K_m K_b}{R}$$

$$M = J_e$$

When the error signals, $q^d - q$, and the change in error $\dot{q}^d - \dot{q}$ in Fig 3.10 are represented as $e(t)$ and $\dot{e}(t)$, the following transfer function can be found (Jung 2006):

$$u(t) = K_P e(t) + K_D \dot{e}(t)$$

$$U(s) = K_P E(s) + K_D s E(s) \tag{3.48}$$

$$C(s)_{PD} = \frac{U(s)}{E(s)} = K_P + sK_D \tag{3.49}$$

Therefore, Fig 3.10 can be redrawn as Fig 3.11:

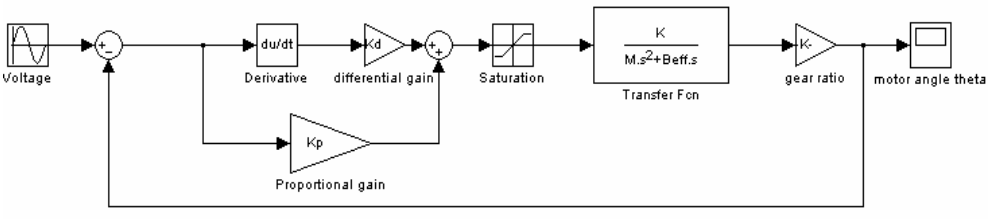

Figure 3.11 Closed-loop system with PD controller

For programming PIC in a discrete system, s domain factors can be presented in discrete time domain with t step size. In fact, the error measurements are directly used as the input to find the control constants, K_P and K_D. When the control period is set as 1kHz, and encoder reading is 2048 counts/rev, for 2233 Faulhaber motor.

3.5 Hand kinematics

For the current research, it is assumed that the tendon cable to have neither mass nor dynamics. The RC servo motors are used as the actuators in the current humanoid robotic hand, and the reaction rate of the DC motors used in other arm joints are much faster than the actuators used for the hand; therefore, it is safe to make such an assumption. Caratheodory's theorem asserts that for a robot with n links, a minimum of n+1 tendons are required to actuate it, while Steinitz's theorem proves that any more than 2n tendons are redundant (Murray et al. 1994). These theorems are also regarded as the configuration for distinguishing the tendon types which are "N+1" types and "2N" types.

For the developed anthropomorphic hand, the N+1 type configuration is adapted. Given the finger architecture in Fig 3.12, the relationship between the joint angle and the extension are given by

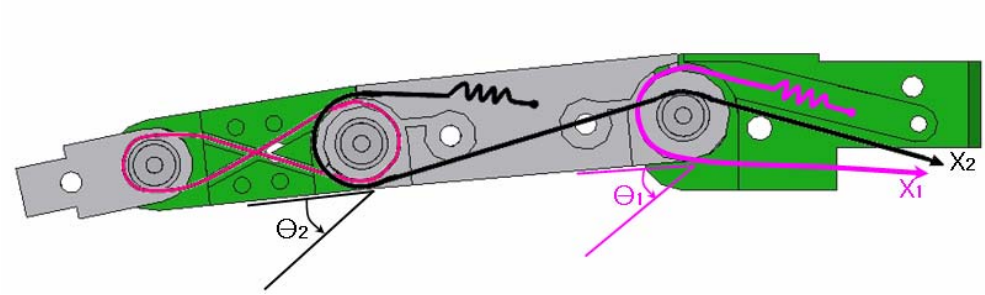

Figure 3.12 2-DoF Finger mechanism

$$\theta_1 = \frac{X_1}{R_{MCP} + R_{Cable}} \tag{3.50}$$

$$\theta_2 = \frac{X_2}{R_{PIP} + R_{Cable}} + \frac{R_{pulley}}{R_{PIP}} \cdot \theta_1 \tag{3.51}$$

Solving for cable extension produces (3.52) and (3.53), X_1 and X_2 are obtained:

$$X_1 = \theta_1 \cdot (R_{MCP} + R_{Cable}) \tag{3.52}$$

$$X_2 = \left(-\frac{R_{pulley}}{R_{PIP}} \cdot \theta_1 + \theta_2 \right)(R_{PIP} + R_{Cable}) \tag{3.53}$$

When R_1, R_2, R_3, R_4 are $R_{cable} R_{pulley}, R_{PIP}, R_{MCP}$ respectively, the coupling matrix, denoted as $P(\theta)$ is

$$P(\theta) = \frac{\partial X^T}{\partial \theta} = \begin{bmatrix} R_1 + R_4 & -\frac{R_2}{R_3} \cdot (R_3 + R_1) \\ 0 & R_1 + R_3 \end{bmatrix}. \tag{3.54}$$

Since all of the extension functions are linear, the coupling matrix is a constant. To compute the relationship between the actuator position and the joint torques, I use

the stiffness matrix, K.

$$K = \begin{bmatrix} k_1 & 0 \\ 0 & k_2 \end{bmatrix}, \text{ where } k_i > 0 \text{ is the stiffness of the } i^{th} \text{ tendon.}$$

Letting e_i be the extension of the tendon as commanded by the actuator and $h_i(\theta)$ be the extension of the tendon due to the mechanism, I assume that when $\theta = 0$, and $e_i = 0$, the tendon is under no tension. Then, the net force applied to the tendons is given by

$$f_i = k_i(e_i + h_i(0)) - h_i(\theta)). \tag{3.55}$$

When K is the stiffness matrix, the elastic behavior of tendons with extension e, the equation $f = K(e + h(0)) - h(\theta))$ holds. For position controlled actuators,

$$P(\theta)Ke = \tau \text{ and } e_i + h_i(0) - h_i(\theta) > 0, i = 1,..., p. \tag{3.56}$$

The overall stiffness is given by S. If the input positions are constant, this gives the restoring force generated as:

$$S(\theta) = PK(X(\theta) - X(0))$$

$$= \begin{bmatrix} k_1\left[(R_1 + R_4)^2 - \frac{R_1R_2R_4}{R_4} - R_2R_4 - \frac{R_1^2R_2}{R_3} - R_1R_2\right] & -k_1\left(R_1R_2 + R_2R_3 + \frac{R_1^2R_2}{R_3} + R_1R_2\right) \\ 0 & k_2(R_1 + R_3)^2 \end{bmatrix}\theta \tag{3.57}$$

The coupling matrix between the actuator extension and the joint torques is given as Q in (3.58):

$$Q = PK = \begin{bmatrix} k_1R_1 + k_1R_4 & -k_1R_2 - k_1\dfrac{R_1R_2}{R_3} \\ 0 & k_2R_1 + k_2R_3 \end{bmatrix}. \qquad (3.58)$$

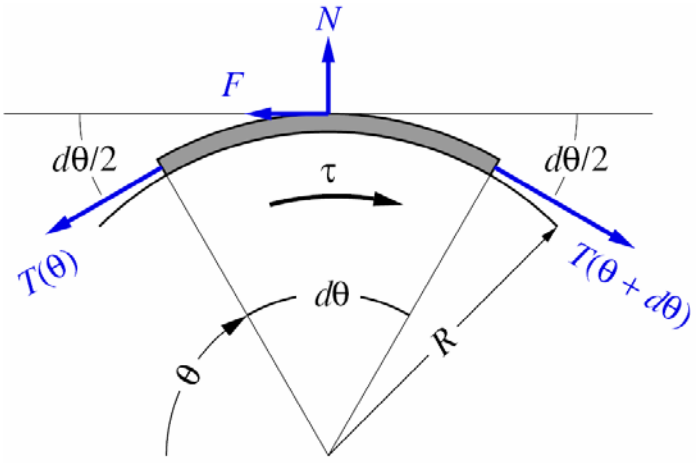

Figure 3.13 The free-body diagram of torque and cable wrap around a pulley

Now consider the torque exerted by the pulling of the cable. When R is the radius of the joint pulley, and the angle $d\theta$ is the wrapped radius around the arc, the force and torque relationship on the finger joint is as shown in Fig 3.13. Here, F , N and T are the forces acting on the cable, the normal force, and the tension from the rest of the cable respectively.

$$N = T(\theta)\sin(d\theta/2) + T(\theta + d\theta)\sin(d\theta/2) \qquad (3.59)$$

$$F + T(\theta)\cos(d\theta/2) = T(\theta + d\theta)\cos(d\theta/2) \qquad (3.60)$$

Assuming $d\theta$ is very small,

$$\sin\left(\frac{d\theta}{2}\right) \cong \frac{d\theta}{2} \quad \text{and} \quad \cos\left(\frac{d\theta}{2}\right) \cong 1$$

$$T(\theta + d\theta) \cong T(\theta) + \frac{dT}{d\theta} d\theta \tag{3.61}$$

Accounting those, (3.59) and (3.60) can equate to

$$N \cong T(\theta) d\theta \tag{3.62}$$

$$F \cong \frac{dT}{d\theta} d\theta \tag{3.63}$$

From Coulomb's Law, $F = \mu N$, therefore, (3.63) becomes

$$\mu T(\theta) d\theta = \frac{dT}{d\theta} d\theta \text{, or} \tag{3.64}$$

$$\mu d\theta = \frac{dT}{T}$$

Taking the integral of (3.64) from the known position $\theta = 0$, the relationship between the pulley and the tension cable is given by (3.65):

$$\int_0^\theta d(\ln T) = \mu \int_0^\theta d\theta$$

$$T(\theta) = T_0 e^{\mu\theta} \tag{3.65}$$

This cannot fully represent the mechanics of the tendon as there are frictions applied by the cable housing. Depending on the radius of the arc in the housing, the total friction force acting on the cable is determined. Fig 3.14 displays the free body diagram of the finger actuating system. θ_a, θ_b and θ_c represent the wrapped contact angle between the tendon and the shield at the contact locations. Since the coefficient of friction here is constant, (3.65) can be written out as (3.66), where θ_2 is the sum of θ_a, θ_b and θ_c, and μ_2 is the coefficient of friction

between polyurethane (shielding) and nylon (fishing string tendon).

$$T_f(\theta) = T_0 e^{\mu_2 \theta_2} \tag{3.66}$$

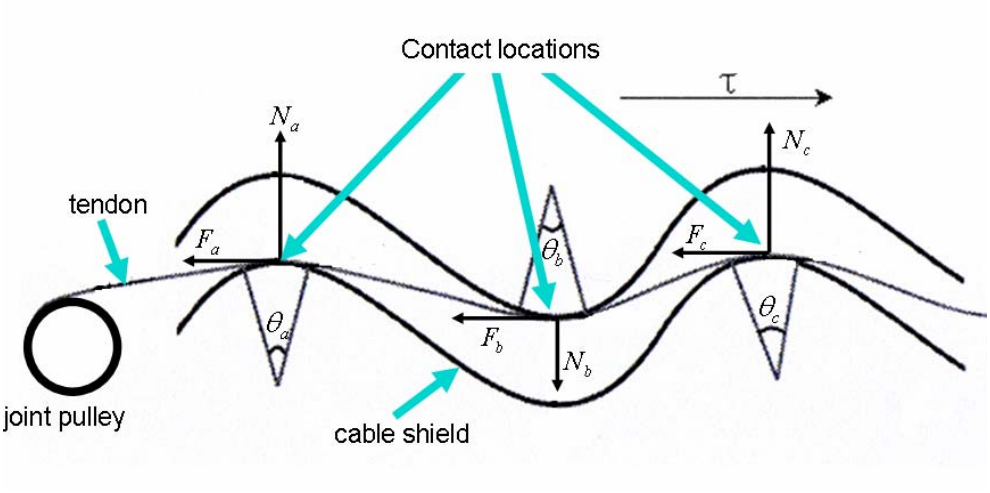

Figure 3.14 Tendon within the windy shielding

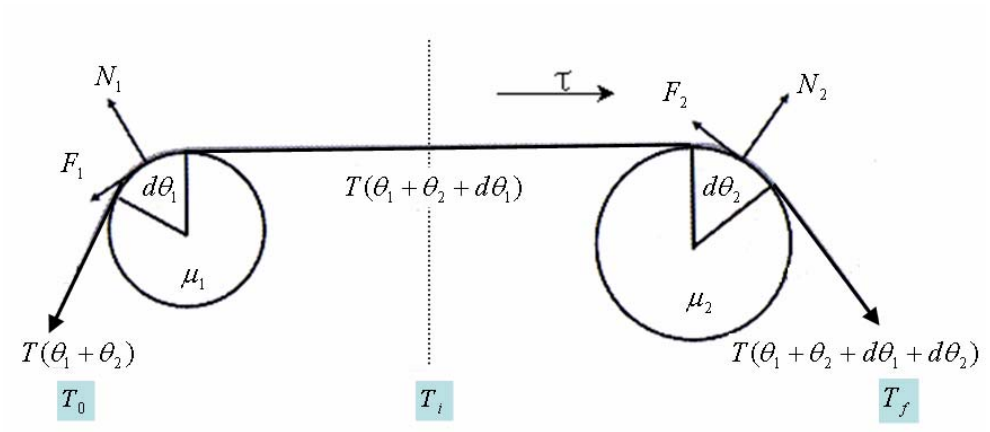

Figure 3.15 The free-body diagram of the finger actuation

Now, when considering the friction in the pulley and the tendon (Fig 3.15), μ_1 is the coefficient of friction between aluminum / nylon, and θ_1 is the wrapped contact angle in the finger joint (200 deg).

$$T_f(\theta) = T_0 e^{\mu_1 \theta_1} \tag{3.67}$$

Therefore, if the initial pulling tension is T_0, the intermediate tension is $T_i = T_0 \cdot e^{\mu_1 \theta_1}$ (through the finger pulley only) and likewise, final pulling tension in the cable is

$$T_f = T_0 \cdot e^{\mu_1 \theta_1 + \mu_2 \theta_2} \tag{3.68}$$

Chapter 4:
Trajectory planning for safety

This chapter presents the method of creating motion trajectory of the developed anthropomorphic robotic arm. This method can apply to most robotic manipulators (even with redundant DoF) without using the conventional sensors; instead, it monitors the motor current level to analyze the torque on the actuator. The results of the algorithm show successful detection of the collision while the new trajectory reduces the damage on both the robot and the human operator.

4.1 Torque-sensor-less torque sensing

The developed anthropomorphic arm and hand is designed for interactive humanoid robot application. A robot gains information on its physical status and surroundings through sensor readings and for multi linked manipulators, various torque and gyro sensors, vision sensors are popular choice for this. Humanoid robot arms are often equipped with torque sensors in each joints and multi-axis F-T sensor at the end-effector (HUBO, ASIMO, HRP-2, DLR's Light Weight Arm, RRC-K1207i). However, the anthropomorphic arm does not use any sensors such as multi-axis F-T sensors, torque sensors or contact sensors to measure torque or

estimate incoming disturbance's load and direction. It uses a unique method of acquiring torque on the joints by observing the motor current which is proportional to the produced motor torque. Since, the motor speed is decreased using a gear train, the reading should compensate for the gear ratio and the back-drivability efficiency. Then the found torque is the resulting torque with all the effect of dynamics of the arm movement, gravity, and collision force, if applied. Fig 4.1 illustrates these steps to convert the current reading to the torque on the joints.

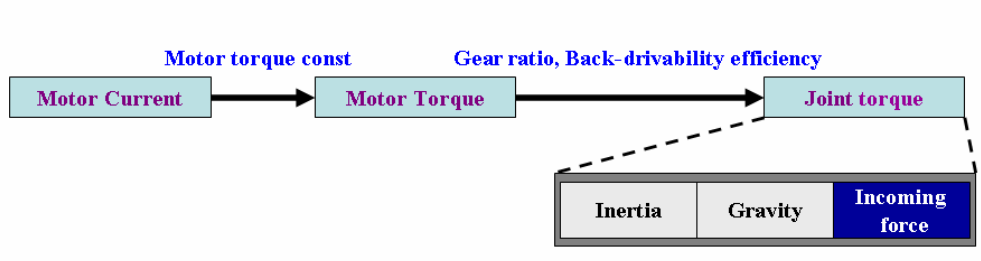

Figure 4.1 External impact estimation by sensing the motor current

4.2 Motion teaching: knot point acquisition

For motion teaching, the anthropomorphic robotic arm and hand uses the same algorithm that we first applied to the Kendo robot, MUSA (Bang et al. 2005). For MUSA, instead of using the typical motion teaching methods such as teaching pendant method, vision or an exoskeleton motion capturing system, we have used the motor current measuring method to acquire motion knot points. Unlike other motion teaching methods, it requires no other infra-structure or equipment and it is

quite intuitive for the operator: the robot arm can be set up at a desired position as if setting up a mannequin arm (see Fig 4.2) and the set position can be saved as a knot point. This algorithm also measures joint torque by observing the motor current change, but the robot's dynamics does not need to be concerned in this case (only the weight of the arm is of the concern). Each torque reading (converted from the motor current measurement) is compared with the undisturbed joint torque value for each position. If disturbance is detected, the joint rotates toward the direction of disturbance.

Figure 4.2 Setting up robot arm as if setting up a mannequin on MUSA

4.3 Motion teaching: polynomial curve fitting

There are largely two methods in fitting curves into discrete points. Firstly the curve is made to pass through all the points by interpolation. And the other is to find the general trend by regression. When the interpolation method is used, the created path needs to pass all points and this will make cusps which will in turn

distort the trajectory. When regression method is used, the starting and the finishing points of motion are unlikely to match the initial input points. Therefore, in this research, high-order polynomial regression is used with restrictions of starting and finishing points and velocities.

The polynomial function up to 9th power produces the trajectory. (4.1) shows the generic 9th order polynomial with boundary conditions.

$$y = a_0 + a_1 t + a_2 t^2 + \cdots + a_9 t^9 \tag{4.1}$$

Initial time: $t_1 = 0$

position: y_1

velocity: y_1'

Final time: t_n

position: y_n

velocity: y_n' (n: number of discrete points)

Using the boundary condition, a_0, a_1 are found in (4.2) and (4.3).

$$f(t_1) = f(0) = a_0 = y_1 \tag{4.2}$$

$$f(t_1) = f'(0) = a_1 = y_1' \tag{4.3}$$

Also, relative (4.4) and (4.5) for a_8, a_9 are yielded.

$$a_8 = \frac{1}{t_n^8}\left(9y_n - t_n y_n' - 9a_0 - \cdots - 2a_7 t_n^7\right) \tag{4.4}$$

$$a_9 = -\frac{1}{t_n^9}\left(8y_n - t_n y_n' - 8a_0 - \cdots - a_7 t_n^7\right) \tag{4.5}$$

When these are substituted in (4.1), and reorganized, the error of the i[th] point is (4.6).

$$e_i = y_i - \left(a_0 + a_1 t + \cdots + a_9 t_i^9\right) \tag{4.6}$$

Then, the sum of squares error is a shown in (4.7).

$$\begin{aligned} S &= \sum_{i=1}^{n} e_i^2 = \sum_{i=1}^{n}\left(y_i - a_0 - a_1 t - \cdots - a_9 t_i^9\right)^2 \\ &= \sum_{i=1}^{n}\left\{y_i - k_{0i}a_0 \cdots - k_{7i}a_7 - \left(1 - k_{oi}\right)y_n + \left(\frac{t_i^8}{t_n^7} - \frac{t_i^9}{t_n^9}\right)y_n'\right\}^2 \end{aligned} \tag{4.7}$$

Here,

$$k_{mi} = \left\{t_i^m - (9-m)\frac{t_i^8}{t_n^{(8-m)}} + (8-m)\frac{t_i^9}{t_n^{(9-m)}}\right\} \tag{4.8}$$

, where

$$m = 0,1,2,\cdots,9 .$$

For the least-squares fit of the polynomial, we minimize *S* with respect of the unknown coefficients $a_2, a_3, \cdots, a_7$. For this, we set the partial derivatives of *S* with respect to the coefficients equal to zero:

$$\frac{\partial S}{\partial a_2} = -2\sum_{i=1}^{n} k_{2i}\{y_i - k_{0i}a_0 - k_{1i}a_1 - \cdots - k_{7i}a_7 - (1-k_{oi})y_n + \left(\frac{t_i^8}{t_n^7} - \frac{t_i^9}{t_n^9}\right)y_n'\} = 0$$

$$\vdots$$

$$\vdots$$

$$\frac{\partial S}{\partial a_7} = -2\sum_{i=1}^{n} k_{7i}\{y_i - k_{0i}a_0 - k_{1i}a_1 - \cdots - k_{7i}a_7 - (1-k_{oi})y_n + \left(\frac{t_i^8}{t_n^7} - \frac{t_i^9}{t_n^9}\right)y_n'\} = 0 \qquad (4.8)$$

(4.8) can be rewritten as a system of linear equations in the unknowns $a_2, a_3, \cdots, a_7$ as

$$\begin{bmatrix} \sum k_{2i}k_{2i} & \cdots & \sum k_{2i}k_{7i} \\ \vdots & \ddots & \vdots \\ \sum k_{7i}k_{2i} & \cdots & \sum k_{7i}k_{7i} \end{bmatrix} \begin{bmatrix} a_2 \\ \vdots \\ \vdots \\ a_7 \end{bmatrix}$$

$$= \begin{bmatrix} \sum k_{2i}\left\{y_i - k_{0i}a_0 - (1-k_{oi})y_n + \left(\frac{t_i^8}{t_n^7} - \frac{t_i^9}{t_n^9}\right)y_n'\right\} \\ \vdots \\ \sum k_{7i}\left\{y_i - k_{0i}a_0 - (1-k_{oi})y_n + \left(\frac{t_i^8}{t_n^7} - \frac{t_i^9}{t_n^9}\right)y_n'\right\} \end{bmatrix} \qquad (4.9)$$

With (4.8), all the coefficients of (4.1) are determined.

(4.1) through (4.8), a common way of the polynomial curve fitting is

shown; Fig 4.3 shows the ball throwing motion of the arm using the trajectory from polynomial curve fitting.

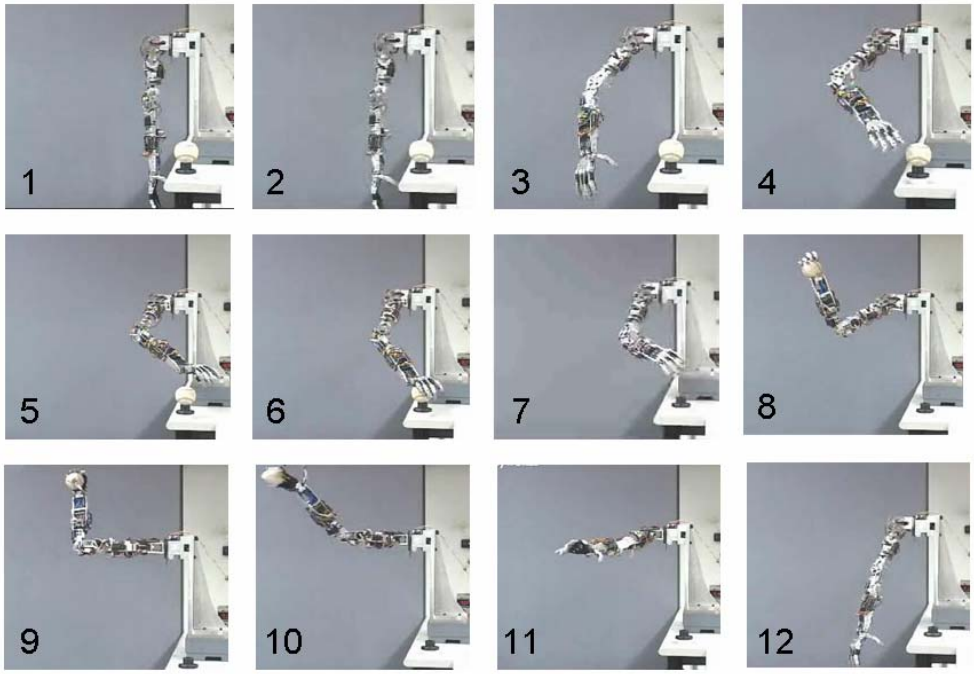

Figure 4.3 Baseball grabbing and throwing

4.4 Motion teaching: weighted knot points

The importance of task execution usually concerns the path planning of the end-effector. However, with redundant robotic manipulators, the form trajectory itself can often be the required task. For example, holding a cup of liquid and transporting it to the other side of table would be the case. For a successful

execution of this task, two tasks must be completed: the content of the cup cannot be spilt while transferring the cup from point A to point B. When creating the motion trajectory for the anthropomorphic arm, the knot points are chosen and used to create the motion trajectory by fitting the knot points in polynomial equations. For such a task, minimum knot points would be 2 and the initial point as shown in Table 4.1.

Table 4.1 Knot points for a cup serving motion

[deg]	**Joint numbers** (shoulder=0 ~palm=6)						
	6	5	4	3	2	1	0
Initial position	0	0	0	0	0	0	0
Point A	0	30	35	-50	-55	-25	-30
Point B	0	5	10	-50	-130	-35	-20

Having more knot points often guarantees more accurate motion trajectories. However, it is a cumbersome process to find all the knot points and unless higher ordered polynomial equations are used, a complete deviation from the original knot points is easy. Especially for the case of humanoid robots with multiple redundant joints, little change in the angles make awkward move even if the condition of knot points are met. Therefore, for generating motion trajectory in simpler way without loosing the essence of the motion to complete the task, an

algorithm to consider weighting the importance of the knot points is considered. By weighting the importance of each knot points, while still using the same linear regression method, this algorithm can reduce unexpected overshoot in the curve without acquiring new knot points. Fig 4.4 shows two sets of polynomial trajectory created based on the 3 knot points. The solid lines show the weighted version of the trajectory.

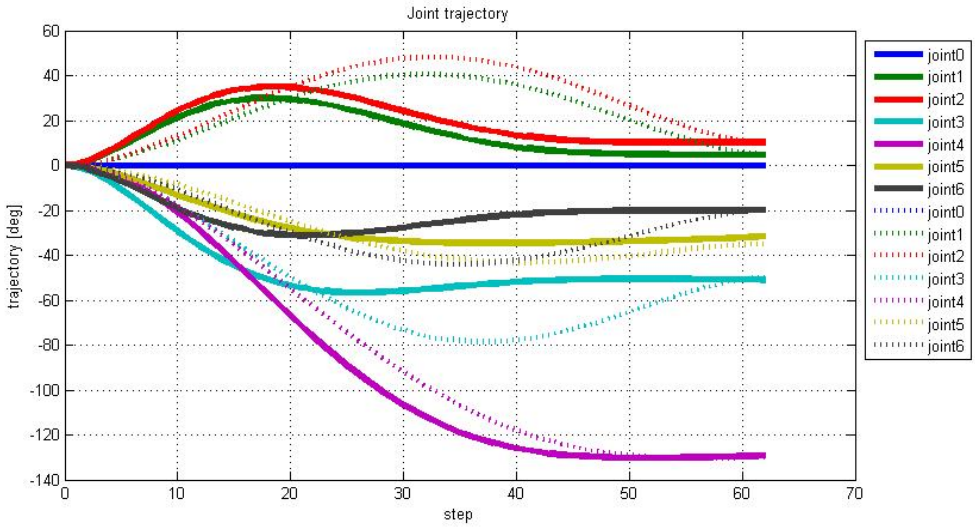

Figure 4.4 Joint motion trajectories for serving a cup

The dotted line shows the default trajectory created without weighting (or equal weights). Both start from initial point with zero velocity and the knot points are the same at time step 20 (point A) and 63 (point B). Both line sets use polynomial functions and if there are more knot points the trajectory profile can vary. For the point B, it is weighted to be 4 times more important than the point A.

Therefore, around point B, the trajectory curve flattens faster. By employing this algorithm, deviating motion trajectory resulted from lack of knot points can be reduced while the curve form can be customized.

4.5 Impact force estimation

Since, the motion dynamics can be completely solved out following Chapter 3, the expected torque on each joint should be found. For a given trajectory, this toque value can then be constantly compared to the new measurements. Depending on the threshold, if the reading of the moving arm does not match the expected torque values, it can be considered as the effect of collision. The flowchart of determining the incoming torque is shown in Fig 4.5.

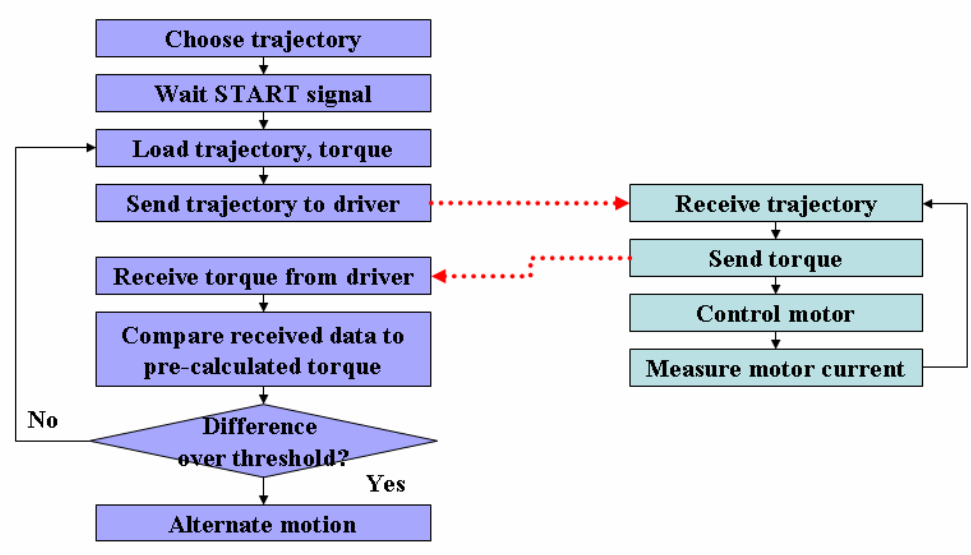

Figure 4.5 Anthropomorphic arm motion teaching algorithm

To determine the direction of the unknown incoming impact on the arm, seven joint torque values at the point of impact are collected and their value difference over the threshold is compared. The following 3 figures display the process of detecting impact force from the joint torque reading form a task execution determined using the algorithm. Fig. 4.6 compares the given motion trajectory's expected torque with the actual reading of the motor torque during a task execution. Fig. 4.7 displays the reading of the motor torque when the arm jams into an obstacle. The deviation of the curve is shown toward the end of the task. The impact force reading is filtered through a threshold torque and the impact force is determined (Fig. 4.8).

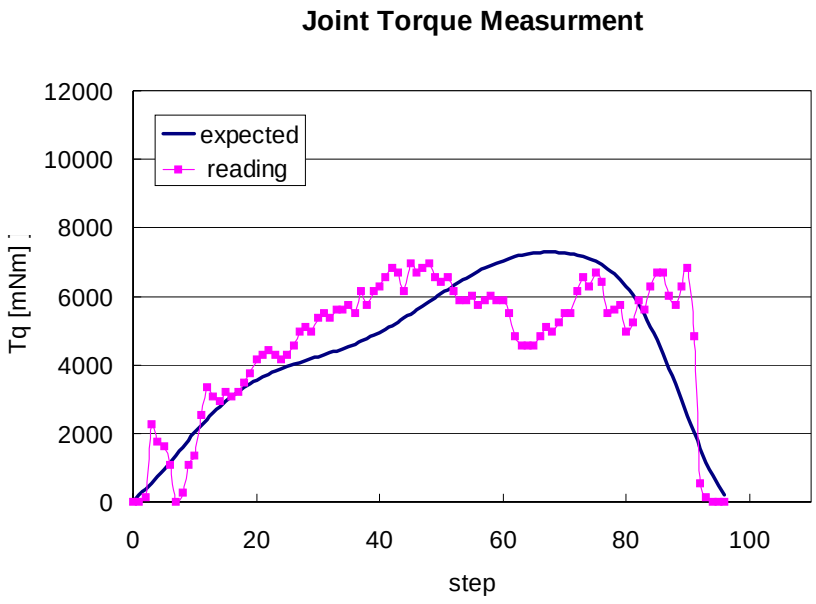

Figure 4.6 Joint torque measurement during a task

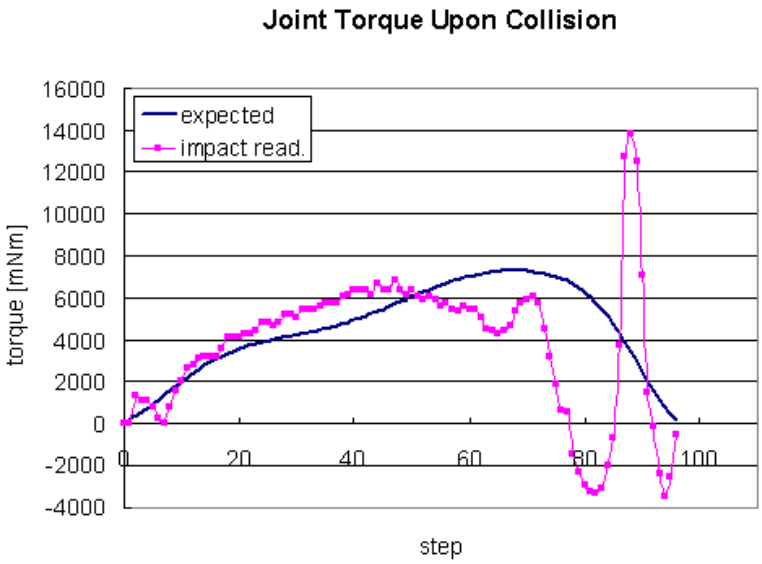

Figure 4.7 Joint torque measurement with an impact

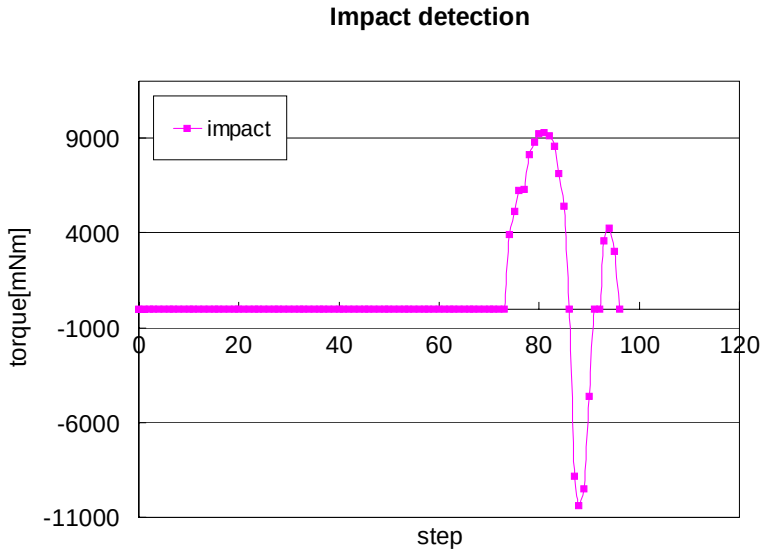

Figure 4.8 Impact force on one joint

Likewise, the impact forces on each of seven joint is collected for estimating the load, and the direction. Figure 4.9 shows the graph of the disturbance force applied to the palm of the anthropomorphic robot. This graph shows varying magnitude of forces pushed in two directions; the stars are the forces applied on the palm toward the body and the circles are the forces pulling away from the body.

Once estimating the direction and the load of the incoming force, a new trajectory is chosen accord to the "intent criteria" that has been developed for the anthropomorphic robotic arm.

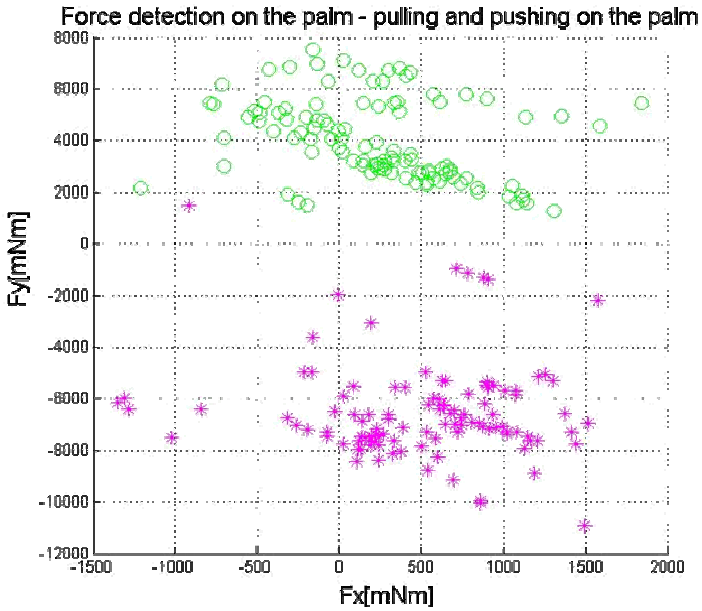

Figure 4.9 Multiple impact forces with varying load and direction the palm

4.6 Trajectory generation for safety

For generating a new trajectory to minimize further physical damage, analyzing the estimated impact force for its actual danger level is necessary. The quantification of the safety of humanoid robots had been first proposed by Ikuta et al.(2003)'s group calculated the danger level using the danger index, α, which is the ratio of the impact force, to the critical impact force. They examined robot's weight, cover material, joint flexibility, shape and the surface friction to determine the complete danger index of a robotic arm (see the Danger Index in Fig.4.10).

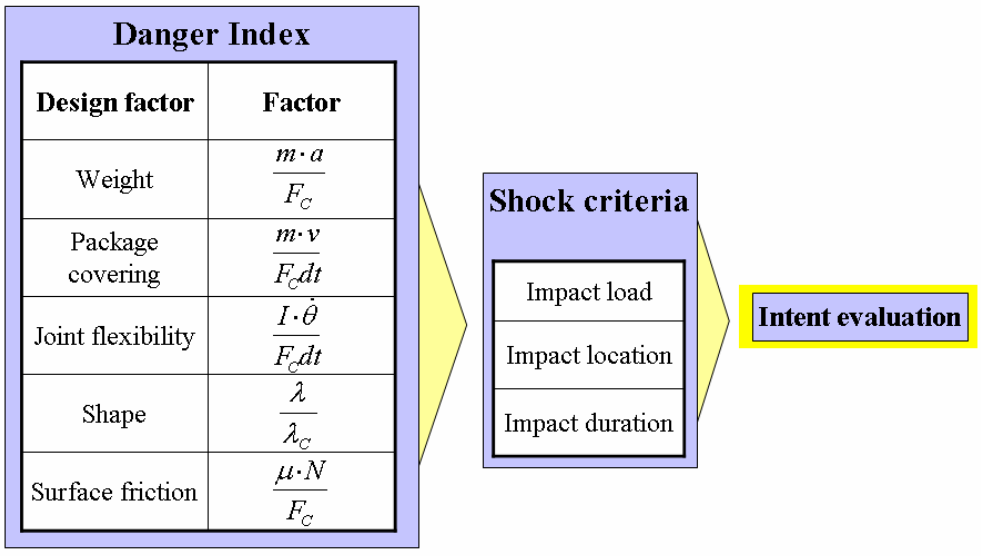

Figure 4.10 Intent evaluations suited to the anthropomorphic robotic arm

Given the danger index, safety level of the mechanism can be quantified for a collision within a given trajectory. Upon collision, the algorithm narrows

down the collected data considered for the Danger Index to three factors suited for the anthropomorphic robotic arm: the impact load, the impact location and the impact duration. These shock criteria are evaluated to determine the work environment and the intent of the user.

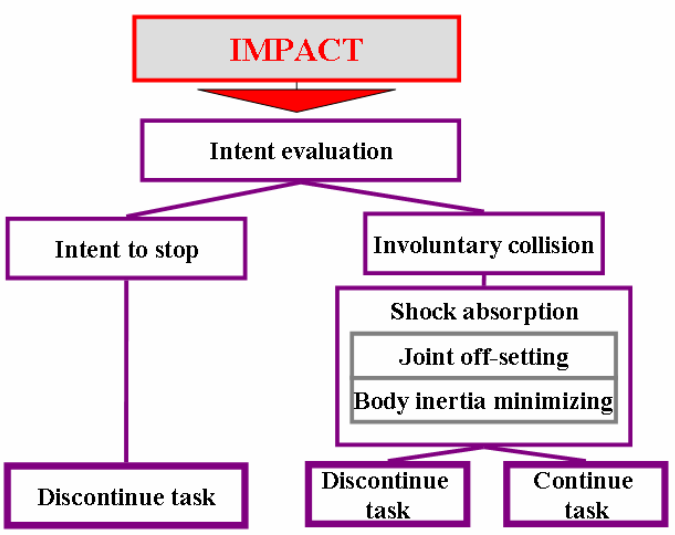

Figure 4.11 intent evaluation processes upon impact on the arm

The anthropomorphic arm is developed for real-life sized humanoid robots bearing much similitude to real humans. By analyzing the intent evaluation criteria, the robot arm can proceed to the next motion trajectory based on the intent of its user. Depending on the intent, the robotic arm may not complete the task or proceeds to finishing the task after taking appropriate measure of absorbing the shock. Instinctively, there is one way of reacting to the incoming collision shock:

by moving in the direction of the applied force proportional to the magnitude of the load. And another is by proceeding to the direction of minimizing the body energy level: meaning moving in to the direction where the robot needs minimum voluntary movement. Currently, upon impact, the robotic arm moves in the direction of the impact load while minimizing the body potential energy in all the links. Fig 4.13 and Fig 4.14 shows the movement of the arm upon impact when Fig 4.12 is the controlled movement. For both movements, the impact came in at frame 3 of Fig 4.12.

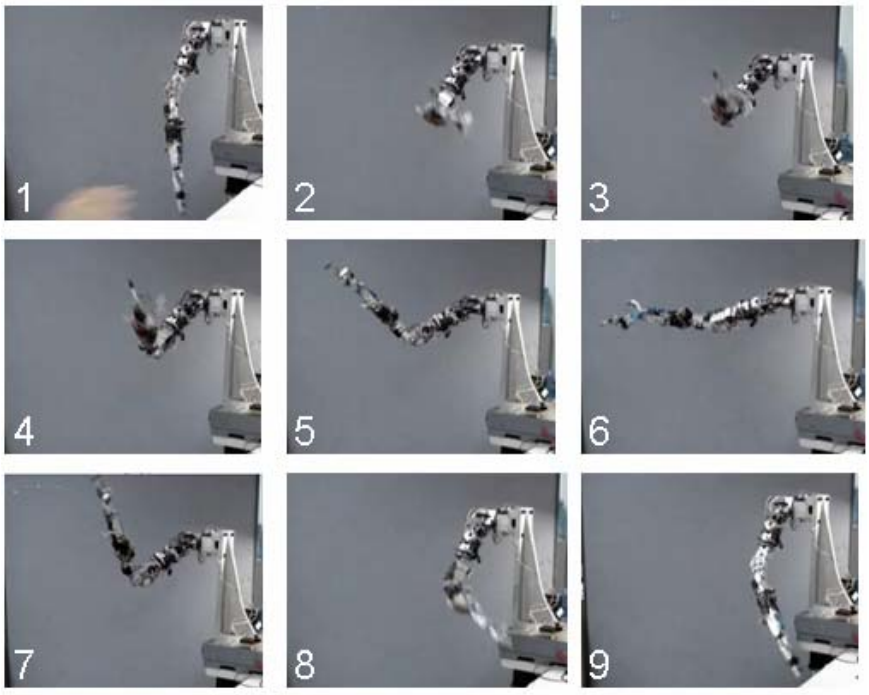

Figure 4.12 Controlled trajectory

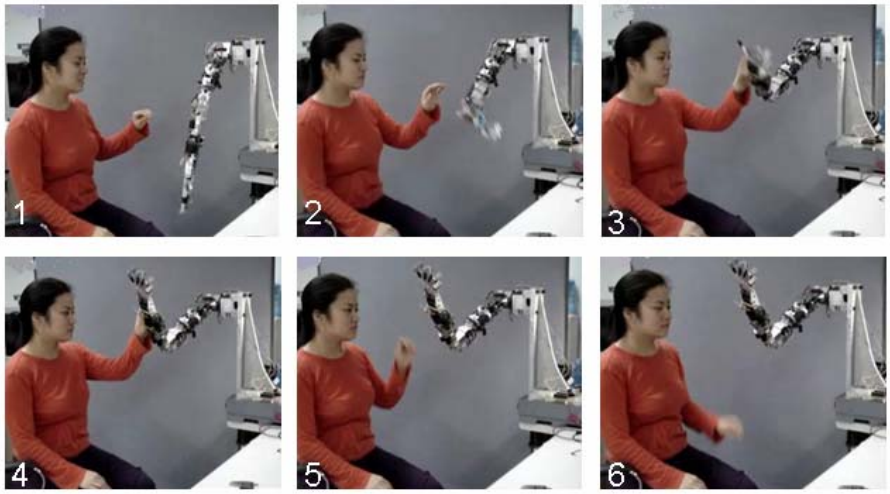

Figure 4.13 Collision with an intention to stop

At time frame 3 of the controlled trajectory (Fig 4.12), a collision occurs. The impact is analyzed with the intent evaluation, and the motion comes to a halt.

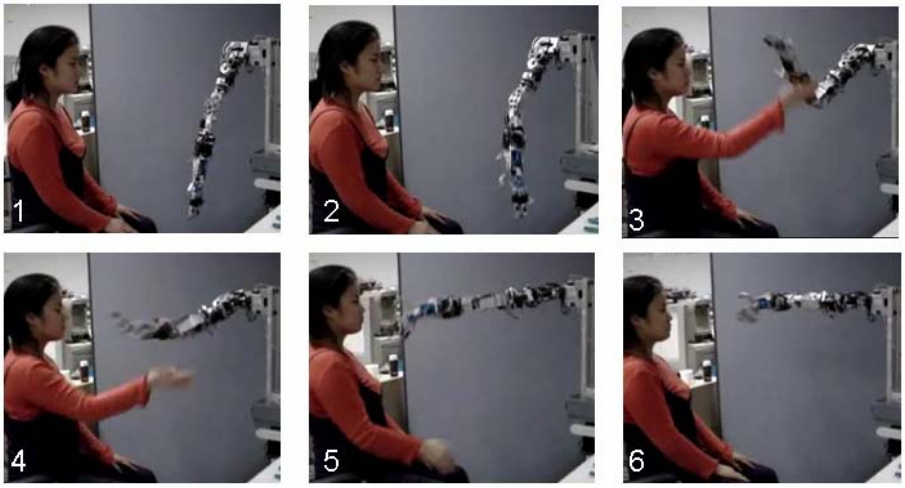

Figure 4.14 Involuntary collision

This time, involuntary collision is made at the forearm link location. First the arm moves in the direction of the incoming torque then proceeds to move in the

direction to the original trajectory. In this case, at frame 3, the forearm experiences an impact force downward. To reduce shock on the body, the elbow unbends and the forearm joint rotates toward the forced direction. Then, the current position and the time are compared with the original trajectory to choose the next motion. In this case, frame 6 motion of Fig 4.12 is chosen to continue with the task.

Chapter 5: Mechanism Design

This chapter details the biologically-inspired mechanical design of the humanoid arm and the hand, including the unique gear-train for a humanoid robot that is made up of back-drivable spur and bevel gears instead of harmonic drive. The biometric conscious parameters such as the endowed degrees of freedom, the working range, and the volume validate the effort to building the robotic arm is suitable for size and flexibility critical humanoid applications.

5.1 Mechanical Architecture

Having the human figure in mind, the anthropomorphic arm has 7-DoF from the shoulder to the wrist. This is very close to that of the human as the shoulder rotates in 3-DoF (can extend to 5-DoF for finer manipulations (Lenarcic 1999, Sakai et al. 2006), elbow in 1-DoF and the wrist in 3-DoF. This architecture proves to be effective and suitable when mimicking the human-like movements with finesse. Figure 5.1 shows the location and configuration of the arm joints while Table 5.1 compares the developed anthropomorphic arm to a real human arm.

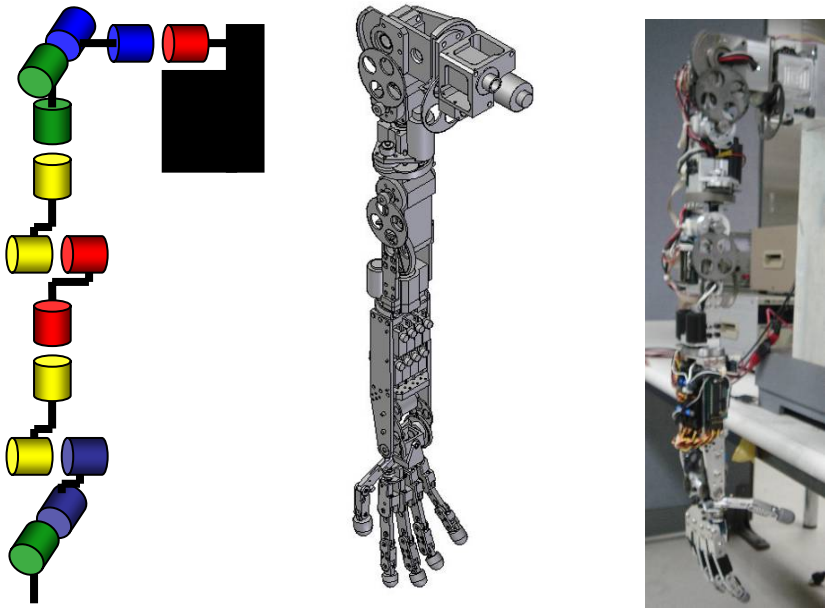

a) **b)** **c)**

Figure 5.1 Mechanical architecture of the anthropomorphic arm

a) Illustration of available DoF from the shoulder to the wrist

b) CAD drawing of the anthropomorphic arm

c) Developed humanoid applicable robot arm

Table 5.1 The anthropomorphic robotic arm vs Human arm

	Anthropomorphic humanoid arm	Human
DoF	7	7 (roughly)+ 2 (shoulder)
Length	Shoulder to wrist (500mm) Elbow to wrist (242mm)	550mm
Weight	3.7kg (with hand 200g)	3.6kg
Joint	Revolute joints	Ball-socket joint
Payload (Arm forward)	4.5kg	~10kg
Safety feature	- Light weight - Controllable joint compliancy	- Light weight - Actively varying compliancy - Soft skin covering

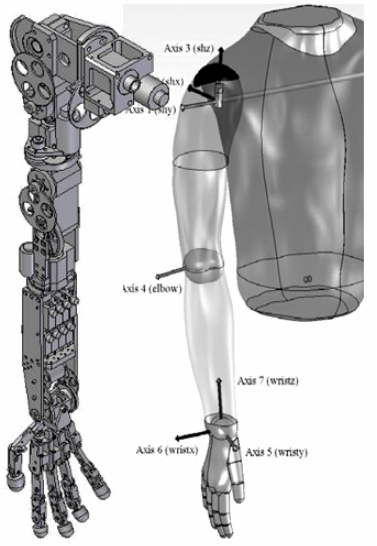

5.1.1 Hollowed joints

The custom made motor driver control individual joints from the shoulder to the wrist. This driver is small enough (see Fig 6.1) to be installed on each link for a embedded and modularized control having RS-485 communication in between the modules. Although the multi-point communication network that RS-485 provides minimizes the wiring between the modules, the power lines, and a single node communication wiring is still necessary. Due to the flexibility of the designed mechanism, the cabling can still be tedious and they can easily get tangled between the moving joints during task operations. In order to clear the wires out of the, the

joints are designed to have a hollowed out centers where the wires can run through. This not only eliminates unsightly protruding wires but also minimizes the risk of them getting caught in the gears while in motion. Since this arm has a multi-DoF with a large range of motion, without having the wires gathered in the center, it is quite challenging to position the wires unless having them braided and giving additional length for the mobility. Fig. 5.2 shows the hollowed joint centers where the wires can run through without interfering with the robot motion.

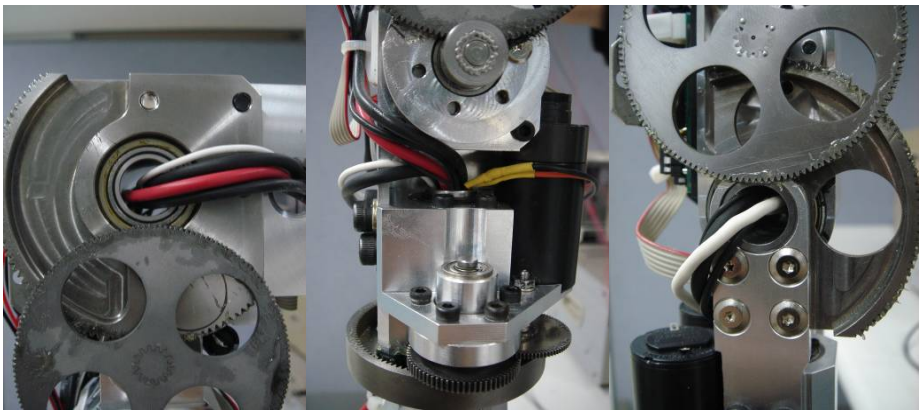

a) Shoulder **b) Forearm** **c) Elbow**

Figure 5.2 Hollowed joint centers in the arm

5.1.2 3-DoF wrist mechanism

In order to produce closely imitate human motions, it is critical to design the arm to have 3-DoF in the wrist. Having the extra DoF allows for fine and precise

movements which easily can resemble human's motions. Due to the limited space in the forearm section of the robotic arm, 1-DoF is placed in the forearm and the two other DoF is placed at the end of the wrist. All three joints share the same center of rotation for minimizing body inertia and reducing computational effort. To realize this architecture, bevel gearing is used as shown in Fig. 5.3.

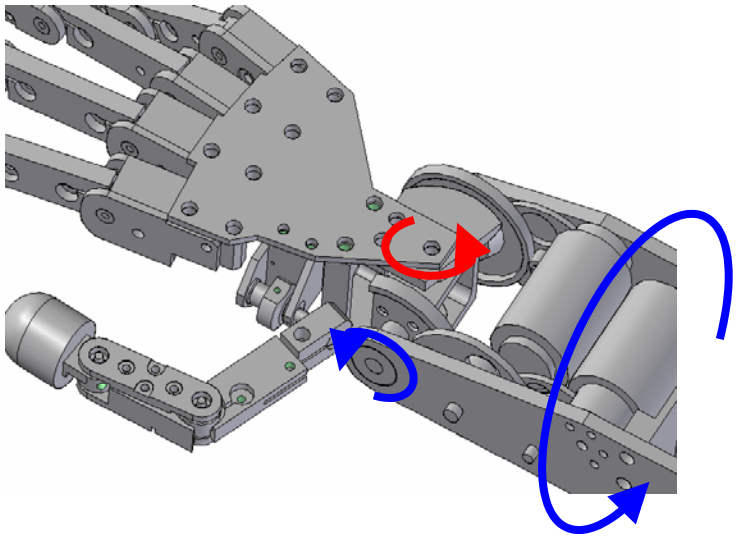

Figure 5.3 3-DoF in the wrist

5.1.3 Hand and finger mechanism

Human fingers are said to have around 20 DoF to execute most tasks and a couple more DoF in the palm. Human fingers' motions can be largely divided in to enveloping grasp (power grasp) and fingertip grasp (precision grasp) (Borst 2002). As the names suggest, power grasp would use the palm for larger force

transmission where the precision grasp would use the finger tips for tasks that require precision more than the force. For the currently developed robotic arm, the fingers have a total of 15 joints and 8 of them are actively actuated by 8 RC servo motors. There is no extra DoF endowed in the palm. Instead, the thumb connects to the palm by a spring-loaded hinge which is composed of and a ball joint (actively actuated in one direction). This design imitates most motions required of a thumb for grasping. All the finger joints are tendon driven with fishing wire. The little and the ring finger have one actively actuated DoF which controls movement in the rest of the three joints, DIP (Distal Interphalangeal), PIP (Proximal Interphalangeal) and MCP (Metacarpophalangeal) joints (see Fig.5.4).

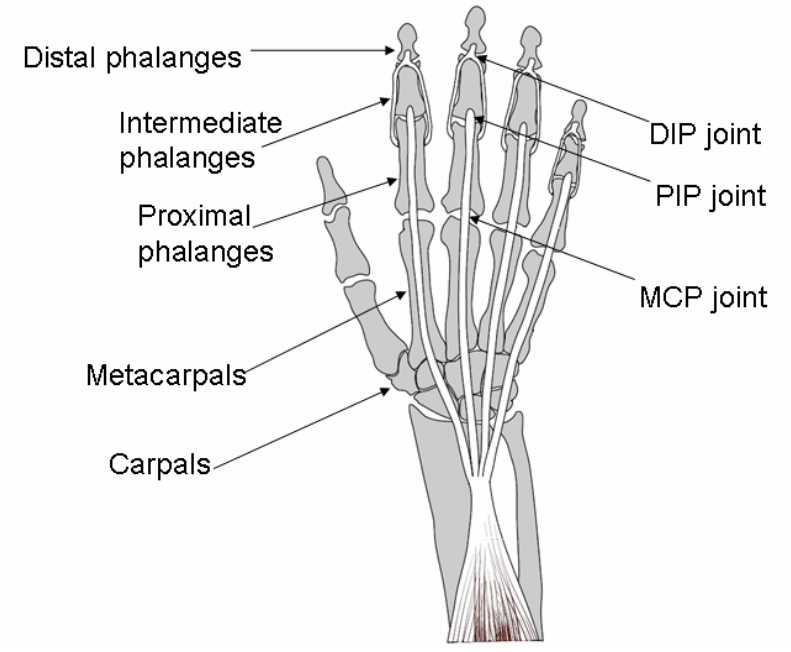

Figure 5.4 The human hand anatomy

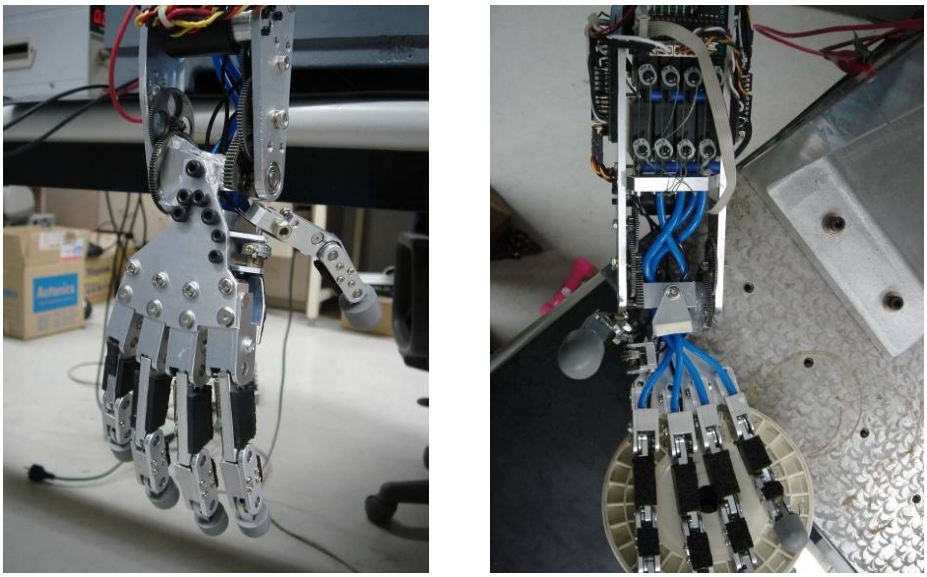

Figure 5.5 Developed robotic hand

The rest of the fingers all have two actively actuated DoF while having coupled movements. For the thumb, DIP and MCP are coupled and the base carpal joint moves independently. For the index and middle fingers, DIP, PIP and MCP are coupled for one DoF and DIP and PIP are coupled for the other DoF (see Fig. 5.6 and 5.7). For the coupled movements, the angular change was mechanically set to be in a ratio of 1:1. According to former biomechanical statistics, (Lang & Schieber 2004, Andrew 2003) the angular velocity ratio between the joints varies depending on the total angle change of the joints. Therefore, for the purpose of grasping multiple and/or various objects, this ratio is 1:1. Currently the fingers

have been tested to hold and grab in power grasp mode and have shown successful performances with the given angular velocity ratio in the coupled joints.

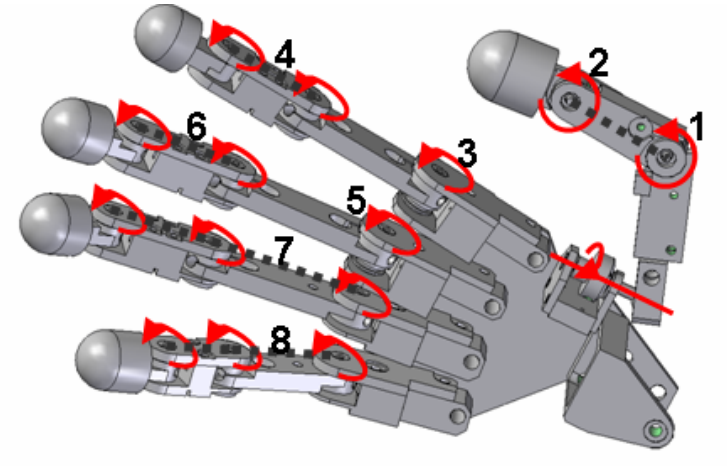

Figure 5.6 Endowed degrees of freedom in hand

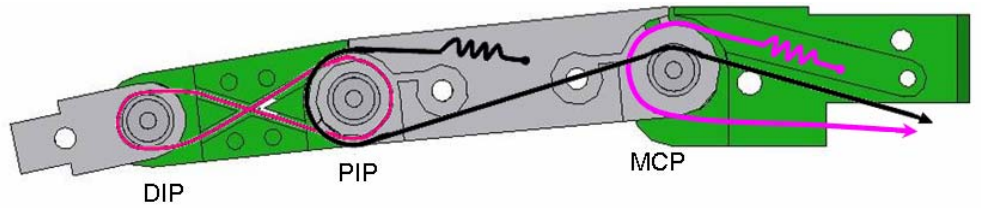

Figure 5.7 Finger joints

Many researchers have used tendon/wire driven hand designs to actualize multi degree of freedom hand while keeping the weight down (see Appendix A and chapter 2 for the statistics). The hand mechanism presented in this thesis also uses tendon driven joints. When cables are used to actuate finger joints, in most cases,

they are antagonistically actuated: when joints are moved in one direction, they need to be actively pulled back to the other direction to go back to the origin. It is unrealistic to use two actuators to create one joint motion when it is crucial to keep the whole arm mechanism compact and light. Therefore, in this humanoid applicable hand mechanism, finger joints are spring loaded to get the required recoil motion when returning the fingers. From the test results springs have shown to recoil the finger joints back to the origin; however, it when the unloading shock is greater than the threshold, the fingers can jitter lightly upon the impact of a shock. This problem is likely to be solved with a high stiffness springs and corresponding high torque motors. This way of actuation can be seen as an anthropomorphic behavior of the hand, as human hands, too, display greater force when gripping than when opening the hand.

Wires cross link between the coupled joints and as it can be seen in Fig. 5.7, the grooves in the links allow minimizing the number of assembly parts. The wires go around the grooves and get affixed to the links by screw bolts. The bolts can tighten up the wires to change the preloading force if required.

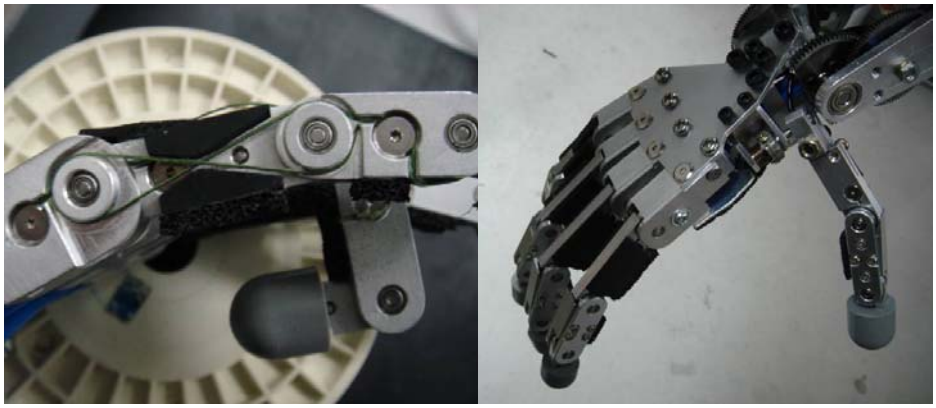

Figure 5.8 Robotic hand's finger joints: machined groove and ball joint thumb

5.1.4 Wire Shield

The tendon wires are 0.4~0.5mm in diameter flexible but a non-stretching fishing string. In order to have the actuators pull the joints, these wires must be connected to the actuator. However, due to its flexibility and thickness, the wire cannot support tension and is bound to collapse. In order to maintain its position and prevent tangling, and transmit the tension from the actuator to the joints, external shielding tube is fitted from the end joint to the actuator. It is a similar mechanism used in bicycle breaks; when the break handles are pulled, the cable inside the external tubing is pulled while the shielding tube takes the reaction force from the hinge. Similarly, the hand mechanism utilizes external tubing made of urethane that encases the wire; the tubing maintains enough flexibility to route the wire in the

desired direction while being stiff enough to anchor the reaction force.

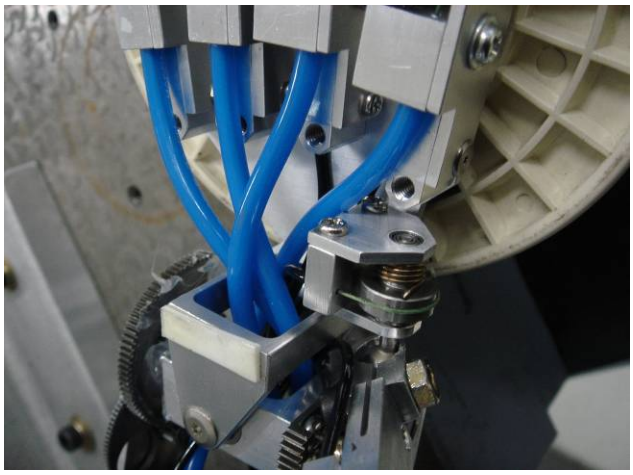

Figure 5.9 Spring loaded and ball-socket joint thumb & shield tubing

5.1.5 Thumb joint mechanism

There is no hinge in the actual palm part of this robotic hand. However, in order to grab an object, it is difficult to do it smoothly and "human-likely" without the motion equivalent to that of the human palm. In order to compensate for the lack of a palm hinge, in this mechanism, the base carpal joint is designed as a ball and socket. This design allows the base joint to move in the shortest path of the wire when actuated; however, it remains compliant to the object that it holds. The flexibility of the thumb and in turn, the flexibility of the whole hand is maintained with the given 8-DoF with this joint. Currently power grasp of up to 0.5kg load is enabled with this design.

5.1.6 Exterior covers

The humanoid applicable hand is designed for both types of holding controls: power and precision grasping. In order to improve the grip of the finger tips, they are fitted with silicon thimbles. Inside the palm and each phalange are covered with foam rubber tapes for the same reason. They provide approximately 4mm thick cushion for protecting the grabbed objects from scratching while increasing the friction coefficient to minimize slipping.

5.2 Gears and actuators

This section covers actuators and the gear-train of the developed arm. In this anthropomorphic arm architecture, spur gears are used instead of harmonic drive gears. They are custom built to satisfy the dimensional needs and to enable to use sensor-less joint driving algorithm.

5.2.1 Gears

The humanoids with an extremely compact mechanical designs favors the application of harmonic drives which provide high gearing ratio in a smaller package.. However due to the nature of the harmonic drives, the joints loose the

compliancy and back-drivability. The currently developed robotic arm has no additional sensor to retrieve the torque on the joints but instead uses spur gears and its back-drivable nature to acquire joint torques. It is unarguable that harmonic drives' application in the architecture decreases the joint backlash. However, the distance between the shaft axis of each gear in a gear train are designed to be adjustable to minimize the effect of backlash (the backlash in each joint is compiled in Table 7.4).

Table 5.2 compares the pros and cons of the use of spur gear and harmonic drives and writes how the problems of using spur gears have been addressed.

Table 5.2 Harmonic driver vs. Spur gear

	Harmonic drive	Spur gear	Current design
Volume	Compact	Depends	Strategic design required
Gear ratio	Usually over 50	Adjustable	Gear ratios 65:1 ~ 135:1
Efficiency	Worse than spur gear	Better than harmonic drive	Back-drivability efficiency over 80%
Price	Relatively expensive in Korea	cheaper	Custom made spur gears
Backlash	Usually better than spur gear	Usually worse than harmonic drive	Mechanical feature to minimize backlash
Back drivability	Difficult	Possible	Uses this feature to estimate motor torque
Compliancy	Limited compliancy	Compliant	Adjustable joint compliancy

5.2.2 Actuators

There are a total of 7 joints from the shoulder down to the wrist: for the ease of reading and visualizing the joints, the joints are numbered from one to seven starting from the wrist joint as one. Eight different DC motor models are used and the following table shows them in a list matching the motors and their locations in the arm from the shoulder to the wrist.

All finger joints are actuated by the same RC digital servo motor from Hitec (model HS-5125MG). The selected servo motors are thin and light which are the characteristic wanted in this robotic arm application. Currently developed robotic hand uses RC servo motors that do not require changing the rpm. Therefore, there is no need for a gear-train.

Table 5.3 Joint driving actuators and gear ratios

Joint number	DC Motor (FaulHaber)	Weight [kg]	Stall torque [Nm]	Motor const. [Nm/A]	Gear ratio
0 (shoulder)	3257 048CR	0.242	0.547	0.0762	1:100
1	3257 048CR	0.242	0.547	0.0762	1:81
2	2642 048CR	0.114	0.137	0.082	1:96.25
3	3242 048CR	0.175	0.189	0.0698	1:70
4	2232 024SR	0.062	0.0487	0.0321	1:65
5	2232 024SR	0.062	0.0487	0.0321	1:135
6	2232 024SR	0.062	0.0467	0.0321	1:135

Chapter 6: Motor control

One of the novel features of the developed anthropomorphic arm is its modularized links. Each arm link has its own embedded motor drivers to control the actuators while all the drivers communicate via multi-point RS-485 communication. This section covers the motor drivers and the communication protocol involved in the anthropomorphic robotic arm motor control.

6.1 Motor drivers

There are a total of fifteen motors in the developed humanoid arm. Each of them is controlled by custom-made motor drivers which are specially designed to be slim, compact and light. For this reason, an effort has been made to use an all purpose microcontroller chip that enables multi functional I/Os. Among the vast choice of microcontrollers, we required one that features a robust architecture, a flexible memory mapping and peripheral supports. AVR® and DSP 24001® are popular options for such applications; however, the physical size of the chip is of a concern in this robot arm application as we wanted modularized drivers for an installment on each individual link. More details on the RS-485 communication specifications, control methods, command configurations for the motor driver modules are covered in the following sections. For the motor driver modules, Microchip's PIC

18L2431 microcontroller was implemented. PIC® satisfies the requirements (RS-485 communication operations, 10-bit resolution power control PWM output, 10-bit A/D converter, flash program memory, internal RC oscillator) and is an economic, one chip solution for modularization of the joint actuators.

6.1.1 DC motor driver

There are a total of 7 DC motor drivers for the robotic arm and they consist of National's LMD18200 and Maxim's RS-485 interface chips. The LMD18200 chip internally has an H-bridge circuit to drive DC motors and also measures the current flow. Table 6.1 summarizes the specifications of the compact DC motor driver that is developed to be installed on the arm links. Figure 6.1 shows the circuit diagram of the DC motor driver.

Table 6.1 DC motor driver specifications

Motor	FaulHaber DC motor
Size	27mm x 43mm
Voltage	48V
Max. current	3A (6A peak)
Communication	RS-485
Control method	Position control
Feature	Current level feedback

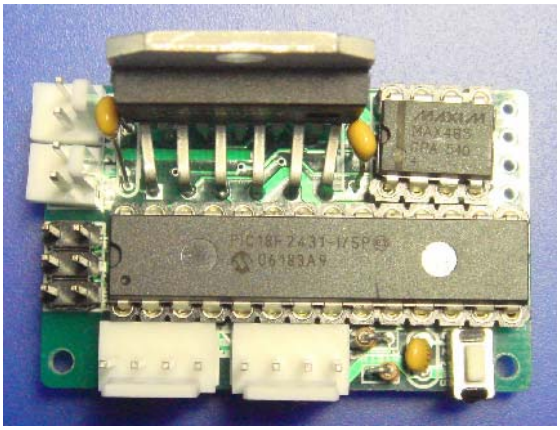

Figure 6.1 DC motor driver (27.5mm X 43mm)

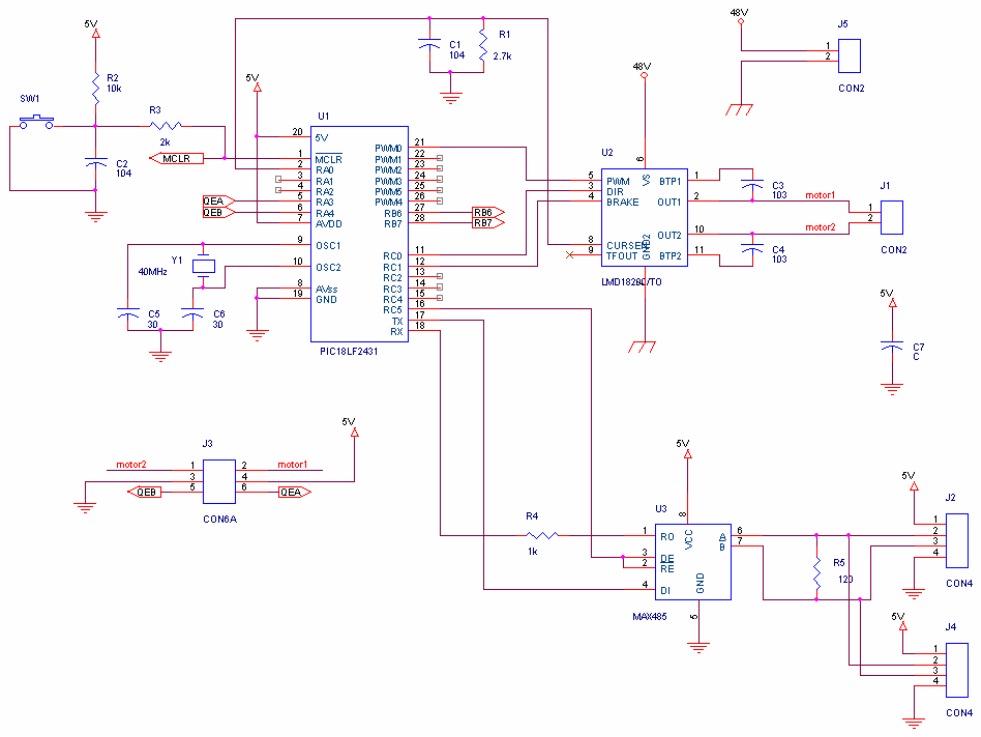

Figure 6.2 DC motor driver circuit diagram

6.1.2 RC digital servo motor driver

To control 8 servo motors in the fingers, 2 servo motor drivers designed and they are installed on the forearm of the humanoid arm. Because RC servo motor drivers do not use DC motors' LMD18200 chip, in order to extract the current flow level, additional resistance was attached to pull out current reading. Currently developed hand has a total of actively actuated eight DOF driven by eight RC servo motors. Table 6.2 shows the specifications of currently used RC servo motor driver.

Table 6.2 RC Servo motor driver specification

Motor	Hitec HS 5125MG
Size	27mm x 43mm
Voltage	6V
Communication	RS-485
Control method	Position control
Feature	Simultaneous 5-driver operation (4-motor current feedback)

Figure 6.3 RC Servo motor driver (28mm X 48mm)

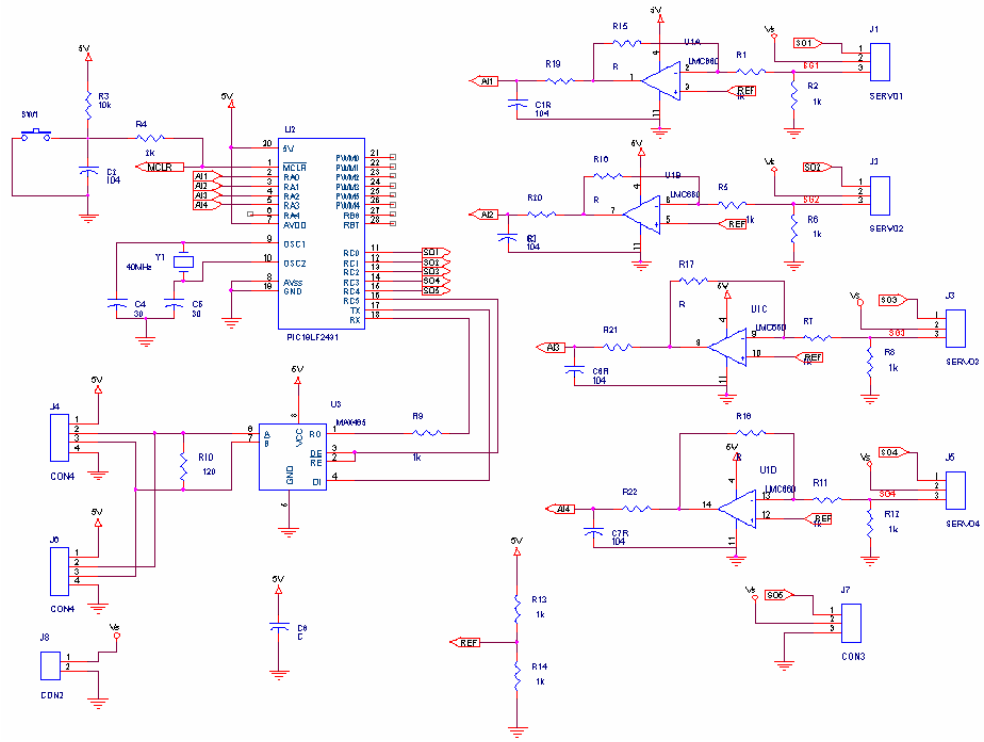

Figure 6.4 RC servo motor driver circuit diagram

6.2 RS-485 communications

The motor driver modules receive the central command through RS-485 communications network. Mostly industries and plants used, RS-485 system is faster and more resistant to noise compared to general use serial RS-232 system. RS-485 communication system inherits the same protocol and configurations as RS-232 standard. However, it can have multiple transmitters and receivers when

RS-232 is meant only for one to one communication. The adaptation of RS-485 communication system minimizes complex and numerous cabling because all the connections can be transmitted via single node. (see Fig. 6.5). Due to the nature of multi communication with a single source controller, it is imperative to have a safe communication protocol. For a successful communication, the transferring message bits and responding bits must be confirmed to eliminate any malfunctioning in the system due to communication error and noise. For the developed humanoid arm, this communication protocol has been designed and implemented. The details on the RS-485 command protocol will be covered in the following section.

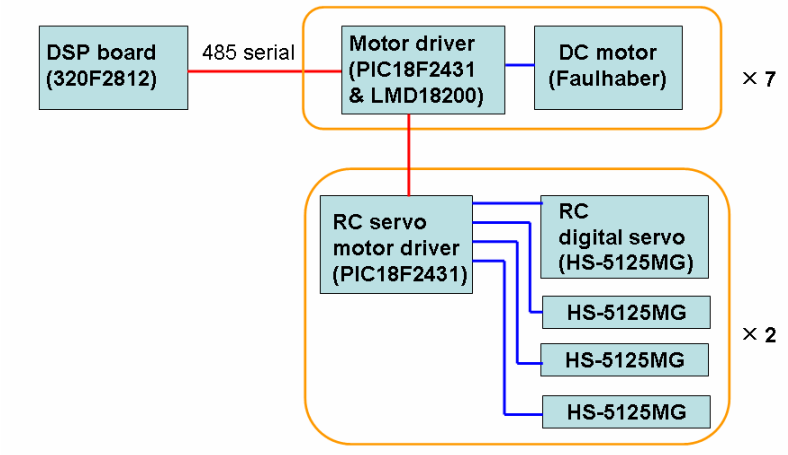

Figure 6.5 RS-485 communication system of the arm

The humanoid robotic arm and finger joints are controlled by the main DSP microcontroller. As it was mentioned previously, individual motor driver for joint motion (one driver for each DC motor and one driver for a set of four servo

motors) communicate via RS-485 system with the main microcontroller. The main DSP controller is responsible for producing trajectories that are sent to the motor drivers ran by PIC® microcontrollers. Then the question arises who will compare and make decisions upon reading in torque values. For the current application, torque load on every joint is analyzed to make the next move, and this process is done for each trajectory points. If the main microcontroller would takes the job of making the decision, the acquired torque values of the joints (collected by PIC®) must be transferred back to the main microcontroller: and this communication takes time even though the calculation load on the PIC® microcontroller reduces. If the extra transferring of received packet is eliminated, and instead PIC® makes the required calculations to make decision for the next movement, the computational load on PIC® increases. In this research, the communication rate is set to be 40Hz and the main microcontroller does the necessary dynamics calculation.

When using the default RS485 receivers with an input resistance of 12 kΩ, it is possible to connect up to 32 devices to the network. Currently, nine drivers and one master transmitter are in the network while the RS-485 buses are in tri-state with high impedance. In designing the communication protocol, the communication rate is set to 19200bps. The master DSP controller sends and receives 5 byte command packet in the form of Table 6.3 including the check sum

byte. Every sending and receiving packet is checked to ensure secure communication. This format is all defined during this arm development and showed satisfactory communication capabilities.

Table 6.3 RS-485 communication protocol for humanoid arm

Motor driver	Tx / Rx	Byte #1 Header	Byte #2 Address	Byte #3 Value	Byte #4 Value	Byte #5 Checksum
DC	To driver	0xAA	ID	Position Low-byte	Position High-byte	Check sum
	From driver			axxx xxbb a: direction b: 2bits for toque	bbbb bbbb	
Motor driver	**Tx / Rx**	**Byte #1 Header**	**Byte #2 Address**	**Byte #3 Address**	**Byte #4 Value**	**Byte #5 Checksum**
RC servo	To driver	0xAA	151 152	1~4 add.	Position 0~255	Check sum
	From driver			aaaa xxbb a: upper 4bits b: lower 2 bits for value	bbbb bbbb 10 bits returned.	

Address

The first byte is always set as 0xAA which is followed by the ID byte. The DC motor IDs are numbered 131~133 for the shoulder (3-DoF), 121 for the elbow (1-DoF), and 111~113 for the wrist (3-DoF). As mentioned before, four servo motors are controlled by one motor driver and there are two motor drivers to control eight DC motors. Therefore, the address numbering starts from 1511~1514 for the first driver and 1521~1524 for the second RC motor driver.

Position

The DSP controller sends preplanned position data produced from set of equations that are found from interpolation software. The interpolation software we had used for developing MUSA (Bang et al. 2005) is modified for the currently developed 7-DoF arm: this software takes in a minimum of three knot points and produces equation that interpolates the knot points. These values are updated for each packet. The pulse conversion for each joint is set accordingly depending on the encoder specification. The range of motion and the effective number of encoder pulse count are considered in setting the displacement [deg / encoder pulse] ratio to maximize the resolution of joint position control. The produced joint displacement in degrees is as follows.

Joint displacement [deg] = 360 * (m / n)

, where n = number of encoder pulse / 1 command pulse,

m= number of encoder pulse / 1 rev

The RC servo motors that actuate finger joints use different conversion parameter from the DC motor drivers. Servo responds to variations in the duty cycle of a 50 Hz rectangular pulse train. The rotation range of -60~60 deg is translated to 0~ 250 pulses where the pulse width varies 1.1~1.9ms. When the command value is not within the scope of the preset motion range, the program set to give out error

message. And for convenience, preset numbers are used to perform specified tasks as summarized in Table 6.4.

Table 6.4 Preset commands for motor drivers

Address input	Driver tasks
32100	Emergency stop for all motors
32101	Power on for all motors
32110	Reset all motor positions to the origin
32111	Send current motor position reading to the controller

In addition to the commands above, if ID is set to 0x33 all the driver reacts with LED signal without return value. Such definitions are not directly used during the actual motion control process; however, these simple commands are frequently used while testing the drivers and trajectory motions.

Torque reading

The motor torque is initially received as the motor current values which are received in 10bits. For this measurement, 5 Ohm resistor is connected (if 1A current flows, 1.0V is measured). Then the conversion ratio is calculated from the maximum torque (current), which is measured when the potential difference is 5V. For a 10bit-system, 1024 pulse is the maximum count and it is equivalent to 5V; 208.262pulse/A conversion ratio is used to calculate the actual torque. From the

pulse reading, torque is calculated inversely; where, the joint torque is found to be pulse count * 1A / 208.262 count * motor torque constant * gear ratio. The joints from the shoulder to the wrist have no coupling effect on each other during the movement; however, the finger joints show dependency.

Checksum

The *Checksum* byte indicates the sum of all the pulse that has been sent.

ID + Address + Value + Chksum = 0

This byte makes sure if the communication is made successfully. This checks if a correct driver is responding or if there's a clash in responses or transfers. By checking both check sum and id values is necessary for safe and accurate communication. During this process, it needs 5.5ms for transferring and checking the packets using 192000 bps communication speed.

ie. (8bit * 5bytes / 19200bps + 0.1ms wait time) * 15joints = 33ms

This means, for immediate checking of the received torque value happens only after 33ms elapses (12ms for when moving joints only from the shoulders down to the wrist). For current purpose of the humanoid arm, this value was found to be sufficient using the DSP microcontroller.

Chapter 7: Hardware Evaluation

The humanoid robotic arm with the mechanical architecture described in the previous chapters is built and it is tested for various hardware specifications including the motor capacity, the joint backlash, the back-drivability and the torque reading resolution in the joints. Also the hand's contact force sensitivity is compared to the result of a contact sensor reading.

7.1 Motion range and speed

The developed anthropomorphic humanoid arm assembly measures a total of 500mm from the shoulder to the wrist; the upper arm measures 258mm and the forearm measures 242 mm. The wrist to the middle finger tip (the longest finger) measures 180mm. The total mass of this arm is 3.7 kg including the hand, motor drivers and controller. Table 7.1 shows the maximum angular range of motion in the joints compared to human (partly taken from Appendix B and the averaging measurements from the laboratory members). Most joints are designed to have an exceeding range of motion compared to the human's.

Table 7.1 Angular motion range in joints compared to human

	Joint	Human [deg]	Anthropomorphic arm Motion range [deg]
shoulder	0	245 (-200~45)	265 (-205~60)
shoulder	1	189 (-91~98)	180 (-45~135)
shoulder	2	209 (-109~100)	270 (-135~135)
Elbow	3	150 (0~150)	150 (-15~135)
Wrist	4	240 (-120~120)	210 (-105~105)
Wrist	5	150 (-70~80)	180 (-90~90)
Wrist	6	43 (-10~33)	40 (-10~30)

To execute most human like motions, the joint angular velocity at each joint is designed to be higher than 200 deg/s. Each joint and their maximum velocity are shown in Table 7-2. These values are superior to an average human capability.

Table 7.2 Maximum angular velocity without load

	Joint	Maximum angular velocity [deg/s]
Shoulder	0	350
Shoulder	1	430
Shoulder	2	390
Elbow	3	460
Wrist	4	650
Wrist	5	310
Wrist	6	310

7.2 Joint Bandwidth

Like any other robotic arms, a high bandwidth performance is desirable in

controlling humanoid robot arm joints. However, the response rate for humanoid robot arm joints is often jeopardized as much sensor information and data communication must be taken into consideration for multi-joint, multi-DoF redundant mechanisms. Figures below show the bode diagram of the joint motion responses of the developed robotic arm. The plotting is done for the motor responses when each joint is commanded to move 180 degrees. Fig 7.1 and Table 7.3 display the resulting data plot. As it can be expected, the wrist joints which take the least load; thus, they have the highest bandwidth among the other joints.

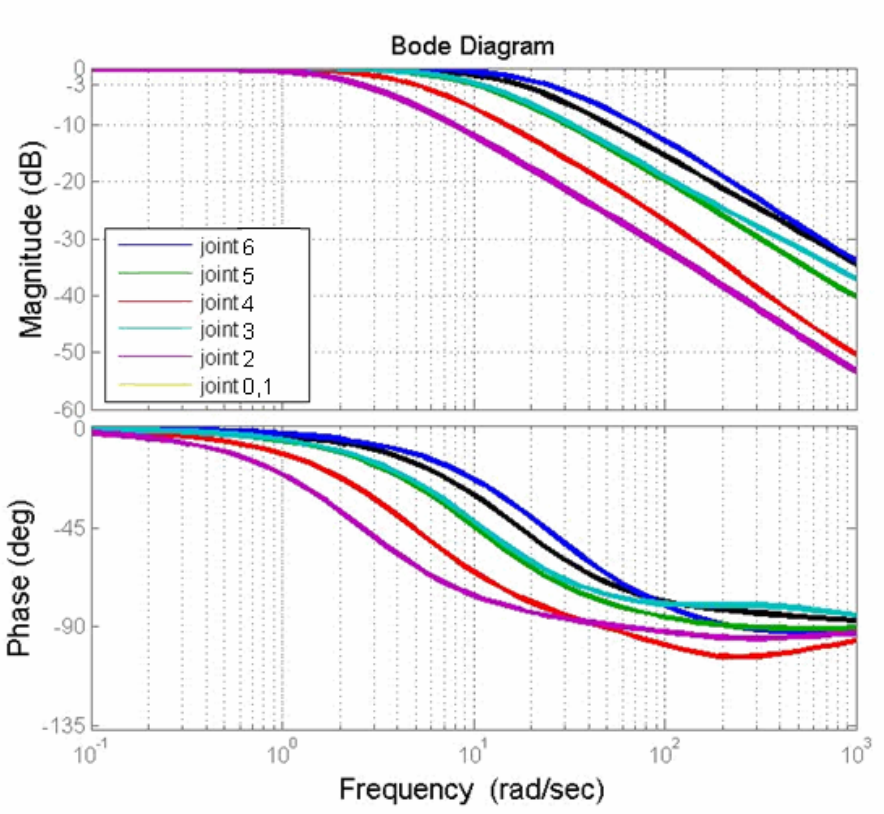

Figure 7.1 Bode plot of the arm joints

Table 7.3 Bandwidth of each arm joint (for rotating 180 deg)

	Joint	Bandwidth [Hz]
Shoulder	0	0.4
Shoulder	1	1
Shoulder	2	1.6
Elbow	3	1.8
Wrist	4	3.0
Wrist	5	4.4
Wrist	6	4.4

7.3 Back-drivability

The back-drivability of each joint is found and compared with the actual torque output from the motors. The actual torque output is calculated from the product of measured current and the motor torque constant. The applied torque is derived from adding incremental weight to the lever arm. In Fig 7.2 and 7.3, x-axis represents the applied torque and y-axis represents the measured torque in Nm. As the graphs display, the relationship is linear and show efficiency of minimum 70%.

The torque measurement range is within 1~5Nm while the sensing resolution is within 2% of the measurement: a sample of 10 readings is made for each incident of measurement and has used its average for comparison. Having less than 5% of error in measurement compared to the calculation, they are still

extremely conservative due to the quality of the gears: joints that have better machined gears showed superior performance in all tests. Fig. 7.2 and 7.3 show the measurements made for the top shoulder joint for resolution and accuracy. Fig 7.2 shows the maximum torque range up to 5Nm and clear linear trend up to that range. Fig 7.3 shows the same joint where the 2% resolution reading is shown. Subsequent shoulder joint 1 and joint 2, which take less torque than joint 0, are also shown in Fig. 4 and 5. The lower joints of the arm only a take fraction of the load compared to the upper joints.

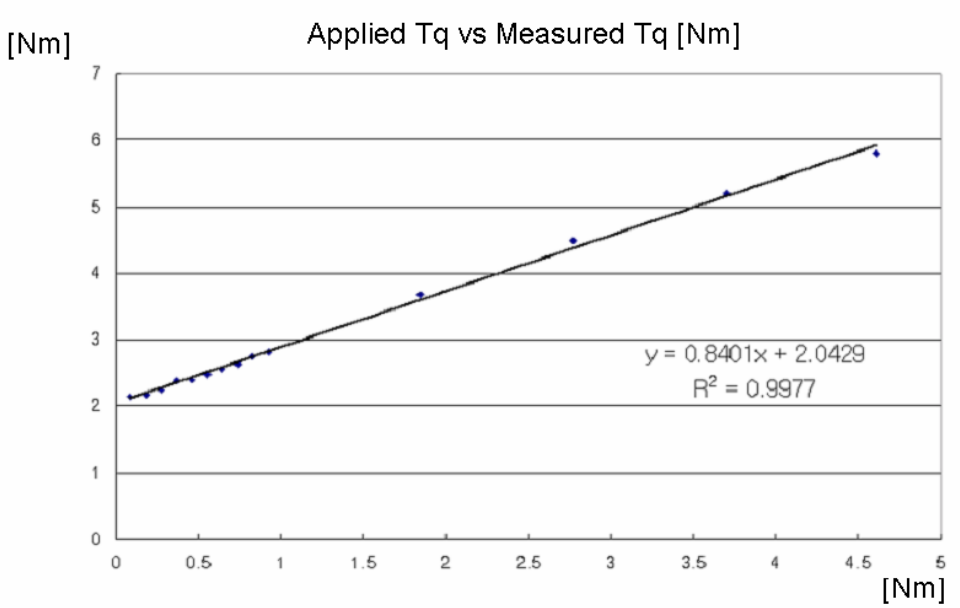

Figure 7.2 Torque detection in shoulder in its maximum range

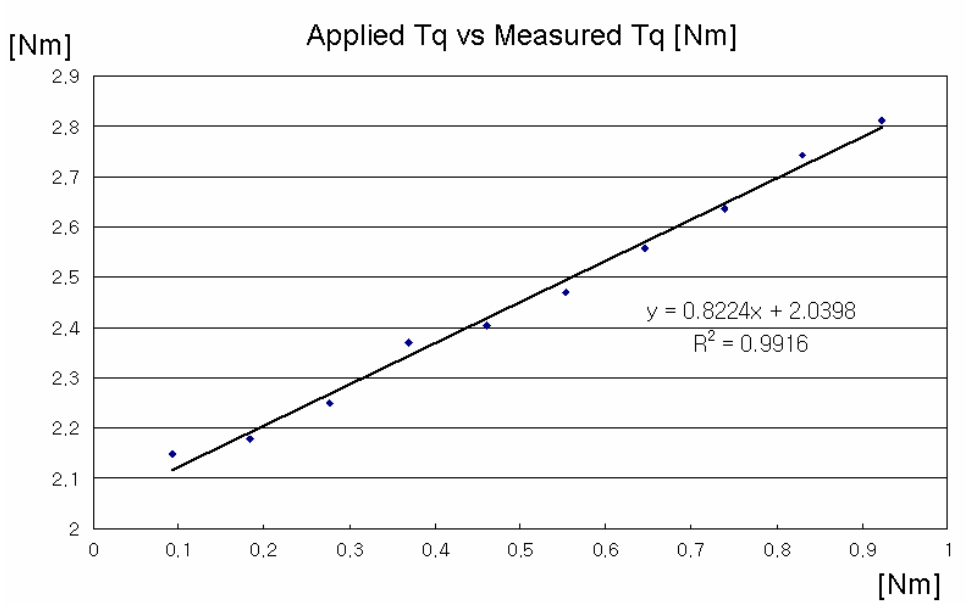

Figure 7.3 Torque detection in shoulder in its resolution range

For measuring the sensitivity of the joints, force is applied on each link separately and this force is measured with a load cell. Figures 7.4, 7.5 and 7.6 show the resulting joint torque readings and the applied torque when the force is applied. As it can be seen, the joint is sensitive to less than 10mNm for the worst joint (the shoulder joint 0, which takes the most load) and it is smaller for other joints.

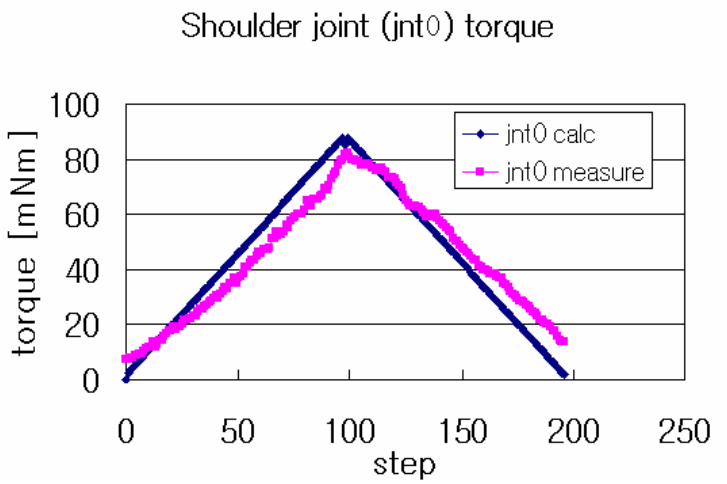

Figure 7.4 Shoulder torque reading for loading and unloading

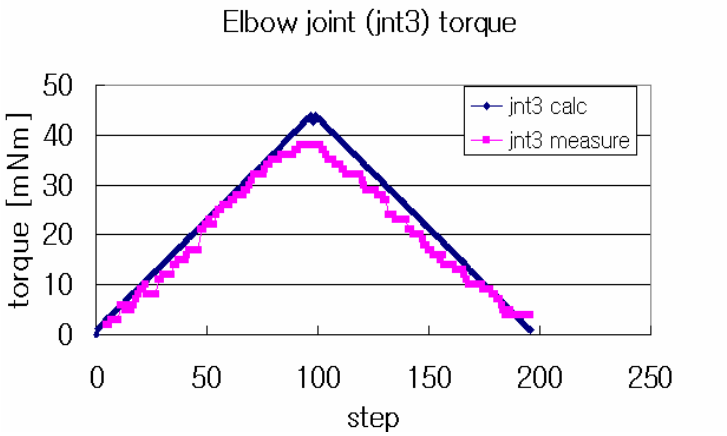

Figure 7.5 Elbow torque reading for loading and unloading

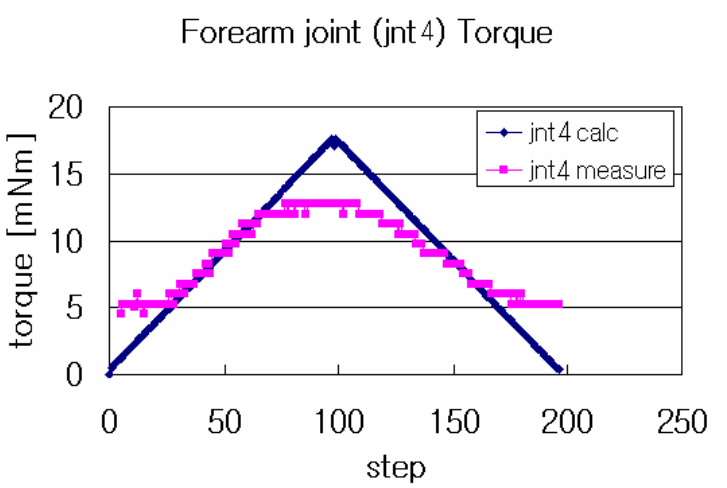

Figure 7.6 Forearm torque reading for loading and unloading

7.4 Backlash

Ideally, gears should have no backlash for accurate positioning, and minimizing the friction loss. However, using spur gear trains in this multi jointed humanoid arm, the effect of backlash on the performance is inevitable. Table 7.4 compiles the backlash in each joint. These values are isolated by restricting movements in other joints while the measuring joint is rotated back and forth to check for the range of the backlash. Since the scope of the deflection is small, its range was amplified with a lever arm attachment and this deflection is measured using a micrometer. Once the reading was made, its tangent value was taken to be the backlash of the joint.

Table 7.4 Backlash in the arm joints

	Joint	Backlash [deg]
Shoulder	0	0.19
Shoulder	1	0.11
Shoulder	2	0.16
Elbow	3	0.13
Wrist	4	0.04
Wrist	5	N/A
Wrist	6	N/A

The wrist joint 5 and 6 are built with module 0.3 bevel gears, and actuators transmit the torque through double gear trains. Measuring the backlash is difficult in this case using the same conventional method.

7.5 Hand contact force sensitivity

Instead of using contact or conventional torque sensors, the developed hand detects object grabbing by watching the motor current level change. The effectiveness of using this method and conventional contact sensors are compared in Fig. 7.7 and 7.8. Fig 7.7 shows contact sensor reading of GIFU hand III when a contact is made. Similarly, using the motor current detection method, Fig 7.8 also displays apparent contact point. To see the sensitivity level of the finger joint, force is applied to a finger joint in Fig 7.9.

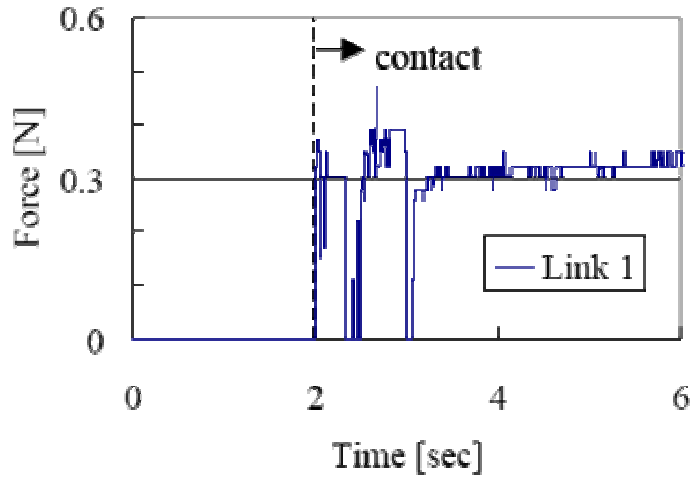

Figure 7.7 GIFU hand III's contact sensor reading (Mouri et al. 2002)

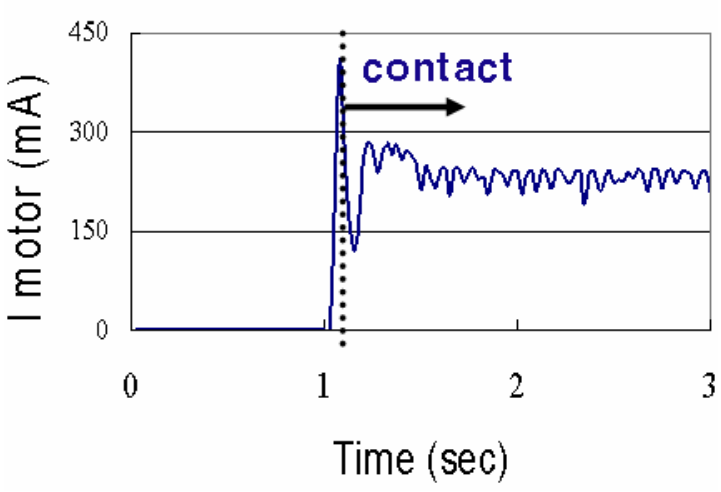

Figure 7.8 Load detection by monitoring the motor current

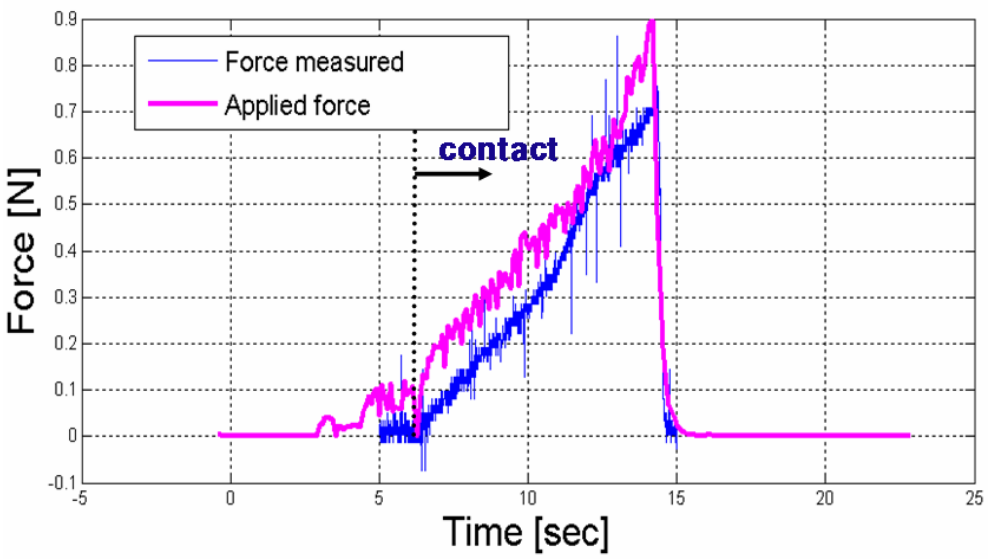

Figure 7.9 Sensitivity of the anthropomorphic robotic finger

Fig 7.8 displays the resulting force measurement when constantly increasing force is applied to the finger. The point of contact is marked with a dotted line in the figure. The finger starts to make measurements (*applied force* in Fig 7.9) earlier than the actual force application (*force measured* on Fig 7.9). This is due to the nature of cable actuation system. In other words, this dead zone is the direct result of the friction in between the cable and the shield, and the lagging cable inside the shield. With a tighter pretension in the cable, the finger can be more sensitive as the amount of friction loss due to the cable lag can decrease. Current setting of the finger cable tension shows a sensitivity level around 0.1~0.2N which is quite comparable to the result of contact sensor usage shown in

Fig.7.6.

7.6 HIC index experiments

Industrial robots have specifications in all fields including the safety features. Therefore, they have a standardized test for measuring the safe level in the hardware. The most immediate way of achieving safety when sharing work space with robots is a constant monitoring of the control manipulator with sensors. By improving the mechanical design of the robot eliminates potential for hazardous situations. An example of a hazardous situation would be being hit by an operating robot while working closely to the machine. In this research, mechanical frangibility of the human body and its severity is quantified using the empirical formula developed by automotive industry. Among many formula, Head Injury Criteria (HIC) index (McElhaney 1976, Zinn et al. 2004) is adapted to measure the shock level: the solution is to reduce the effective impedance of the whole system.

$$HIC = \left[\frac{1}{t_2 - t_1} \int_{t_1}^{t_2} a dt \right]^{2.5} (t_2 - t_1)$$

Where a is a resultant head acceleration,

$$t_2 - t_1 \geq 36ms$$

2.5 is used for the head, this parameter varies for different parts of body.

For the testing, 5 readings were taken for each of three arm model, which are the conventional robotic arm that uses harmonic gears, MAHRU (Kim et al 2005), the

developed humanoid arm without covering, and the robotic arm with a silicon (porous silicon with 15mm thickness) covering. Each arm is hit with a F-T sensor at 2m/s velocity as shown in experiment set up in Fig 7.9. The force reading is collected every 440usec and plotted in Fig 7.10.

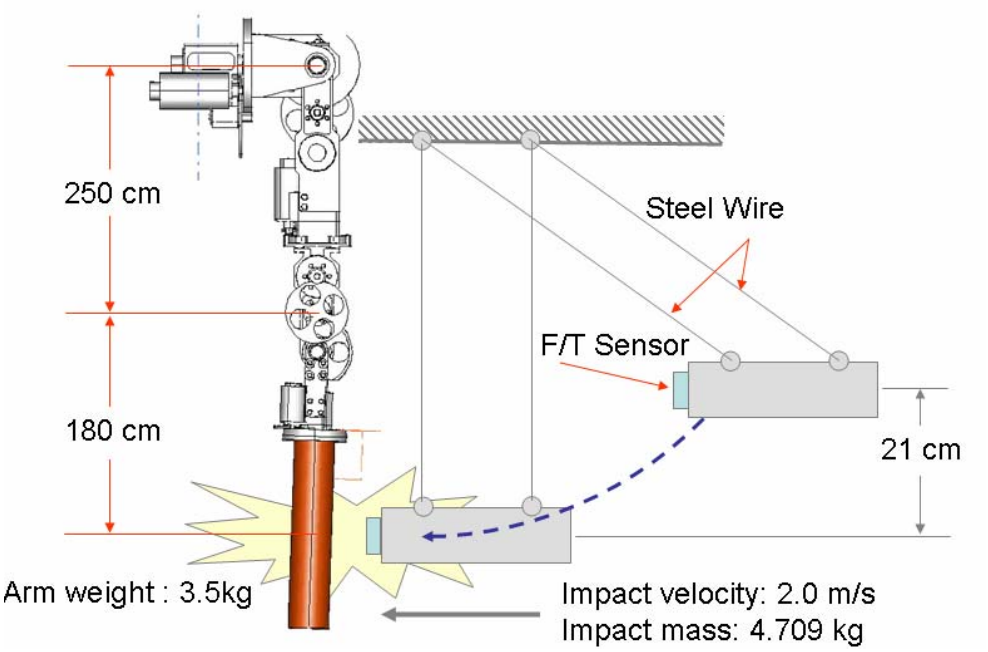

Figure 7.10 Experimental setup for HIC evaluation

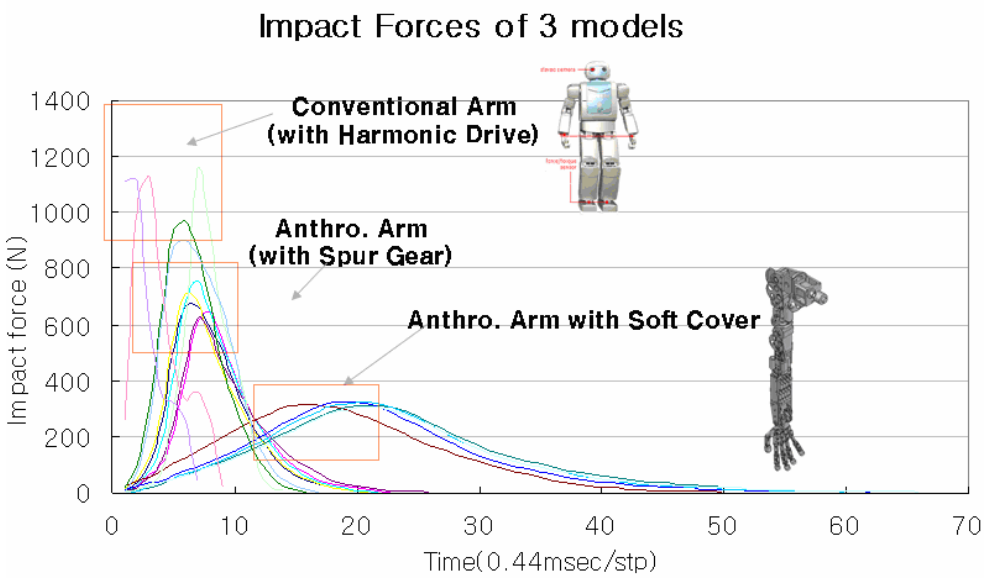

Figure 7.11 Impact force reading in all three arms

Table 7.5 Resulting forces and HIC

Trials	Conventional (MAHRU Arm)		Anthropomorphic humanoid arm		Anthro. arm + Silicon Cover	
	Max. Force [N]	HIC	Max. Force [N]	HIC	Max. Force [N]	HIC
1	1148.99	286.12	664.98	148.71	315.97	91.87
2	972.55	392.07	648.59	95.94	314.16	73.49
3	903.46	422.50	721.00	140.90	326.14	66.62
4	1127.23	585.24	756.49	153.56	325.31	77.26
5	1115.52	558.21	619.42	81.58	305.18	60.67
Average	1053.54	448.83	680.30	124.14	317.35	73.98

The resulting numbers in Table 7.5 show a dramatic reduction with the developed humanoid arm that is much more compliant than the arm using harmonic gears. With the reduction in over all impedance and weight, the maximum shock force is reduced 35% and HIC is reduced 72% compared to the harmonic gear using humanoid robotic arm of MAHRU. With a silicon covering, the effect is even higher being reduction of 70% and 84% respectively.

Chapter 8:
Conclusions and Recommendations

This thesis presents a novel anthropomorphic 7-DoF arm completed with 8-DoF hand for interactive humanoids. The mechanical design of the humanoid arm is compact enough not only to be compatible with currently available narrator-mannequin type humanoid robots, but also powerful and flexible enough to be functional; the redundant DoF joints allow flexible robot arm and dexterous hand manipulations. The detailed mechanism design, the embedded and modularized hardware, the "conventional-sensor-less" trajectory planning for safety, and the actuator control method have been presented. Hardware-wise, it is designed to be light and compliant to minimize any system impedance; software-wise, the proposed method recognizes any accidental collision in all the joints including the fingers. Upon a collision, the intent evaluation chooses the subsequent reaction trajectory for safe HRI.

9.1 Summary of Contributions

The multi-DoF anthropomorphic humanoid applicable robotic arm and hand

The anthropomorphic arm and hand that display realistic mechanical parameters for intuitive human interactions have been designed and built. The human biometric conscious parameters such as, the joint operation speed, weight, length, motion range, thickness and flexibility, all conjunctively exhibit human quality in its motions. The embedded and modularized controllers of the arm enable a direct application of the full mechanism to a human-sized humanoid robot.

The "conventional-sensor-less" torque sensing

A simple yet unique method of torque sensing without using the conventional multi-axis F-T sensors, torque sensors, or contact sensors is proposed in this work. The load torque on the joints (both the arm and fingers) is proportional to the motor current level of each actuator. Therefore, the motor current value is monitored for joint torque changes for task execution and safe manipulations of the developed arm and hand.

Impact force estimation and intent evaluation criteria for safe HRI

An algorithm for an aberrant impact force quantification and localization has been suggested in this thesis for safe HRI. This algorithm can distinguish the joint load

from the load resulting from its own weight and motion dynamics from an aberrant impact during a task execution. Upon impact, it evaluates the collision force with the "intent evaluation criteria" which is an objective and simple safety criterion suited for the developed hardware. This evaluation quantifies the intent level of the collision and chooses a new trajectory minimizing any future damage on the robot and the human operator.

Inherently safe hardware: controllable joint stiffness

An inherently safe arm mechanism design is suggested for safe HRI; the arm displays an exceptionally low link inertia, and compliant joint stiffness. Eliminating the use of the torque sensors and stiff harmonic drives has increased the range of joint stiffness which is adjustable.

9.2 Future Work

Currently the arm is designed to pose minimum danger to humans (according to the ISO standards on industrial robots, HCI, and humanoid robotics danger index). Therefore, in this research, only the impact force on the hand is watched and analyzed. This focused research is sufficient as no critical danger would be posed by other links. However, if the actuators were replaced with a higher torque capacity and result in an increase in the overall volume and weight, the arm may no

longer be safe and possibly require additional research on developing a different safety protocol and algorithm.

Apart from the tendon-pulley pulled, 8-DoF hand that has been covered in the thesis, an improved second version hand has been designed. This robotic hand model has an additional DoF to have a total of 9-DoF. Comparing it to the previous model, it weighs only 20g more but the new mechanism has eliminated the problem with cable lagging in-between the joints. A future work on a sophisticated grasping algorithm in conjunction with the previously developed contact sensing method is likely to increase the dexterity of the hand.

Bibliography

Akin D, Carignan C, Foster A (2002), “Development of a Four-Fingered Dexterous Robot End Effector for Space Operations”, Proc of the ICRA 2002, p2302–2308.

Alba, D.,Armada, M., and Ponticelli, R.(2005),"An Introductory Revision to Humanoid Robot Hands", Climbing and Walking Robots, Springer Berlin, Heidelberg, p701-712.

Altintas, Y. (2000) “Manufacturing automation”, Cambridge University Press.

Andrew E. et al. (2003) "The Fibonacci Sequence: Relationship to the Human Hand" The J of Hand Surgery, 28(1), January 2003, p157-160.

Bang, Y., Lee, W.S., Lee, K.M., Kim, I.S., Paik, J., Shin, B.(2005), "Motion Teaching Method for Complex Robot Links Using Motor Current Sensing", Int Conf on Control, Automation and System ICCAS, Korea.

Biagiotti, L., Lotti, F., Palli, G., Tiezzi, P., Vassura, G., Melchiorri, C. (2005) "Development of UB Hand 3: Early Results", ICRA2005, IEEE Int Conf on Robotics and Automation, Barcelona, Spain, April.

Bicchi, A. & Tonietti, G. (2002), “Design, Realization and Control of Soft Robot Arms for Intrinsically Safe Interaction with Humans”, Proc. IARP/RAS Workshop on Technical Challenges for Dependable Robots in Human Environments, p79-87.

Bicchi, A. & Tonietti, G. (2004) “Fast and soft-arm tactics”,IEEE Robotics & Automation magazine, June, p22-23.

Bicchi, A. et al (2001) “Compliant design for intrinsic safety: general issues and preliminary design” Proc. Of the 2001 IEEE Int. Conf. onIntellifent Robots and Systems, 2001.

Borst, C., Fischer, M. and Hirzinger, G. (2002) “Calculating hand configurations for precision and pinch grasps”, Proc. Of 2002 IEEE Int Conf on Intelligent Robots and Systems, Switzerland, Oct 2002.

Brock et al. "Elastic Strips: A framework for motion generation in human environments” Int. J of Robotics Research Dec. 2002.

Butterfass, J., Grebenstein, M., Liu, H., Hirzinger (2001), “DLR-hand II: Next generation of a dexetrous robot hand”, Proc of the IEEE International Conference of Robotics and Automation, p109–114.

Butterfass, J., Hirzinger, G., Knoch, S., Liu, H. (1998a), “DLR’s Multisensory Articulated Hand, Part I: Hard and Software Architecture”, Int Conf on Robotics and Automation, ICRA’ 98. p2081–2086.

Butterfass, J., Hirzinger, G., Meusel, P., Liu, H. (1998b) “DLR’s Multisensory Articulated Hand, Part II: Parallel Torque/Position Control System”, Int Conf on Robotics and Automation, ICRA’ 98. p2087–2093.

Caffaz A, Cannata G (1998), “The Design and Development of the DIST-Hand Dextrous Gripper”, Proc of Int Conf on Robotics an Automation (ICRA’98). Leuven, Belgium, p 2075–2080.

Carrozza MC, Massa B, Micera S, Zecca M, Dario P (2001), “A “Wearable” Artificial Hand for Prosthetics and Humanoid Robotics Applications”, Proc of the 2001 IEEE — RAS Int Conf on Humanoid Robots.

Craig, J. (2003) "Introduction to Robotics: Mechanics and Control" Prentice Hall, 3rd edition.

Drills and Contini (1966), http://www.pt.ntu.edu.tw/ hmchai/ bm03 / bmmeasure/ anthropometricMeasuremtns

Edsinger-Gonzales, A. (2004), "Design of a Compliant and Force Sensing Hand for a Humanoid Robot", Proceedings of the Int Conf on Intelligent Manipulation and Grasping.

Fisher, M. Smagt, P.D., Hirzinger, D. (1992), “Learning techniques in a dataglove based telemanipulation system for the DLR hand”, IEEE ICRA, p1603-1608.

Folgheraiter, M. and Gini, G. (2003) “Human-like reflex control for an artificial hand”, Proc. of the 5th Int Workshop on information processing in cells and tissues (IPCAT2003). Lausanne, Switzerland, p223–238.

Folheraiter, M., Gini, G. (2000) “Blackfingers: Artificial Hand that Copies Human Hand in Structure, Size and Functions”, Proceedings of Humanoids 2000.

Fukaya, N., Shigeki, T., Afour, T., Dillmann, R. (2000), “Design of the TUAT/Karlsruhe Humanoid Hand”, IEEE/RSJ Int Conf on Intelligent Robots and Systems.

Gomez, G. (2006) "An adaptive neural controller for a tendon driven robotic hand", Proceedings of the 9th Int Conf on Intelligent Autonomous Systems (IAS-9) .Tokyo, Japan, p298-307.

Grimm M, Arroyo A, Nechyba M (2002), “Thing: A Robotic Hand with Realistic Thumb Pronation”, Proc of the FCRAR 2002.

Grinyagin, Bityukova, V., Maier, M.A. (2005), “Kinematic and dynamic synergies of human precision-grip movements”, J of Neurophysiology v94, p2284-2294.

Guru, B. S. & Hiziroglu, H. R. (2001) “Electric machinery and transformers” Oxford University Press. 3rd Ed.

Hans, M., Graf, B. (2004) "Robotic Home Assistant Care-O-Bot II,” Advances in Human-Robot Interaction. Series: Springer Tracts in Advanced Robotics, V14, p371-384.

Helms, E. et al. (2002) "Rob@work: Robot Assistant in Industrial Environments", Proceedings of IEEE ROMAN '02.

Hirzinger, G. (2002) et al. "DLR’s torque-controlled light weight robot III - are we reaching the technological limits now?", Proceedings of the 2002 IEEE lnt Conf on Robotics & Automation, Washington, DC May, p1710-1716.

Hirzinger, G. et al. (2001) "Robonauts need light-weight arms and articulated hands", Harmonic Drive International Symposium, Matsumoto, Nagano, Japan, Nov. p20-21.

InTouch Co., “The Companion”, http://www.intouchhealth.com/products.html

Ikuta, K. et al. (2003) “Safety Evaluation Method of Design and Control for Human-Care Robots”, The Int J of Robotics Research, 22(5), p281-297.

Ishikawa, Y., Yu, W., Yokoi, H., Kakazu, Y. (2000), “Development of Robot Hands with an Adjustable Power Transmitting Mechanism”, Intelligent Engineering Systems Through Neural Networks. Asme Press, v10, p631–636.

Jacobsen, S. C. et al. (1986), “Design of the Utah/MIT dexterous hand”,

Proceedings of the IEEE Int Conf of Robotics and Automation. p1520–1528.

Jung, S. (2006) “Robotics Engineering”, Choongnam University Press. 2nd Ed.

Kahtib, O. et al. (1999) “Robots in human environments: basic autonomous capabilities”, The Int J of Robotics Research, 18(7), p684-696.

Kaneko, K. et al. (2004) “Humanoid Robot HRP-2”, Proceedings of 2004 IEEE Int. Conf. on Robotics & Automation, New Orleans, LA, p1083-1090.

Kaneko, K. et al. (2007),"Development of Multi-fingered Hand for Life-size Humanoid Robots",2007 IEEE Int Conf on Robotics and Automation Roma, Italy, p913-920.

Kawasaki, H., Komatsu, T., Uchiyama, K. (2002) “Dexterous Anthropomorphic Robot Hand With Distributed Tactile Sensor: Gifu Hand II”, IEEE/ASME Trans On Mechatronics. 7(3), p296–300.

Kawasaki, H., Shimomura, H., Shimizu, Y. (2001) “Educational-industrial complex development of an anthropomorphic robot hand ‘Gifu hand’”, Advanced Robotics, 15(3), p357–363.

Kerpa, O., Osswald, D., Yigit, S., Burghart, C., Woern, H. (2003), “Arm-hand-control by tactile sensing for human robot cooperation”, Proc. Humanoids 2003, Karlsruhe, Germany, Oct. 2003.

Kim, B.H. (2006), “A joint motion planning based on a bio-mimetic approach for human-like finger motion”, Int J of Control, Automation, and Systems, 4(2), p217-226.

Kim, D., Choi, Y., Oh Y., and You, B.J. (2005) "Real-Time Generation of

Humanoid Motion with the Motion-Embedded COG Jacobian", ICCAS2005 June 2-5, KINTEX, Gyeonggi-Do, Korea.

Kim, M., Yun, S.K., Kang, S. (2004) “Safe design and vibration control of a manipulator with passive compliant joints”, 2nd Int conf on autonomous robots and agents Dec 13-15, 2004, New Zealand, p180-185.

Kulic, D. and Croft, E.a. (2005) “Real-Time Safety for Human-Robot Interaction”, J of Robotic Systems, 22(7), p383-396.

Kulic, D. and Croft, E.a. (2006) “Real-Time Safety for Human-Robot Interaction”, Robotics and Autonomous Systems, n.54, p1-12.

Lalibert, T., Birgleny, L., Gosselin C. (2002) "Underactuation in robotic grasping hands", Machine Intelligence & Robotic Control, Vol. 4, No. 3, p1–11.

Lang, C. & Schieber, M.H. (2004) "Human Finger Independence: Limitations due to passive Mechanical Coupling Versus Active Neuromuscular Control", J of Neurophysiology 92, p2802-2810.

Lee, W.S. (2007), “An interactive kendo robotic system based on real-time force sensing”, Ph.D. Thesis, Seoul National University (2007).

Lenarcic, J. (1999) "Basic Kinematic Characteristics of Humanoid Manipulators”,1999 John Wiley & Sons, Inc.Lab. robot. autom., v11, p272-278.

Lohman, Timothy G., Roche, Alex F. Martorell, Reynaldo (1988) “Anthropometric standardization reference material”, Human Kinetics Books, Champaign, Illinois 1988. p1~55.

Lovchic C, et al. (2001), “Compact Dexterous Robotic Hand”. United States Patent,

Patent Number 6,244,644

Lovchik C, Aldridge H, Diftler M (1999) “Design of the NASA Robonaut Hand”, Proceedings of the ASME Dynamics and Control Division DSC. Nashville, Tennessee, Vol.67, p813–830.

Lovchik C, et al. (2000) “Robonaut: NASA’s Space Humanoid”, IEEE Intelligent Systems. 15(4), p57–63.

Lovchik, C., Diftler, M. (1999) “The Robonaut Hand: A Dexterous Robot Hand For Space”, Proc of the IEEE Int Conf on Automation and Robotics. Detroit, Michigan, 2, p907–912.

McCammon, I., Jacobsen, S. (1990), “Tactile Sensing and Control for the Utah/MIT Hand”, Dexterous Robot Hands (eds) Springer-Verlag, p 238–266.

McElhaney, J. (1976) “Head Injury Criteria”, Mechanics of Composite Materials 12(3), p411-429.

Mouri, T., Kawasaki, H., Yoshikawa, K., Takai, J., Ito, S. (2002) “Anthropomorphic Robot Hand: Gifu Hand III” Proceedings of Int Conf ICCAS2002, p1288–1293.

Murrary, R.M., Li, Z., Sastry, S.S. (1994) “A mathematical introduction to robotic manipulation”, CRC Press, p63.

Murray, Li, Sastry, “A mathematical introduction to robotic manipulation”, CRC press.

Namiki, Y., Imai, M., Ishikawa, M. (2003), “Development of a Highspeed Multifingered Hand System and Its Application to Catching”, 2003 IEEE/RSJ Int

Conf on Intelligent Robots and Systems. Las Vegas, p2666–2671.

Odashima, T. et al. (2006) “A Soft Human-Interactive Robot RI-MAN”, Intelligent Robots and Systems, 2006 IEEE/RSJ International Conference, p1.

Onishi, M. et al. (2007) “Generation of human care behaviors by human-interactive robot RI-MAN” IEEE Int conf on robotics and automation, Roma, Italy, April, p10-14.

Pervez, A., and Ryu, J. (2007) “Safe physical human robot interaction-past, present and future”, to be published.

Robotics & Automation Magazine, IEEE Volume 11, Issue 2, p12 – 21.
Sahara, S., Imai, M., Anzai, Y. (2004), “CAHRA: Collision Avoidance System for Humanoid Robot Arms with Potential Field”, Int Conf on Systems, Man and Cybernetics (SMC 2004), p 2889-2895.

Sakai, N., Sawae, Y., Murakami, T. (2006) "The Development of A New Joint Mechanism Based on Human Shoulder Morphology" IEEE/RAS-EMBS Int Conf on Biomedical Robotics and Biomechanics (BioRob 2006) on CD-ROM, p341-346.

Salisbury, J.K., Craig, J.J. (1982), “Articulated hands: Force control and kinematics issues”, Int J on Robotics Research, p4–20.

Salisbury, J.K., Roth, B. (1983), “Kinematics and Force Analysis of Articulated Mechanical Hands”, J of Mechanism, Transmissions and Actuation in Design, p105.

Salloum, M., Wang, Z., Moss, S.. et al. Anthropometry for World SID A World-Harmonized Midsize Male Size Impact Crash Dummy SAE Inter. Technical paper Series June 19-21, 2000.

Schulz, S., Pylatiuk, C., Bretthauer, G. (2001), “A new ultralight anthropomorphic hand”, Proc. ICRA IEEE Int Conf Robotics & Automation. Seoul, Korea, pp. 2437–2441.

Shadow Robot Company (2003), “Design of a dexterous hand for advanced CLAWAR applications”, Proc of CLAWAR 2003, p691–698.

Tondu, B. et al. (2005) "A Seven-degrees-of-freedom Robot-arm Driven by Pneumatic Artificial Muscles for Humanoid Robots" , The Int J of Robotics Research v24, p257-273.

Townsend, W. (2000), “The BarrettHand grasper — programmably flexible part handling and assembly”, Industrial Robot: An International Journal. 27(3), p181–188.

Vogt, H., Berns K. et al. (1998), “Design and Control Architecture of an Anthropomorphic Robot Arm”, Int. Cong on Advanced Mechatronics (ICAM’98), Okayama, Japn Aug 1998.

William J Hughes Technical Center (1965), “Anthropometry and biomechatronic” Federal Aviation Administration, http://www.faa.gov.

Zatsiorsky, V.M. “Kinematics of Human Motion”, Human Kinetics 1998.

Zhang, C. (2003), "Robot 'Nurse' Puts a Human Face on Elderly Health Care", The Salt Lake Tribune, June 19, 2003

Zinn M, Khatib, O., Roth, B. and Salisbury, J.K. (2004a) “Paying it safe-a new actuation concept for human-friendly robot design”, IEEE Robotics and automation magazine, p12-33.

Zinn, M. et al (2004b) “A new actuation approach for human friendly robot design”, 2004 IEEE Int Conf on Robotics and Automation, v1, p249- 254.

Zinn, M., Khatib, O., Roth, B., Salisbury, J.K. (2004c) "Towards a Human-centered Intrinsically-Safe Robotic Manipulator", IEEE Robotics and Automation Magazine, 11(2), p12-21.

Appendix A: Robotic hands

I categorized currently known robotic hands here. The actuation method, number of DoF, actuation mechanism, material, sensory skills, path planning method and novel features are summarized.

Table A.1 Barrett hand & DIST hand

NAME	Barrett hand	DIST Hand
Previously AKA	MIT's FSC hand	-
Institution/ company	MIT Barrett technology, inc.	Universita di Genova
country	USA	Italy
Year	1997 - 2004	1998
Status	Commercial use	Research prototype
Novel feature	Modularized force sensing compliant actuators: spring loaded revolute motors to measure torque Cable driven tendon	Pulley and tendons: cable-driven
Structures and materials	3 fingers Electrical revolute brushless motors, Spur and worm gear transmissions, Fair contact surface smoothness	3 fingers and one opposable thumb, Electrical revolute brushless motors,
Sensory-motor skills	9 DoF (4 controlled= 3 fingers + 1 DoF for spreading 2 fingers) Motor position sensors (optical incremental encoders) Strain-gauges based joint torque sensors (force sensing resistor)	16 controlled DOF Motor position sensors hall-effect based joint position sensors 3-axis fingertip force sensors
Feedback control	Joint position control Joint velocity control Embedded DSP u-processor	Position feedback
Path planning	Power grasp and precision grasp	Power grasp and precision grasp
Autonomy	Non autonomous	Non autonomous

Table A.2 Robonaut hand & DLR hand

NAME	Robonaut Hand	DLR Hand II
Previously AKA	UTAH-MIT Hand	DLR
Institution/ company	NASA Johnson Space Center	DLR-German Aerospace Center
country	USA	Germany
Year	1999	2000~2004
Status	Research prototype	Research prototype
Novel feature	Flexshaft , lead screw transmissions	Built-in actuator Pulley-timing belt driven (distal joints) Harmonic drives/gears transmissions (for 2 DoF MP joint),
Structures and materials	4 fingers and one opposable thumb, Electrical revolute brushless motors, Kevlar body armor coated with Teflon	3 fingers and one opposable thumb, revolute BLDC motors, produce up to 30N @ finger tip Silicone finger surface
Sensory-motor skills	16 DoF -- 14 controlled DOF (2 wrist + 3 middle, index + 3 thumb + 1 pinky, ring) Under-actuated palm action Wrist actuators in forearm Motor position sensors, incremental encoders Joint position sensors Tendon tension sensors Tactile force sensors (FSR Force Sensing Resistor technology)	13 DOF (3DOF/finger +1DOF palm) (coupled medial and distal joints) Motor position sensors Joint position (0.1 deg resolution) sensors (potentiometers) Strain-gauged based joint torque sensors temp sensor 6-axis fingertip force sensors 1.8kg/hand 30N @ fingertip
Feedback control	Force feedback	Position feedback Joint level impedance control force control
Path planning	Power grasp, precision grasp and human-like fine manipulation	Power grasp, precision grasp and human-like fine manipulation
Autonomy	Remotely operated via visual feedback	Pre-planning: performs previously stored trajectories and hand poses Tele-operation via data glove control

Table A.3 Ultra light hand & GIFU hand

Name	Ultra light Hand	GIFU Hand
Previously AKA	-	KH (kinetic humanoid) hand
Institution/ company	Research center of Karlsruhe	Gifu University
Country	Germany	Japan
Publication year	2001	2001~2005
Status	Research prototype	Research prototype
Novel Features	Light weight Flexible fluidic actuators, Direct drive transmissions,	Built-in DC Maxon servomotors Modularized fingers: no need for bulky forearm Planar link mechanism in 3rd and 4th joints for under-actuation
Structures and materials	4 fingers and one opposable thumb, Silicone-rubber glove 20g / finger	4 fingers and one opposable thumb, Worm gear transmissions 1.4 kg/hand
Sensory-motor skills	19 DoF (14 controlled = 3 wrist + 2 DoF/finger + 3 DoF thumb) Joint position bending sensors Pressure sensors in finger links 12N @ finger tips	20 DoF (16 controlled = 3 DoF/finger + 4 DoF thumb) Motor position sensors 6-axis fingertip force sensors Distributed resistive tactile sensors: 859 detection points ART-Linux or Windows OS
Feedback control	No sensory feedback Self adaptable properties of the hand	Force feedback glove control Position feedback control
Functional capabilities	Power grasp and precision grasp	Power grasp and precision grasp Peg in hole task using master-slave through force feedback glove control
Autonomy	Pre-planning: performs patterns of movements : position and torque of every joints	Preplanned hand signal

Table A.4 Shadow hand & UB hand III

Name	Shadow Hand	UB Hand III
Institution/ company	Shadow Robot Company Lt	Bologna University
Country	UK	Italy
Publication year	2004	2004
Status	Available for purchase	Research prototype
Novel Features	Air Muscles	Pulling tendons, cable driven Coiled springs in elastic hinges Actuation module in forearm
Structures and materials	4 fingers and one opposable thumb, Tendons, Layer of soft polyurethane flesh, Thin polycarbonate fingernails	4 fingers and one opposable thumb, DC brushed motor, Visco elastic cover
Sensory-motor skills	24 DOF, 20 controlled (16/12 fingers + 5 thumb + 2 wrist + 1 palm) Muscle pressure sensors Hall effect based joint position sensors Distributed tactile force sensors (contact, force, direction)	20 DoF (16 controlled = 4 thumb, index + 3 middle, pinky + 2 ring) Motor position sensors Tendon force sensors strain gauges based joint position sensors 70N tendon pulling force PC based real time control RTAI-LINUX OS
Feedback control	Position feedback (low level joint position and joint stiffness control)	Sensory feedback Motor position control Impedance control
Functional capabilities	Power grasp, precision grasp and human like fine manipulation	Power grasp, precision grasp and human like fine manipulation
Autonomy	Semi-autonomous	Semi autonomous

Table A.5 RCH-1 & Anthrobot dexterous hand

NAME	RCH-1	Anthrobot Dexterous Hand
Previously AKA	WE4-RII arm/hand WENDY arm (7 DoF) / hand (13 DoF) Hadaly, wabian RTR2 (3 fingers) PALOMA Hand	
Institution/ company	Waseda University Scuola Superiore Sant'Anna	Rensselaer Polytechnic Institute (RPI)
Country	Japan, Italy	USA
Developm ent Year	1997~2003	1997
Status	Research Prototype	Research prototype
Novel Features	Built-in actuators (1 motor integrated into the palm, 5 into the forearm)	Cable driven
Structures and materials	4 fingers and one opposable thumb, Electrical revolute brushless motors + gears Fingertip rubber coating 320g (excluding motors in forearm: 2 for thumb is in palm, 4 for other fingers in forearm)	4 fingers and one opposable thumb 4.5kg/hand
Sensory-motor skills	Hand: 16 DoF (6 actuated) Arm: 7 DoF 30N maximum grasping force 16 contact sensors @ phalanges (14) and palm (2) 2 3-D force sensors @ fingertips of thumb and index finger	20 DoF (16 actuated= 3/finger + 4 thumb)
Feedback control	Fingertip pressure control	Force and position control
Path planning	Pre-generated precision and power grasping	precision and power grasping
Autonomy	Preplanned mapping	Preplanned mapping

Table A.6 Rutger hand & UTAH-MIT hand

NAME	Rutger Hand	UTAH-MIT HAND
Previously AKA	Shape memory alloy actuated prosthetic hand	DH (dexterous hand) Now Robonaut hand
Institution/company	Rutger University	University of UTAH, MIT
Country	USA	USA
Development Year	1999~2002	1986
Status	Research prototype	Research prototype
Novel Features	Wire-driven with SMA actuators	Wire-driven
Structures and materials	4 fingers and one opposable thumb, Electrical revolute brushless motors + gears 0.36kg/finger	3 fingers and 1opposable thumb
Sensory-motor skills	20 DoF (4 DoF / finger) Spherical joint for MP's (2 DoF) revolute joint for PIP DIP (1 DoF) 6.67N @ fingertip	16 DoF
Autonomy		Pre-planning: performs previously stored trajectories and hand poses Tele-operated with glove Visual feedback from 2 stereo cameras (25 img /sec) Grasping-laser scanner

Table A.7 Ultra high speed multi-fingered hand & 5-fingered robotic hand

NAME	Ultra High-speed Multi-Fingered Hand	5-Fingered Robot Hand
Institution/company	University of Tokyo	Keio University
Country	Japan	Japan
Development Year	2004	2005
Status	Research Prototype	Research prototype
Novel features	Harmonic drive gear & high powered mini actuator built in each link High torque Active catching enabled	Ultra-sonic motors and elastic elements Pulley + cable (nylon string) driven
Structures and materials	8 DoF in 3 fingers (2 index + 3 R,L, thumbs) 180 deg / 0.1 sec (each finger in yaw dir.)	4 fingers + 1 opposable thumb no palm action
Sensory-motor skills	Active vision image processing	20 DoF (4 DoF/ finger)
Feedback control	Visual feedback	Force control by rotation angle feedback
Path planning	Approaching + grasping phase	Power grasp and precision grasp Produce Cutkosky classification of gasping
Autonomy	autonomous	Non autonomous

Table A.8 SKKU II & HUBO

NAME	SKKU II	HUBO Arm/hand
Previously AKA	Anthropomorphic hand	-
Institution/company	성균관대학교	KAIST
Country	South Korea	South Korea
Development Year	1995~2005	2000~2006
Status	Research Prototype	Research prototype
Novel features	DC Motor driven Universal joints and gears timing belt	
Structures and materials	3 fingers + 1 opposable thumb 10 DOF (2 DoF X 3 + 4 DoF thumb) Reduction rations are about 275:1 840 g	6 DoF/arm 5 fingers/hand 1 DoF/finger 2 DoF /wrist Pressure sensor @ finger tip pulley./belt mechanism F/T sensor @ waist
Feedback control	DSP embedded controller	
Path planning	Power grasp and precision grasp	Power grasp and precision grasp
Autonomy	Non autonomous	Non autonomous

Table A.9 MAHRU & Micro surgery robot

NAME	MAHRU	Micro Surgery Robot OP2
AKA	AHRA	-
Institution/company	KIST	KAIST
Country	South Korea	South Korea
Development Year	2006	1995
Status	Research prototype	Research prototype
Novel features	Freely move both arms for natural handshaking	Master and slave relation for tele-operated surgery : 2 slave arms for micro/macro manipulation Produce 6DOF @ the end effector
Structures and materials	DC motors	Hydraulic actuators for the platform

Table A.10 EveR-1 & POSTECH HandIII

NAME	EveR-1	POSTECH Hand III
Previously AKA	-	POSTECH Hand
Institution/company	한국생산기술연구원	포항공대
Country	South Korea	South Korea
Development Year	2006	1992~
Status	Research prototype	Research prototype
Novel features	Limited to lifelike facial features (15 DoF) Arms and hands: Hand shaking	
Structures and materials	Deduce max of 1~2 actuated DoF in hands	3 fingers
Sensory-motor skills	DC motor driven	DC motor driven
Feedback control	Vision	Force sensing
Path planning	Preplanned path	
Autonomy	Autonomous	Non-autonomous

Table A.11 Actroid arm & CARDEA arm

NAME	Actroid arm	CARDEA arm
Previously AKA	-	-
Institution/company	Kokoro Inc.	MIT
Country	Japan	USA
Development Year	2005	2003
Status	Commercial usage	Research prototype
Novel features		Series Elastic Actuator arms Mechanically modular arms (3 arms in the future)
Structures and materials		5 DoF (2 shoulder + 1 elbow + 2 wrist / arm)
Sensory-motor skills		BLDC motors in each joint Embedded DSP controllers
Feedback control		Vision and whiskers feedback for navigation and arm manipulation Force controlled arm
Path planning		Edge detection around doors and hallways to plan arm link configuration
Autonomy	Non-autonomous	Autonomous

Table A.12

Thing, TUAT/Karlsruhe humanoid hand, and Dexterous robotic hand

NAME	Thing	TUAT/Karlsruhe Humanoid Hand	Dexterous Robotic Hand
Previously AKA	HIGH 5	ARAMAR hand / arm	-
Institution/ company	University of Florida	Tokyo University University of Karlsruhe (FZI)	
country	USA	Japan Germany	USA
Publication Year	1997	2000	1992
Status	Research Prototype	Research prototype	Research prototype
Novel Feature	Actuated by modularized SMA pistons	Spherical & sandwich type ultrasonic motors Ball joints for 2 DoF Rod & link plate parallel Mechanism	Tendon-pulley driven
Structures and Materials	3 fingers + 1 opposable thumb	5 fingers Resin	
Sensory-motor Skills	Flex sensor on power glove controls the Hand	Hand: 20 DoF (1 actuated) 4 under actuated DoF / finger Arm: 7 DoF	
Feedback Control		No sensory feedback	
Path planning	"Power glove" control	Power grasp and precision grasp	
Autonomy	Non autonomous	Preplanned motion	

Appendix B:
Biomechanical models of human arm

In creating the anthropomorphic robotic arm, much attention has gone into building an extremely lifelike humanoid arm that bares high similitude in its physical appearance and capacity. Therefore, anthropometry of adult human has been collected from various sources to determine the design specifications of the robot arm. Ideally it is desired to collect all the anthropometric data from the same controlled group. However, collecting such data is much demanding and there is no guarantee such an effort will produce completely balanced demographic representation of average adult human. Taking measurements from specimens require strict control in measuring techniques (Lohman et al. 1988, William 1965), without which inconsistency in the cumulative error is undetectable and cannot be corrected. Since there are already several ways of determining the proper way of making measurements and we consider two methods here. There are 2 methods: directly measured segment length & projected length. The direct segment measurement method is preferred for this research. Therefore, when the collected measurement was not sufficient, we took the samples of the lab group members.

In the tables below, I summarized specifications of human body that would be concerned when designing the robotic arm that bares the likeness and

performs to the capacity that of the human.

Table B.1 Angular range of human adult male in shoulder, elbow and wrist

(Lohman et al. 1988, William 1965)

	Rotation angles [deg]	Torque[Nm]
Shoulder		
Horizontal abduction	91	-
Forward flexion	188	-
Forward hyperextension	61	-
Lateral rotation	72	-
Medial rotation	109	-
Elbow		
Supination / pronation	80	0.85
Flexion / extension	150	7
Forearm		
Pronation	97	2.5
Supination	105	2.5
Wrist		
Radial	27	-
Ulnar	33	-
Flexion	102	5
Extention	121	5
Rotation	270	-

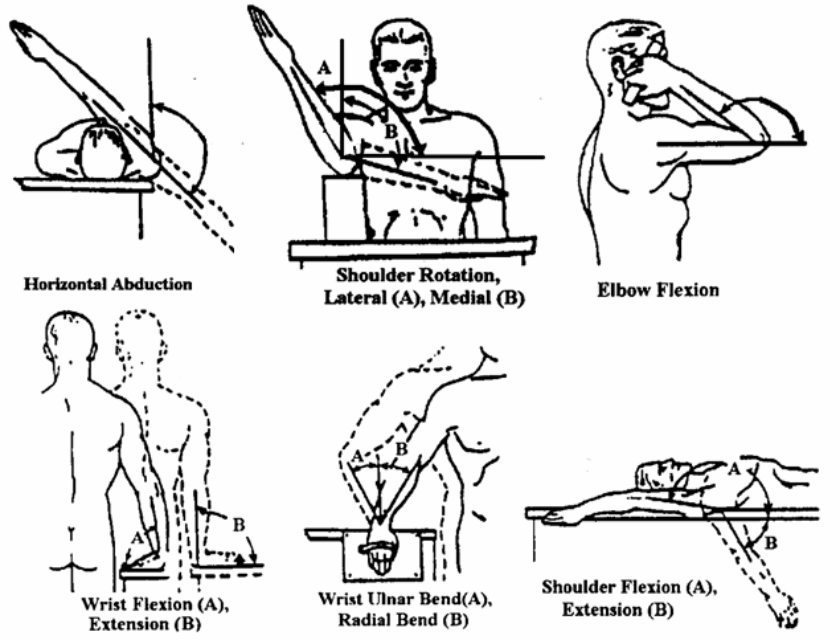

Figure B.1 Nomenclature for arm angles (William 1965)

Table B.2 Length of arm links (Vogt et al. 1998 Drills & Contini 1966)

	% of total body height [%]	measurement [mm]	% of total body weight [%]	weight [kg] (of 78kg male)
upper arm				
length	18.6	296	-	-
Weight	-	-	2.8	2.2
Forearm				
Length	14.6	276	-	1.3
circumference	-	254	-	-
Weight	-	-	1.7	-
Hand				
length	10.8	190	-	-
Breadth	-	88	-	-
weight	-	-	0.6	0.5

Table B.3 Human arm forces in various directions

exertable horizontal force			
condition	applied with	exertable horizontal force	
low traction (u<0.2)	both hands	110	push or pull
medium traction (u=0.6)	both hands	200	push or pull
braced against wall	one hand	240	push
high traction (u>0.9)	both hands	310	push or pull
feet anchored	both hands	490	push or pull
feet anchored	Back	730	push
Hand & thumb-finger strength			
condition	hand grip [N] Fig B.2 a)	thb-fig palmer [N] Fig B.2 b)	thb-fig tip [N] Fig B.2 c)
momentary hold	208	48	48
sustained hold	124	28	28

a) **b)** **c)**

Figure B.2 Directional forces of human arm (William 1965)

초록

휴머노이드용 로봇 개발의 궁극적인 목표는 인간과 흡사한 형상을 가져서 인간의 환경에 적응 하여 인간과 상호작용을 하며 공존하는, 인간의 편의를 돕는 로봇을 만드는데 있다. 이 로봇들은 집이나 병원 같은 특이 환경에서 작업을 해야 하기 때문에 작업영역의 구속을 받을 뿐만 아니라, 경우에 따라서는 사람에게 물리적인 위협이 될 가능성이 있다. 산업용 로봇과 달리 휴머노이드용 로봇은 지정된 동작을 수행하다가도 동작 중에 예상 밖의 외력이 감지되면 즉각 동작을 정지하거나 안전한 동작으로 전환하여 로봇의 동작이 인간에게 피해를 가하지 않도록 해야 한다. 또한 접촉 대상이 인간이 아니더라도 로봇은 물체와의 충돌로 인한 균형 상실이나 손상으로부터 자신을 보호하기 위해 동작을 정지하거나 변형해야 한다. 로봇 몸체 중 특히 팔의 경우는 인간의 팔처럼 외력을 감지하여 적절히 대응할 수 있는 판단의 근거를 필요로 한다.

본 논문에서는 인간의 팔과 유사한 크기, 형상, 자유도를 가진 7-자유도 로봇 팔과 8-자유도 손을 제작하고, 이 팔이 토크센서가 없이도 외력을 감지할 수 있도록 프로그램하며, 앞서 말한 자기 보호 및 인간 보호를 가능 하게 하였다. 기존의 휴머노이드 팔들이 느린 속도로 부자연스럽게

움직이는 것에 반하여, 개발된 로봇 팔은 인간이 일상생활을 행하는 정도의 속도로 움직일 수 있다. 특히 각 7개의 관절들을 하나의 독립된 모듈로 개발하여, 외부와는 최소한의 배선을 이용한 RS-485 통신으로 안정적인 제어가 가능한 완결된 구조를 가지도록 했다. 이렇게 기어로 외력을 감지하여 지능적으로 동작하는 팔은 안전도가 높아서 인간과 상호작용하는데 적합할 뿐만 아니라 다른 모양의 다관절 로봇에도 적용 가능하다. 이 연구에서 얻어진 성과를 정리하면 다음과 같다.

인간을 닮은 안전성을 고려한 팔과 손의 개발

전체적인 크기와 질량이 성인 여자의 팔과 손과 비슷하도록 설계하였다 (전체 질량 3.7kg, 어깨 관절부터 손목 관절까지 500㎜). 팔은 7-자유도로 사람과 흡사한 대부분의 동작을 구현할 수 있으며 전체 관절 각속도도 200deg/sec가 충분히 넘게 설계되어 사람과 비슷한 속도로 넓은 구동 범위를 가지며 운동할 수 있다. 기존의 휴머노이드 팔보다 가볍고 관절 강성이 낮아서 안전도가 높은 팔임을 HIC 실험을 통하여 확인했다. 또한 필요에 따라서 실시간으로 관절 강성을 조정할 수 있어서 다양한 작업이 가능하다.

외력에 반응하여 안전한 경로 생성

다른 외력이 없어도 각 관절에서는 항상 중력과 관성력에 의한 토크 부

하가 걸리게 된다. 이때, 로봇 팔의 역기구학과 동역학을 해석하여 외력이 없을 시의 부하 토크를 알 수 있고, 이 값을 실시간으로 수집된 토크 값과 비교하여 관절에 가해지는 외력만을 검출할 수 있다. 이러한 외력 검출 기능을 이용하여 외력의 위치, 값, 방향을 구할 수 있으며, 현재의 경로에서 들어온 외력에 따라서 새로운 안전한 경로를 실시간으로 생성한다. 이를 위해서 외력을 위험 정도에 따라 분류하는 알고리즘을 개발하였으며 그 수치에 따라 안전 경로를 택하여 움직이게 된다

인간과 상호 작용하는 손

개발한 로봇 팔과 손을 동시 제어하여 위치가 파악된 물건을 집을 수 있다. 손에 잡힌 물체로 인해 발생하는 외력을 별개의 센서 없이 감지하여 확실하고 안정적으로 반응할 수 있으며, 이 기능을 이용하여 인간이 건네준 물건을 신속하고 안전하게 받을 수 있다. 또한 사람의 팔, 손과 구동범위가 비슷하여 사람과 거의 동일한 동작 수행이 가능하다.

주요어: 휴머노이드, 로봇 팔, 로봇 손, 로봇 인간 상호작용, 안전 운동 경로

학생번호: 2002-21182

Acknowledgements

First, I would like to thank my supervisor Professor Bang Yongbong for his support and guidance during writing thesis. I am grateful for all the great advice, many sleepless nights of building and testing the robot together. His expertise and insights have been invaluable.

My appreciation also goes to my advisors, Professor Lee Kyoil, Professor Kim Jongwon, Professor Lee Kunwoo, Professor Pahk Heui Jae, and Professor Park Shinsuk, whose comments and suggestions have been indispensable to completing this thesis.

I should also thank Samsung Electronics Co. and Dr. Shim Youngbo's group for their funding and support. I hope they are happy with the results. I am especially indebted to Dr. Shim for his understandings with my ambitions with the arm. Without his generosity and patience, this thesis may never have been bounded.

I have formed a close bond with everyone in my lab during my graduate studies. I thank Dr. 신부현, Dr. 이원석, Dr. 이경민, Mr. 김인수, Mr. 배현기, Mr. 임원규, Mr. 국주호, Mr. 백장균, Mr. 오승률, Mr. 주춘식, Mr. 정성원, Mr. 김호연, Dr. 김호상, Mr. 유제홍, and Mr. 양승철 for their friendship and partnership. I should give a special thanks to Dr. 신부현, with whom I am graduating, for his knowledge in the motor drivers and many other things that I continuously bugged him for.

I thank my friends and advisors from my other hometown, Vancouver. My supervisors from UBC, Dr. Croft, Dr. Altintas and Dr. Frigaard, they have taught me the foundations for my work today. I value the friendship with my "J group": James, Jason, Jeannie and Jennifer. The ongoing memories we share are invaluable. Thanks you Jennifer always for your blunt advices and brownie points. I cannot think of engineering without remembering my EMECH crew: Arman, big Neil, small Neil, Rocky, Tom, Darren, Cecilia, Chris, and Aaron, who I shared the craziest timetable ever. Arman, my project partner Neil, and small Neil, I am thankful for your assistances and discussions with the loads of assignments that never seemed to lessen. My red E-Angel's, Mary, Anne, Sharon and Shue, I am

lucky to have known you ladies. Annie, I am always grateful for your sincerest care and concerns. Kimmy and Alan, thank you for your support, honesty and heartwarming words. Dr. Sara Stafford, Dr. Emi, and Eriko, I treasure our long-lasting friendship, always. And I must thank Pastor 김경진 for keeping me in his prayers.

My deepest appreciation goes to Ms. 박소윤 and Ms. 곽현영, who have provided me with endless support and phone calls when I needed to cool my head from many mishaps in the lab. You are my 이아모 and my blood sisters. I cannot think of my past years in Seoul without you girls. I have to thank Mr. 안승우 for keeping me sane during the times of insanity after many nights of awful experiments that just would not work. Your encouragements along with EBM's have honestly kept me from running out of building #302.

I thank you, Ross, for feeding me when I am in dire need of meat, good wine and stimulating conversations. Matthias, I am grateful for our Pepsi time and Hariboos. Dr. Minara, who I had a pleasure of having as a roommate, I thank you for your heartfelt advices on school, on life and on myself. Dr. Simon, Dr. 이해성, Dr. 김학창, Mr. 이희상, and Mr. 변정원, my appreciation goes to you for your caring words and the de-stressing coffee breaks. Thank you, Ms. 이주은, as you have shown me how to keep the cool and smile during the most stressed of times. Ms. 이규진 & Ms. 이문환, thank you for being the support and my excuse to visit the far land, building #301. Ms. 최혜진, Ms. 이종미 and Dr. 이현숙, you are one of the warmest groups of people that have known. Thank you for being infectiously generous and kind.

I must give my sincerest appreciation to my forever heart warming choir family. Ms. 한정혜 for always being the big sister, always being by my side and caring for me. I am forever indebted to your blinded love.

I am grateful to Ms. 김정미 and Ms. 노정현 for their beautiful and professional advices and cheers; to Ms. 김은정 and Mr. 김동혁 for their tireless efforts and the most beautiful musical talents; to Ms. 심지연 and Dr. 강기민, Dr. 김흥규, Ms. 김영신, and Mr. 송충헌 thank you always for being so inviting and warm; and Pastor 김영신 for your devotion and prayers.

I need to thank Ms. 우해경, whose voice inspires me, and listening ears gives me comfort always. I thank Ms. 최미혜 and Ms. 나미경 who have enriched my life with beats and hip-circles. I am indebted to Ms. 김수연 for her sincerest friendship that first began in the big bamboo jungle. I am always thankful to Ms. Eugenia, Ms. Anna, Ms. Jeeyoung, Ms. Mina, Ms. Jasmin, Ms. Pie, Ms. Jineun and Dr. Karen for their honesty, blunt advices, and their infectious unflagging energy. I thank especially Ms. Anna for her kindness until dawn when helping me with the formatting of this thesis. I am just as indebted to Ms. 김성진, Ms. 박지예, Ms. 장애리, and Ms. 현지윤 for being patient with my complete absence and still sending me the best support, and the warmest words.

I would like give my greatest thanks to my 이모 and 이모부 for their undoubted cheers and love. I only wish to make them proud. Thank you always for your guidance and support.

And of course, I MUST thank my family, mom, dad, Christopher, and 할머니 for their endless prayers, the deepest trust, and unconditional love. You have stood by me during the best of times and the worst of times. You are my inspiration, role model, and coach. You give me reason to work harder and I try my best to give you reason to be proud.

Finally, I thank God for continuously blessing me with such beautiful and loving acquaintances, and an exciting life full of challenges.